Dark Matter in Clusters & Large-Scale Structure

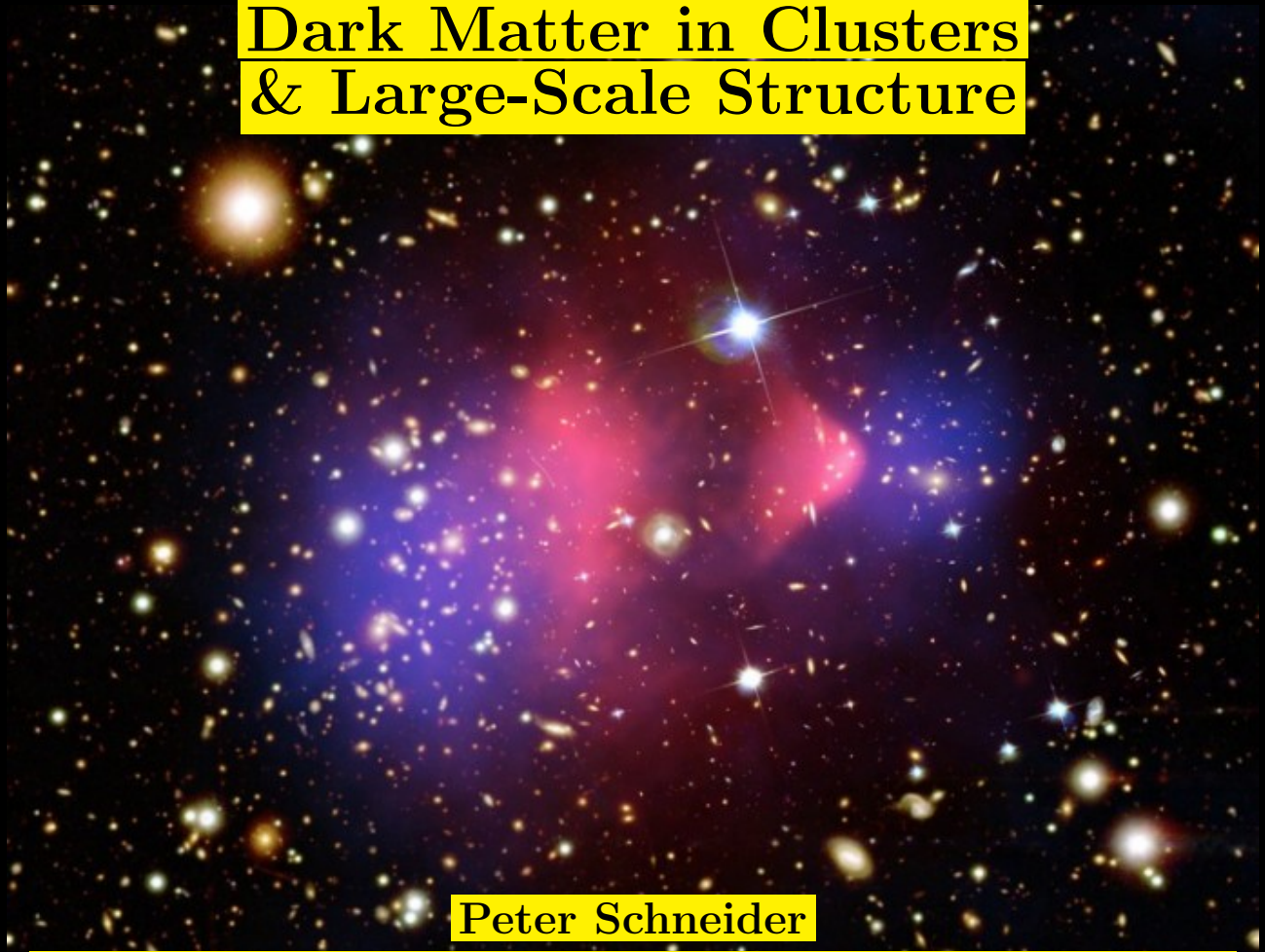

Peter Schneider

Argelander-Institut für Astronomie, Universität Bonn

Gravitational light deflection ...

- ... independent of nature and state of deflecting matter
- ... causes changes of apparent position; multiple imaging
- ... differential light deflection causes magnification and shape distortion

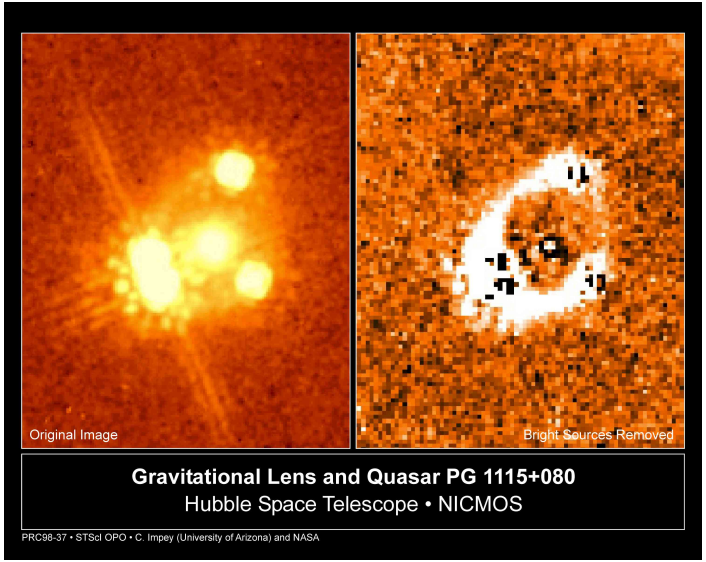

The gravitational lens effect can be used to learn something

- about the lens
  – e.g., mass distribution
- about the source
  – e.g., brightness distribution
- about the geometry of space between source, lens, and observer
  – e.g., the geometry of the Universe and its expansion history.

These Lectures

(I) Basics of weak gravitational lensing

- Distortion and Magnification
- Brightness moments and ellipticities
- Principle of shape measurements; shear estimates
- Observational issues

(II) Galaxy clusters as lenses

- Arcs, arclets and multiple images
- Strong lensing results
- Clusters as 'natural telescopes'
- Weak lensing in clusters – mass reconstruction
- Mass determinations and degeneracies

(III) Lensing by the large-scale structure

- Principle of cosmic shear – from 3D to projected power
- Shear correlations and related statistics
- E- and B-mode shear
- Measurements of cosmic shear
- Intrinsic alignments
- Future surveys and forecasts

(IV) The galaxy-mass correlation in cosmology

- Principle of galaxy-galaxy lensing
- Measures of GGL lensing
- Galaxy bias and correlation coefficient
- GGL and the halo model
- Cosmology from GGL
- Higher order mass-shear correlations

Dark Matter in Clusters & Large-Scale Structure

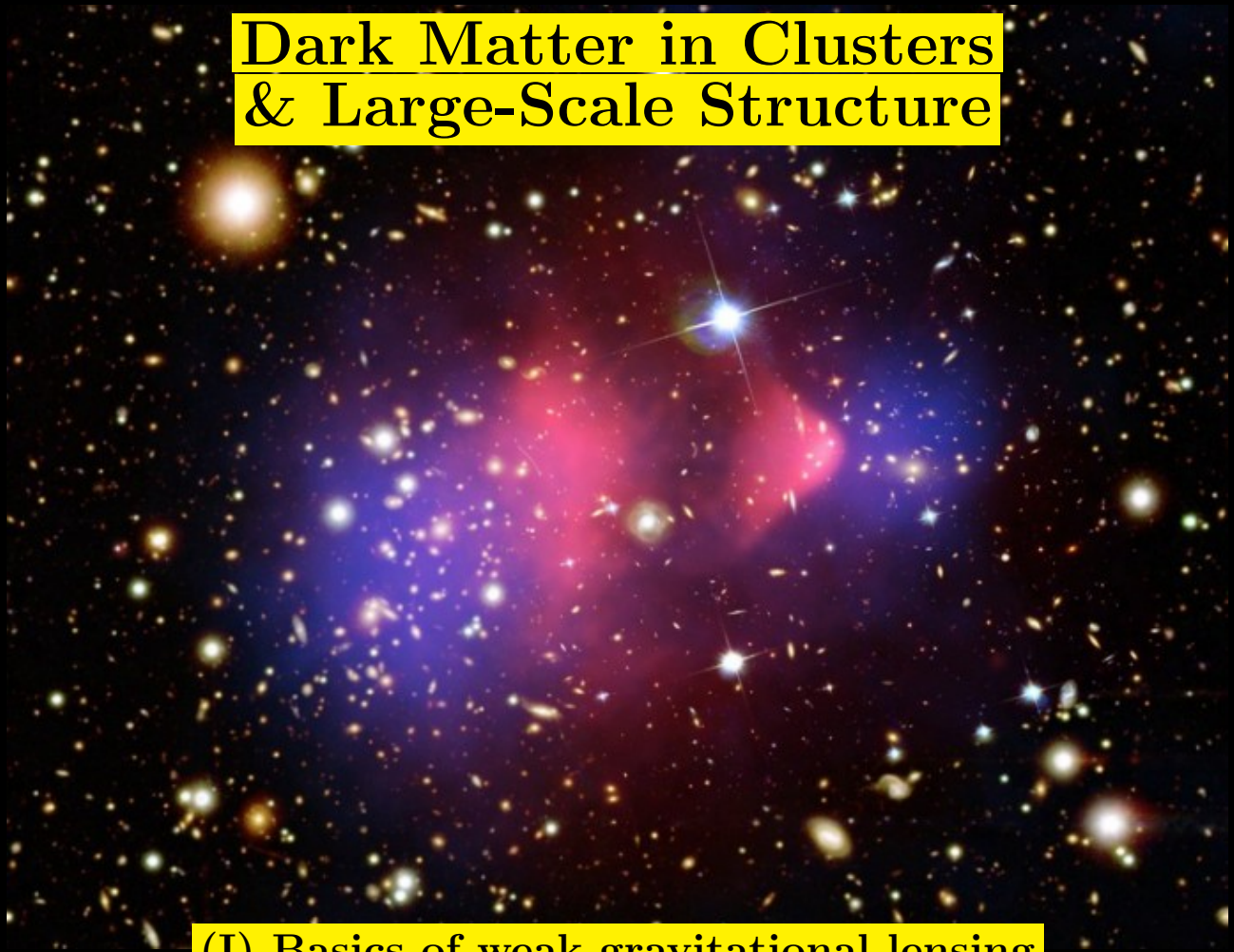

(I) Basics of weak gravitational lensing

Weak gravitational lensing: Introduction

- Multiple images, microlensing (with appreciable magnifications) and arcs in clusters are phenomena of *strong lensing*.
- In *weak gravitational lensing*, the Jacobi matrix $\mathcal{A}$ is very close to the unit matrix
  $\Rightarrow$ **weak distortions, small magnifications.**
- Those cannot be identified in individual sources, but only in a statistical sense;
- weak lensing studies therefore require large number of source;
- the basics of these effects will be descibed here.

Principles of weak lensing

Images of distant, extended sources are distorted in shape and size;
this is described by **conservation of surface brightness**,

$$I(\boldsymbol{\theta}) = I^{(\mathrm{s})}[\boldsymbol{\beta}(\boldsymbol{\theta})] \;, \tag{1}$$

where $\boldsymbol{\beta} = \boldsymbol{\theta} - \boldsymbol{\alpha}(\boldsymbol{\theta})$, together with the locally linearized lens equation

$$\boldsymbol{\beta} - \boldsymbol{\beta}_0 = \mathcal{A}(\boldsymbol{\theta}_0) \cdot (\boldsymbol{\theta} - \boldsymbol{\theta}_0) \;, \tag{2}$$

with

$$\mathcal{A}(\boldsymbol{\theta}) \equiv \frac{\partial \boldsymbol{\beta}}{\partial \boldsymbol{\theta}} = (1-\kappa) \begin{pmatrix} 1-g_1 & -g_2 \\ -g_2 & 1+g_1 \end{pmatrix} \;,\; g_i = \frac{\gamma_i}{(1-\kappa)} : \text{ reduced shear} \tag{3}$$

$$\text{magnification : } \; \mu = \frac{1}{\det \mathcal{A}} = \frac{1}{(1-\kappa)^2 - |\gamma|^2} = \frac{1}{(1-\kappa)^2 \; (1-|g|^2)} \;, \tag{4}$$

and the shape distortion is given by the **reduced shear** g.

Reminder

Dimensionless surface mass density

$$\boxed{\kappa(\boldsymbol{\theta}) := \frac{\Sigma(D_\mathrm{d}\boldsymbol{\theta})}{\Sigma_\mathrm{cr}}} \quad \text{with} \quad \boxed{\Sigma_\mathrm{cr} = \frac{c^2}{4\pi G}\,\frac{D_\mathrm{s}}{D_\mathrm{d}\,D_\mathrm{ds}}}\;;$$

Σ_cr: *critical surface mass density*, depends only on the distances D between source, deflector and observer.

$$\text{Deflection angle:} \qquad \boxed{\boldsymbol{\alpha} = \nabla\psi}\,,$$

with the *deflection potential*

$$\boxed{\psi(\boldsymbol{\theta}) = \frac{1}{\pi}\int_{\mathbb{R}^2} \mathrm{d}^2\theta'\;\kappa(\boldsymbol{\theta}')\;\ln|\boldsymbol{\theta}-\boldsymbol{\theta}'|}\,,$$

which satisfies the 2-D *Poisson equation*,

$$\boxed{\nabla^2\psi = 2\kappa}\,.$$

Shape distortions are described by trace-free part of Jacobian matrix $\mathcal{A}$,

$$\gamma_1 = \frac{1}{2}(\psi_{,11} - \psi_{,22}) \ , \quad \gamma_2 = \psi_{,12} \ : \quad \text{shear components;}$$

$$\mu = \frac{S}{S_0} = \frac{1}{\det \mathcal{A}} = \frac{1}{(1-\kappa)^2 - |\gamma|^2} \ , \ \text{with} \ \ |\gamma| = \sqrt{\gamma_1^2 + \gamma_2^2} \ .$$

The (reduced) shear is 2-component quantity, written as a complex number,

$$\gamma = \gamma_1 + \mathrm{i}\gamma_2 = |\gamma| \, \mathrm{e}^{2\mathrm{i}\varphi} \ ; \quad g = g_1 + \mathrm{i}g_2 = |g| \, \mathrm{e}^{2\mathrm{i}\varphi} \ ; \tag{5}$$

its amplitude describes the degree of distortion, its phase φ the direction.
Reason for factor '2' in phase factor: ellipse transforms into itself after rotation by 180°.

WARNING: The shear is *not* a vector:

vectors are defined through their transformation behavior under rotations;
shear is the traceless part of a symmetric tensor, which determines its transformation behavior as through $e^{2i\varphi}$.

To wit, if the Jacobi matrix $\mathcal{A}$ is considered in a different reference frame which is rotated by an angle φ, $\mathcal{A}$ transforms like

$$\mathcal{A} \to R(\vartheta)\mathcal{A}R^{-1}(\vartheta) = R(\vartheta)\mathcal{A}R(-\vartheta) \; ;$$

this transforms a shear $|\gamma|\, e^{2i\varphi}$ to $\gamma \to |\gamma|\, e^{2i(\varphi-\vartheta)}$

Geometrical interpretation: an ellipse transforms into itself when rotated by 180 degrees.

Consider a circular source with radius R; mapped by the local Jacobi matrix, its image is an ellipse, with axes

$$\frac{R}{1-\kappa-|\gamma|} = \frac{R}{(1-\kappa)(1-|g|)} \quad ; \quad \frac{R}{1-\kappa+|\gamma|} = \frac{R}{(1-\kappa)(1+|g|)}$$

and the major axis encloses an angle φ with the positive θ_1-axis.

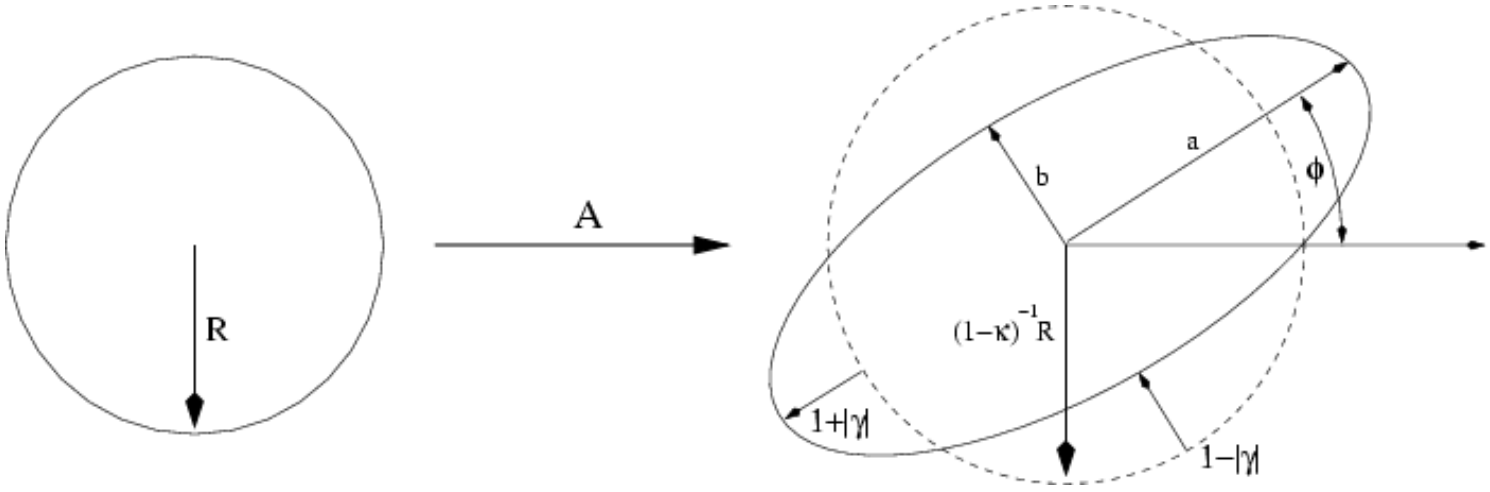

To first order, a circular source is distorted into an elliptical image, with axis ratio

$$r = \frac{1-|g|}{1+|g|}\,, \qquad \text{valid for } \; |g| < 1\,.$$

This shape distortion presents prime weak lensing observable.

Shape distortions very small ($|g|$ typically 1 to 10%), much smaller than intrinsic ellipticity distribution of galaxies

A statistical approach is required !

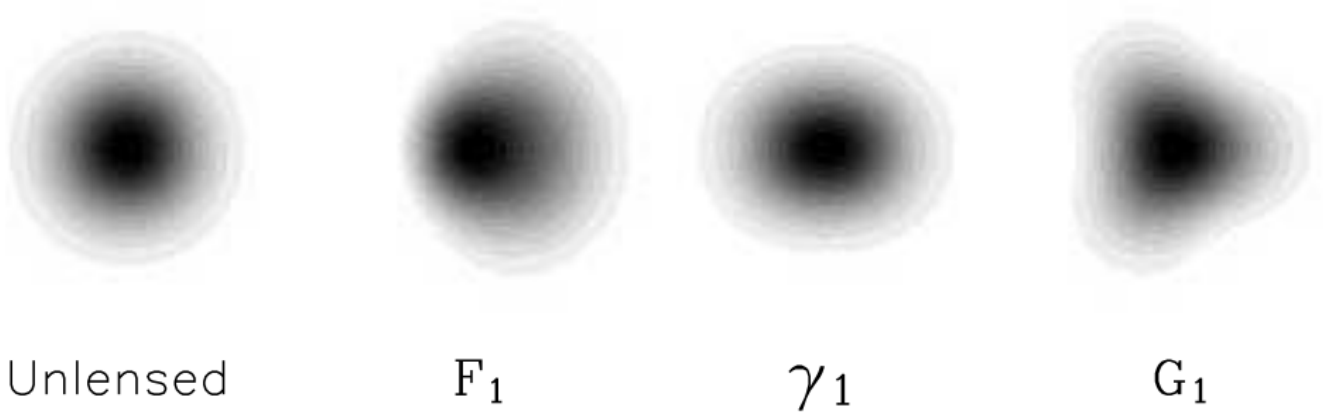

Flexion F and G

If some galaxy images are distorted as strongy as this ...

there will be **many more** galaxy images around the cluster which are distorted much less, where the distortion signal can be extracted only by statistical means.

Hence, if circular sources could be identified, measured image ellipticities would immediately yield reduced shear, through the axis ratio

$$|g| = \frac{1 - b/a}{1 + b/a} \quad \Leftrightarrow \quad \frac{b}{a} = \frac{1 - |g|}{1 + |g|}$$

and the orientation of the major axis φ.

However, faint galaxies are not intrinsically round
$\Rightarrow$ observed image ellipticity a combination of intrinsic ellipticity and shear.

Strategy: locally averaging over many galaxy images, assuming that intrinsic ellipticities are *randomly oriented*, can yield an estimate of the local shear (see below).

But: how to define 'ellipticity' for a source with arbitrary isophotes?

In addition: Seeing by the atmospheric turbulence will blur – and thus cricularize – observed images.

We'll deal with these issues in turn.

Measurements of shapes and shear

- Galaxies are not 'elliptical' (i.e., isophotes are in general not ellipses);
- how to define 'an ellipticty' for an arbitrary image shape?
- Do it in terms of brightness moments!

Let $I(\boldsymbol{\theta})$ be brightness distribution of an image, assumed to be isolated on the sky; define **center of the image:**

$$\bar{\boldsymbol{\theta}} \equiv \frac{\int \mathrm{d}^2\theta \, q_I[I(\boldsymbol{\theta})] \, I \, \boldsymbol{\theta}}{\int \mathrm{d}^2\theta \, q_I[I(\boldsymbol{\theta})] \, I} \; , \tag{6}$$

where $q_I(I)$ is suitably chosen weight function

e.g., if $q_I(I) = \mathrm{H}(I - I_{\mathrm{th}})$, integral would extend over limiting isophote of image

Define tensor of second brightness moments,

$$Q_{ij} = \frac{\int \mathrm{d}^2\theta \, q_I[I(\boldsymbol{\theta})] \, I \, (\theta_i - \bar{\theta}_i) \, (\theta_j - \bar{\theta}_j)}{\int \mathrm{d}^2\theta \, q_I[I(\boldsymbol{\theta})] \, I} \; , \quad i,j \in \{1,2\} \; ; \tag{7}$$

for an image with circular isophotes, $Q_{11} = Q_{22}$, $Q_{12} = 0$.
Trace of Q describes size of image;
traceless part of Q_{ij} contains the ellipticity information.

From Q_{ij}, one defines two complex ellipticities,

$$\chi \equiv \frac{Q_{11} - Q_{22} + 2\mathrm{i}Q_{12}}{Q_{11} + Q_{22}} \; , \tag{8}$$

and

$$\epsilon \equiv \frac{Q_{11} - Q_{22} + 2\mathrm{i}Q_{12}}{Q_{11} + Q_{22} + 2(Q_{11}Q_{22} - Q_{12}^2)^{1/2}} \; ; \tag{9}$$

both have the same phase (since the same numerator), but different absolute value;

note: in both cases, denominator given by the invariants of Q_{ij}, i.e., invariant against rotations.

For an image with elliptical isophotes of axis ratio $r \leq 1$, one has

$$|\chi| = \frac{1-r^2}{1+r^2} \quad ; \quad |\epsilon| = \frac{1-r}{1+r} \, . \tag{10}$$

Which of these two definitions is more conveninent depends on the context; one can be transformed into the other,

$$\epsilon = \frac{\chi}{1+(1-|\chi|^2)^{1/2}} \, , \quad \chi = \frac{2\epsilon}{1+|\epsilon|^2} \, . \tag{11}$$

In total analogy, one defines the second brightness tensor $Q_{ij}^{(\mathrm{s})}$, and the complex ellipticities $\chi^{(\mathrm{s})}$ and $\epsilon^{(\mathrm{s})}$ for the unlensed source.

From source to image ellipticities

From

$$Q_{ij}^{(\mathrm{s})} = \frac{\int \mathrm{d}^2\beta\, q_I[I^{(\mathrm{s})}(\boldsymbol{\beta})]\, I\, (\beta_i - \bar{\beta}_i)\, (\beta_j - \bar{\beta}_j)}{\int \mathrm{d}^2\beta\, q_I[I^{(\mathrm{s})}(\boldsymbol{\beta})]\, I}\,, \quad i,j \in \{1,2\}\,, \tag{12}$$

one finds with $\mathrm{d}^2\beta = \det \mathcal{A}\, \mathrm{d}^2\theta$ and $\boldsymbol{\beta} - \bar{\boldsymbol{\beta}} = \mathcal{A}\left(\boldsymbol{\theta} - \bar{\boldsymbol{\theta}}\right)$ that

$$Q^{(\mathrm{s})} = \mathcal{A}\, Q\, \mathcal{A}^T = \mathcal{A}\, Q\, \mathcal{A}\,, \tag{13}$$

where $\mathcal{A} \equiv \mathcal{A}(\bar{\boldsymbol{\theta}})$ is the Jacobi matrix of the lens equation at position $\bar{\boldsymbol{\theta}}$.

The transformation of second-order brightness moments between source and image is given solely in terms of the locally linearized lens equations, i.e., the Jacobian matrix $\mathcal{A}$.

Using definitions of (complex) ellipticities, one finds the transformations:

$$\chi^{(\mathrm{s})} = \frac{\chi - 2g + g^2\chi^*}{1 + |g|^2 - 2\mathcal{R}\mathrm{e}(g\chi^*)} \; ; \quad \epsilon^{(\mathrm{s})} = \begin{cases} \dfrac{\epsilon - g}{1 - g^*\epsilon} & \text{if } |g| \leq 1 \\ \\ \dfrac{1 - g\epsilon^*}{\epsilon^* - g^*} & \text{if } |g| > 1 \end{cases} \tag{14}$$

Inverse transformations obtained by interchanging source and image ellipticities, and $g \to -g$:

$$\chi = \frac{\chi^{(\mathrm{s})} + 2g + g^2\chi^{(\mathrm{s})*}}{1 + |g|^2 + 2\mathcal{R}\mathrm{e}(g\chi^{(\mathrm{s})*})} \; ; \quad \epsilon = \begin{cases} \dfrac{\epsilon^{(\mathrm{s})} + g}{1 + g^*\epsilon^{(\mathrm{s})}} & \text{if } |g| \leq 1 \\ \\ \dfrac{1 + g\epsilon^{(\mathrm{s})*}}{\epsilon^{(\mathrm{s})*} + g^*} & \text{if } |g| > 1 \end{cases} \tag{15}$$

Thus, image ellipticity is function of source ellipticity and reduced shear.

Estimating the (reduced) shear

Assumption: intrinsic orientation of galaxies is random,

i.e., no direction in the Universe is singled out:

$$\mathrm{E}(\chi^{(\mathrm{s})}) = 0 = \mathrm{E}(\epsilon^{(\mathrm{s})}) \; . \tag{16}$$

This then implies that the expectation value of ϵ is:

$$\mathrm{E}(\epsilon) = \begin{cases} g & \text{if } |g| \leq 1 \\ \\ 1/g^* & \text{if } |g| > 1 \end{cases} \tag{17}$$

Hence, each image ellipticity provides an unbiased estimate of the local shear, though a very noisy one;
noise determined by the intrinsic ellipticity dispersion

$$\sigma_\epsilon = \sqrt{\left\langle \epsilon^{(\mathrm{s})} \epsilon^{(\mathrm{s})*} \right\rangle} \; .$$

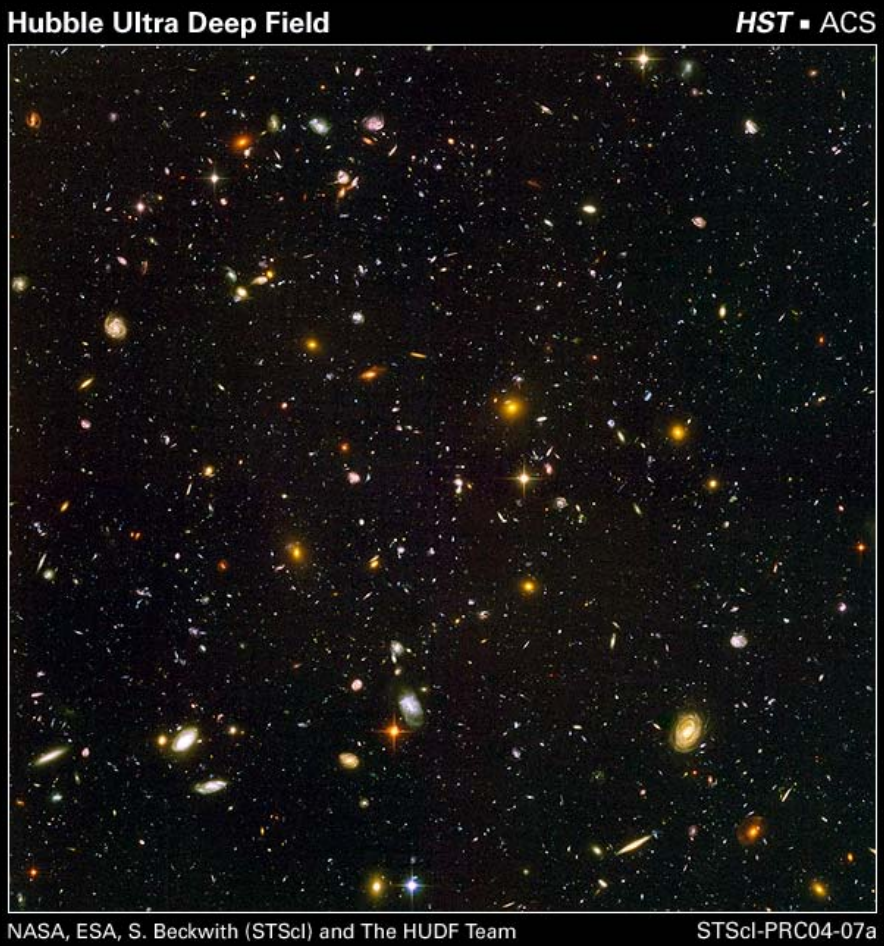

Noise can be beaten down by averaging over many galaxy images; we live in a Universe where sky is 'full of faint galaxies';
accuracy of shear estimate depends then on local number density of galaxies for which shape can be measured – requires deep imaging observations;

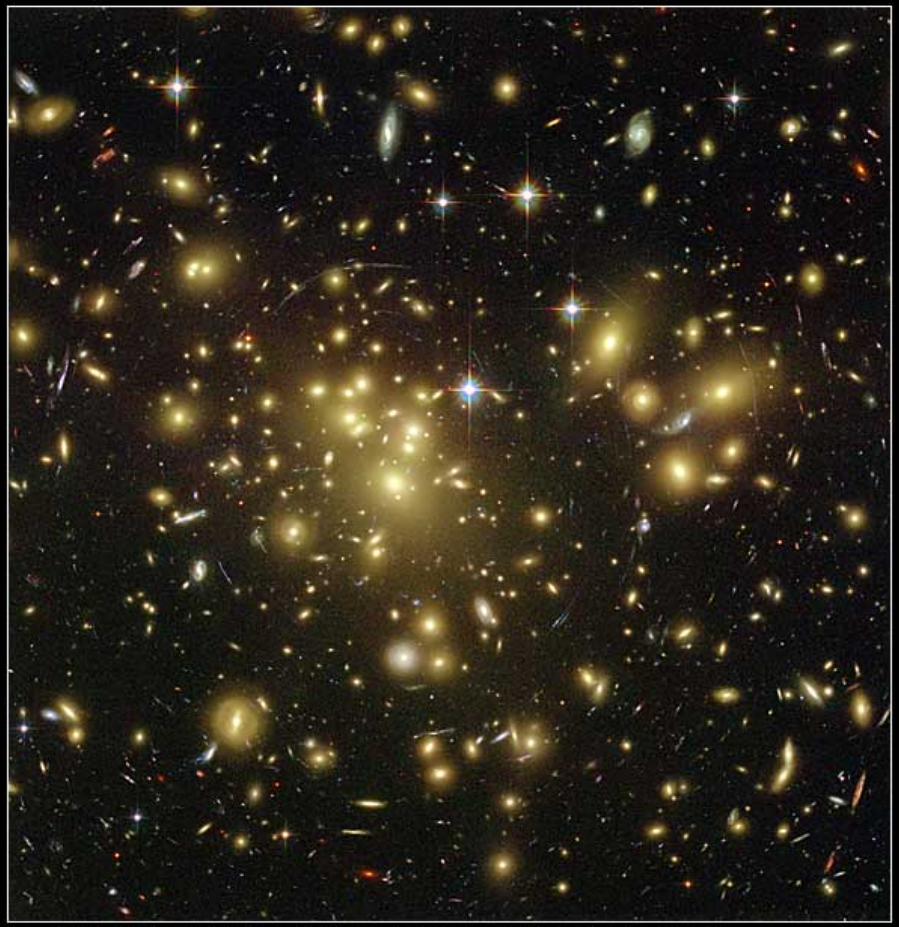

NASA, N. Benitez (JHU), T. Broadhurst (Hebrew Univ.), H. Ford (JHU),
M. Clampin(STScI), G. Hartig (STScI), G. Illingworth (UCO/Lick Observatory),
the ACS Science Team and ESA STScI-PRC03-01a

A massive cluster in front of the HUDF-population:

The current star amongst the strong lensing clusters,
observed with the ACS on-board HST,
full of arcs and multiple images,
everywhere ....

Galaxy Cluster Abell 1689 Details

Hubble Space Telescope • Advanced Camera for Surveys

NASA, N. Benitez (JHU), T. Broadhurst (The Hebrew University), H. Ford (JHU), M. Clampin (STScI), G. Hartig (STScI), G. Illingworth (UCO/Lick Observatory), the ACS Science Team and ESA • STScI PRC03-01b

Note that in the weak lensing regime, $\kappa \ll 1$, $|\gamma| \ll 1$, one finds

$$\gamma \approx g \approx \langle \epsilon \rangle \approx \frac{\langle \chi \rangle}{2} \, . \tag{18}$$

This regime is of prime interest in most weak lensing applications;

only close to strong lenses (like clusters) this 'weak weak lensing' regime no longer holds.

Note: Expectation value of χ depends on the intrinsic ellipticity p.d.f.

Tangential and cross component of shear

The shear components γ_1, γ_2 are defined relative to a reference Cartesian coordinate frame;

often it is useful to measure them w.r.t. a different direction – cf. arcs in clusters, tangentially aligned.

One then wants to measure shear with respect to a certain direction (here: the center of the cluster);

cf.: measuring vector components in rotated reference frames

If ϕ specifies a direction, one defines the *tangential* and *cross components* of the shear relative to this direction as

$$\gamma_{\rm t} = -\mathcal{R}{\rm e}\left[\gamma\,{\rm e}^{-2{\rm i}\phi}\right] \quad , \quad \gamma_\times = -\mathcal{I}{\rm m}\left[\gamma\,{\rm e}^{-2{\rm i}\phi}\right] \;; \tag{19}$$

For example, in case of a circularly-symmetric matter distribution, shear at any point will be oriented tangent to the direction towards the center of symmetry;

thus in this case choose ϕ to be the polar angle of a point; then, $\gamma_\times = 0$.

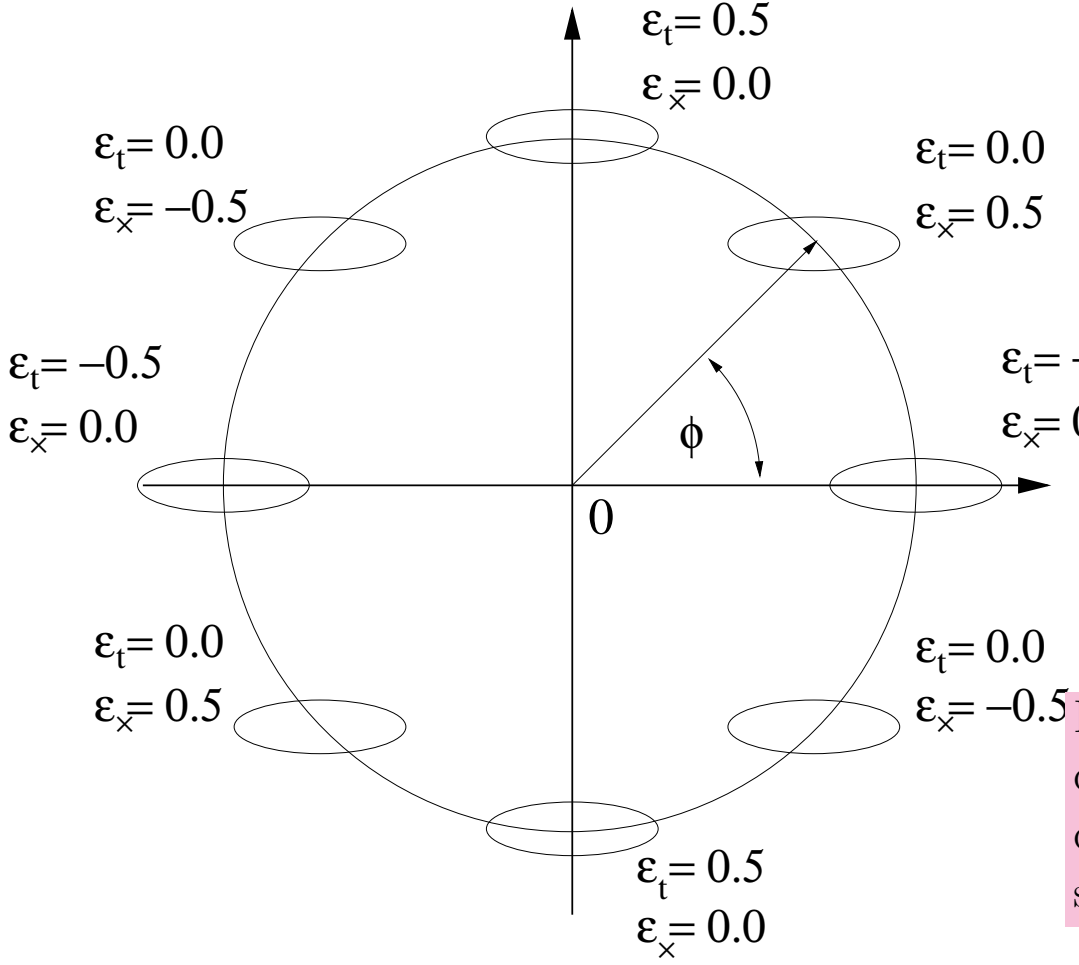

Illustration of the concept of tangential and cross components of shear (or ellipticity)

Magnification effects

Magnification changes apparent brightness of sources; there are two effects:

- the flux from a source is changed according to $S = \mu\, S_0$; if $\mu > 1$, sources appear brighter;
- a population of sources in the unlensed solid angle ω_0 is spread over the solid angle $\omega = \mu\omega_0$ due to magnification.

These two effects affect the number counts of sources differently; which one wins depends on the slope of the number counts.

$$n(>S, z) = \frac{1}{\mu(\boldsymbol{\theta}, z)}\, n_0\left(> \frac{S}{\mu(\boldsymbol{\theta}, z)}, z\right) \ . \tag{20}$$

$n(>S, z)$, $n_0(>S, z)$: lensed and unlensed cumulative number counts of sources.

Illustrative example:

If source counts follow a power law,

$$n_0(> S) = a\, S^{-\alpha} \ , \tag{21}$$

one finds for the lensed counts in a region of the sky with magnification μ:

$$\frac{n(> S)}{n_0(> S)} = \mu^{\alpha - 1} \ . \tag{22}$$

Hence, if $\alpha > 1$ (< 1), source counts are enhanced (depleted);
the steeper the counts, the stronger the effect.

E.g., QSO number counts are steep at bright end, flat at faint end;
in regions of magnification > 1, bright QSO should be overdense, faint ones underdense.

This *magnification bias* is the reason why fraction of lensed sources *much* higher in bright QSO sample than in fainter ones!

Magnification in weak lensing

Provided $\kappa \ll 1$, $|\gamma| \ll 1$, then

$$\mu \approx 1 + 2\kappa \; ; \quad \text{and} \quad \frac{n(>S)}{n_0(>S)} \approx 1 + 2(\alpha - 1)\kappa \; . \tag{23}$$

Thus, from measurement of local number density $n(>S)$, κ can be inferred directly;

for galaxies in B-band, $\alpha \sim 1$, but in redder bands, $\alpha < 1 \;\Rightarrow$ depletion expected for them.

Further effect: $\mu > 1$ causes galaxies with same surface brightness to be larger than unlensed galaxies;

in addition, surface brightness of galaxies strong function of redshift [Tolman effect, $I \propto (1+z)^{-4}$]

However: Magnification effect in weak lensing difficult to measure due to required calibration accuracy.

Minimum lens strength for its weak lensing detection

Consider a lens modeled as a singular isothermal sphere (SIS) with σ_v, where

$$\rho(r) = \frac{\sigma_v^2}{2\pi G r^2} \; ; \tag{24}$$

density distribution of a self-gravitating sphere where velocity distribution of particles is isotropic and independent of radius;

it is a Maxwellian with one-dimensional velocity dispersion σ_v;

three-dimensional velocity dispersion is $\sqrt{3}\sigma_v$;

Einstein radius of this lens model is

$$\theta_{\rm E} = 4\pi \left(\frac{\sigma_v}{c}\right)^2 \frac{D_{\rm ds}}{D_{\rm s}} \; , \tag{25}$$

in terms of which one obtains

$$\kappa(\theta) = \frac{\theta_{\rm E}}{2|\theta|} \; ; \quad \bar{\kappa}(\theta) = \frac{\theta_{\rm E}}{|\theta|} \; ; \quad |\gamma|(\theta) = \frac{\theta_{\rm E}}{2|\theta|} \; ; \quad \alpha(\theta) = \theta_{\rm E} \frac{\theta}{|\theta|} \; . \tag{26}$$

Assume shape measurements in the annulus $\theta_{\rm in} \leq \theta \leq \theta_{\rm out}$, with galaxy number density n. One finds for the S/N of the shear measurement:

$$\begin{aligned} \frac{\rm S}{\rm N} &= \frac{\theta_{\rm E}}{\sigma_\epsilon} \sqrt{\pi n} \sqrt{\ln(\theta_{\rm out}/\theta_{\rm in})} \qquad (27) \\ &= 8.4 \left(\frac{n}{30\,{\rm arcmin}^{-2}}\right)^{1/2} \left(\frac{\sigma_\epsilon}{0.3}\right)^{-1} \left(\frac{\sigma_v}{600\,{\rm km\,s}^{-1}}\right)^2 \\ &\times \qquad \left(\frac{\ln(\theta_{\rm out}/\theta_{\rm in})}{\ln 10}\right)^{1/2} \left\langle \frac{D_{\rm ds}}{D_{\rm s}} \right\rangle \, . \end{aligned}$$

Conclusion:

- Clusters of galaxies ($\sigma_v \gtrsim 600\,{\rm km/s}$) can be detected from weak lensing;
- individual galaxies ($\sigma_v \sim 200\,{\rm km/s}$) too weak to be detected individually

As we shall see, weak lensing by galaxies can be detected (and measured with very high accuracy) from statistical samples of galaxies;

$\Rightarrow$ Galaxy-galaxy lensing

Observational issues and challenges

Weak lensing relies on the shape measurements of faint galaxy images.

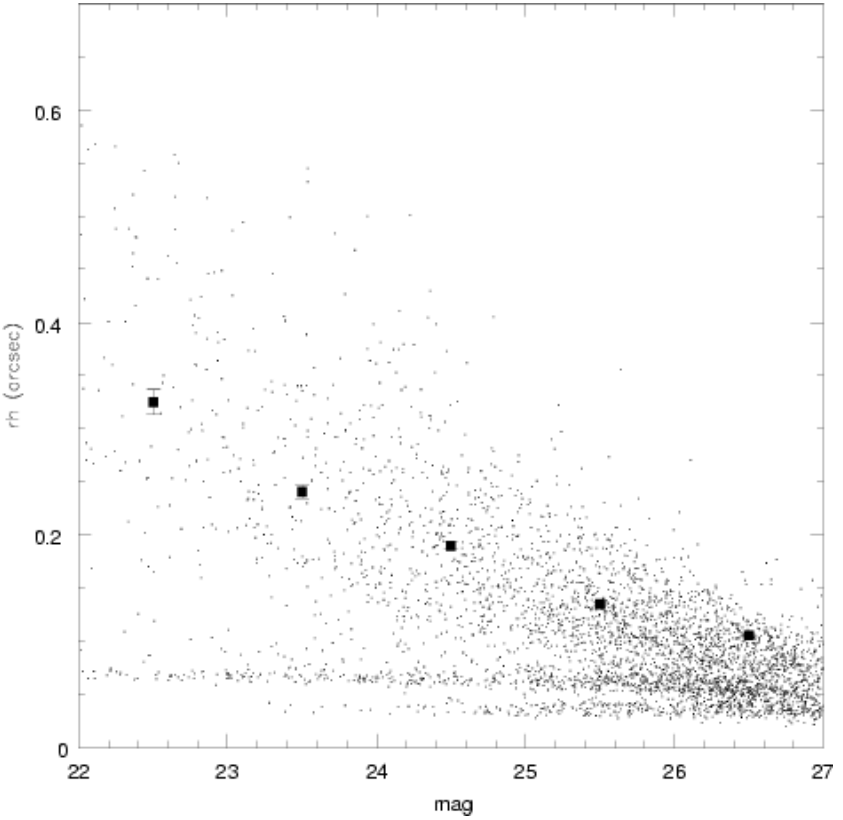

Noise due to intrinsic ellipticity dispersion $\propto \sigma_\epsilon/\sqrt{n}$

$\Rightarrow$ one needs high number density n to beat this noise down.

Larger $n \Rightarrow$ fainter magnitudes $\Rightarrow$ smaller galaxies.

Note that typical size $\ll$ seeing disk!

Fainter galaxies tend to probe higher-redshift galaxies, increases lensing signal due to $D_{\rm ds}/D_{\rm s}$-dependence.

Strategy

Presently, only the optical sky is densely populated with sources;

therefore, weak lensing observations are performed with optical CCD-cameras

N.B.: photometric plates not linear enough to measure these subtle effects – first attempts to detect weak lensing effects have failed due to this non-linearity and the inability to correct for PSF effects

to obtain high number density, long exposures are needed:

to get a number density of $n \sim 20\,\mathrm{arcmin}^{-2}$, one needs $\sim 2\,\mathrm{hours}$ integration on a 4-m class telescope in good seeing $\sigma \lesssim 0.8''$.

Large solid angles are desired, either

- to get large areas around clusters for their mass reconstruction, or
- to get good statistics of lenses on blank field surveys (galaxy-galaxy lensing, cosmic shear)

Large format CCD cameras are needed;

e.g., MegaCam@CFTH has $(18\mathrm{K})^2$ and covers 1 sq.deg;

OmegaCAM@VST has $(16\mathrm{K})^2$ and covers 1 sq.deg.

DES and PanSTARRS-1 even larger cameras.

Note: pixel size of these cameras $\sim 0\farcs2$, needed to sample the seeing disk in times of good seeing.

It is now possible to cover large area in reasonable amounts of observing time.

Data rate: one night of observing with OmegaCAM yields $> 100\,\mathrm{GB}$ of science and calibration data.

Data reduction requires large disk space!

Data reduction

Individual frames

- CCD pixels have different sensitivity
  $\Rightarrow$ **flatfielding**, to calibrate this;
  - dome-flat: a uniformly illuminated screen in the telescope dome is exposed; the counts in the pixels are then proportional to their sensitivity;
    Problem: the screen is not really of uniform brightness
  - twilight-flat: in the period of twilight after sunset, or before sunrise, the cloudless sky is nearly uniformly bright;
    short exposures of regions of the sky without bright stars are then used to calibrate the pixel sensitivity

– superflat: if many exposures with different pointings are taken with a camera during a night, then any given pixel is not covered by a source for most of the exposures (because the fraction of the sky at high galactic latitudes which is covered by objects is fairly small, as demonstrated by the deep fields taken by the HST);
hence, (exposure-time normalized) counts of any pixel will show, in addition to a little tail due to those exposures when a source has covered it, a distribution around its sensitivity to the uniform night-sky brightness; flat-field given by median of this distribution

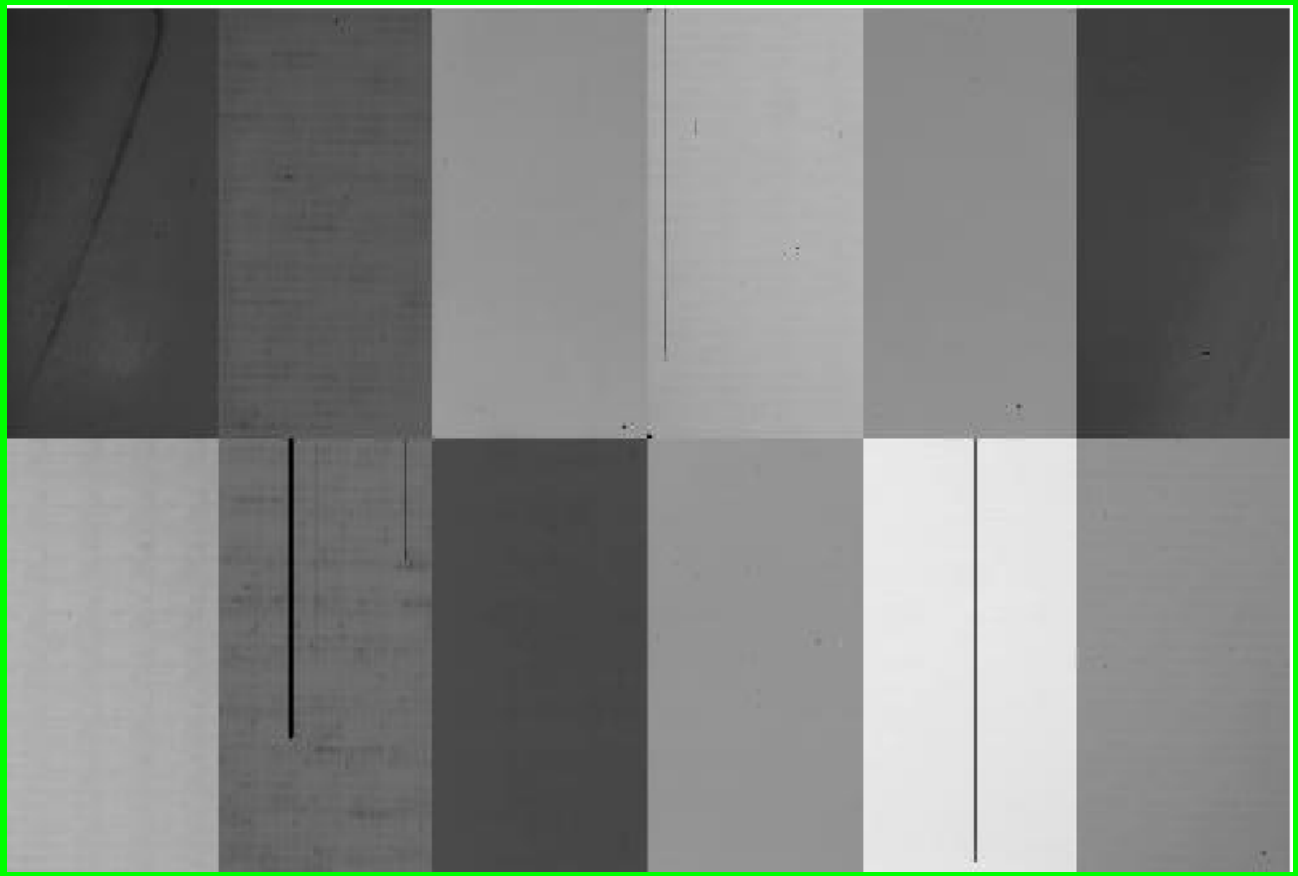

A flat field for the CFH12K camera, showing the sensitivity variations between pixels and in particular between chips. Also, bad columns are clearly seen

- bad pixels: each CCD has defects; some pixels are dead or show a signal unrelated to their illumination
  this can occur as individual pixels, or whole pixel columns
  no information available at these positions
  $\Rightarrow$ dithering, take several exposures of the same field with slightly different pointing;

- cosmic rays: mimic groups of bad pixels
  $\Rightarrow$ take several exposures, identify them (they do not repeat, and are smaller than the seeing disk), and mask them;
  also: width of its track is typically much smaller than the seeing disk, the minimum size of any real source;

- bright stars: cause large diffraction spikes, reflection rings, etc.
  $\Rightarrow$ try to avoid them, otherwise mask them;

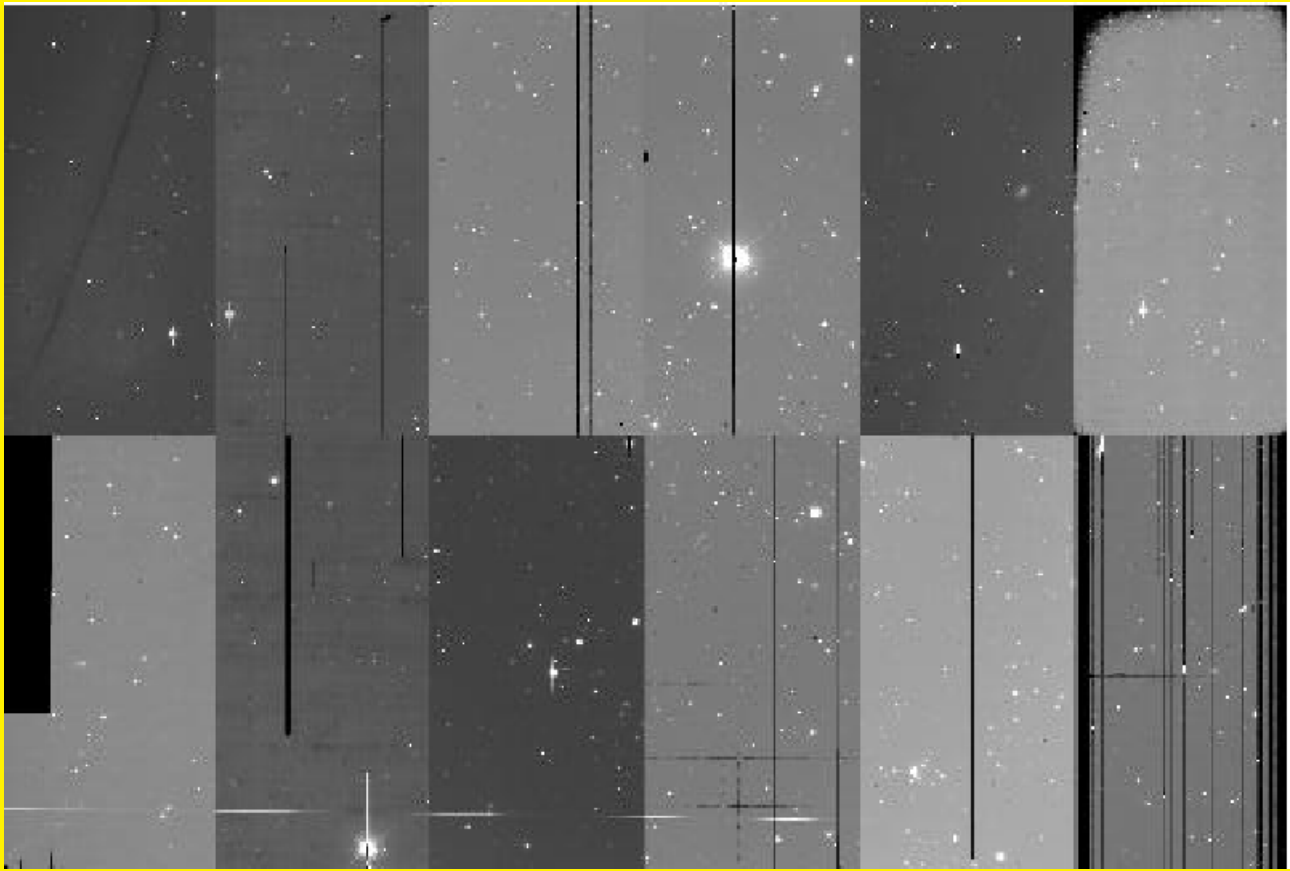

Raw frame from the CFH12K camera, showing: bad column, saturation of bright stars, bleeding, and sensitivity variations across the field

- fringes: pattern occurring due to reflection within the CCD (problem occurs at longer wavelengths in thinned CCDs)
  $\Rightarrow$ in clear nights, fringe pattern stable; then, model for it can be constructed and subtracted; otherwise, observe at shorter wavelengths ...

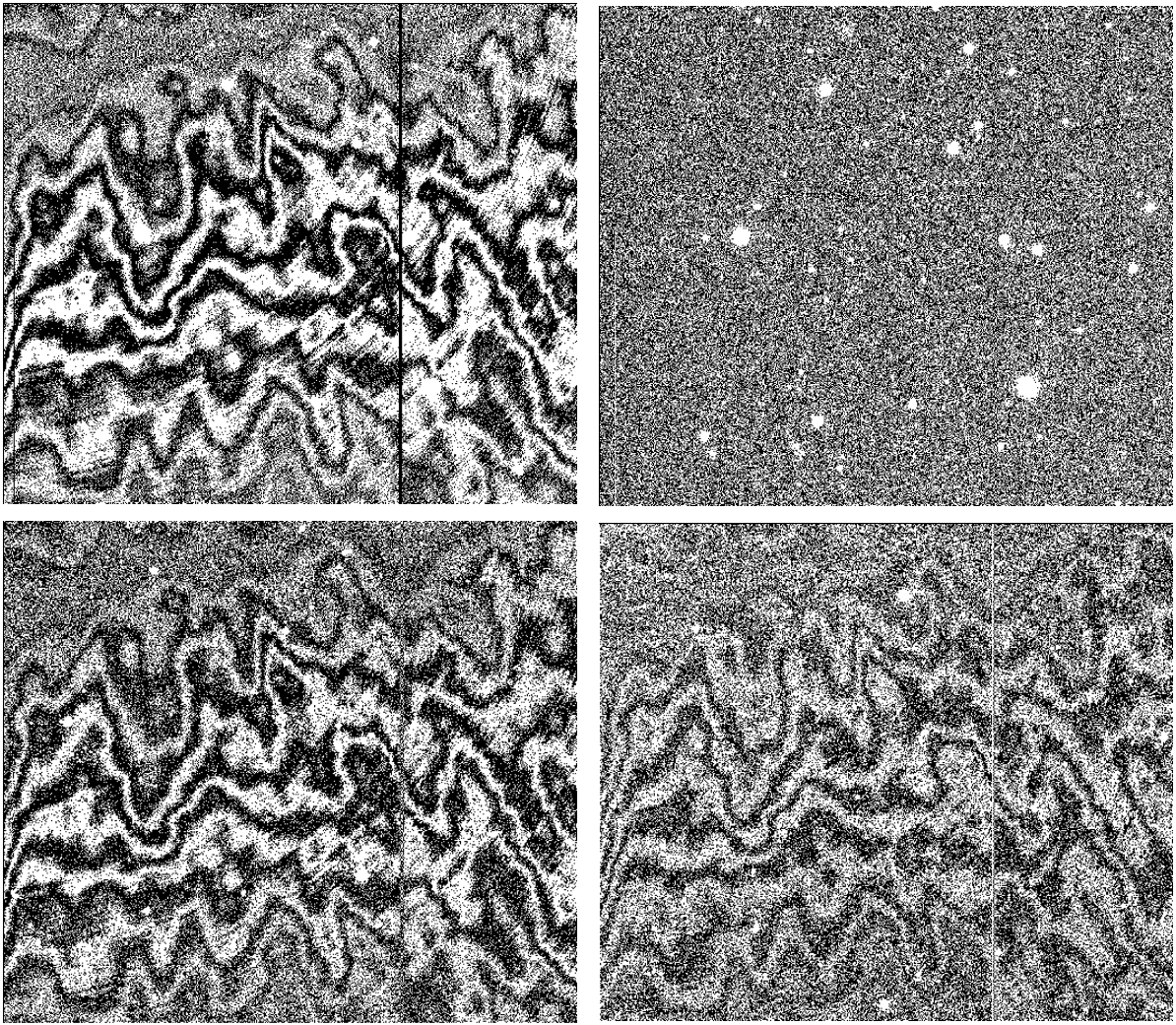

- gaps between chips in multi-CCD cameras
  $\Rightarrow$ use dithering to cover the gaps, if needed

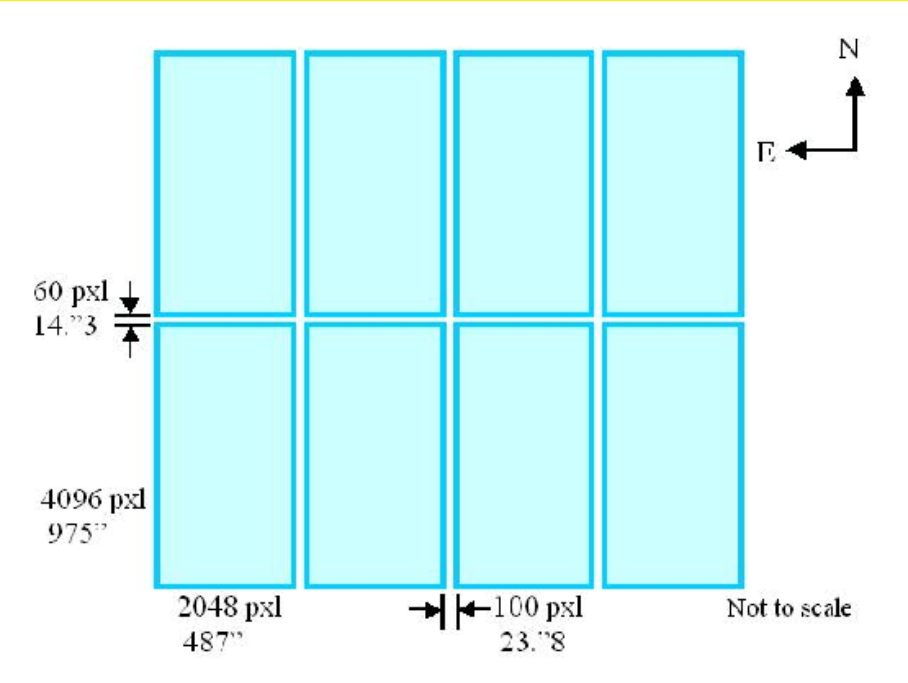

- satellite trail, asteroid trails
  $\Rightarrow$ identify and mask (masking currently often 'by hand'; software solution needed)

Coaddition

After taking several exposures with slightly offset positions (reasons given above), frames shall be coadded to sum-frame;
major steps here are:

- Astrometric solution: one needs a very precise mapping from sky coordinates to pixel coordinates;
  field distortions make this mapping non-linear;
  mapping sky $\rightarrow$ CCD pixels has to be obtained from data itself;
  external reference catalog: USNO, contains ~ 2 point sources per arcmin^2 (at large $|b|$) with 0.3 arcsec positional accuracy, or 2MASS;
  internal astrometry: sky coordinates constant, pixel coordinates change between dithering positions $\Rightarrow$ same objects on different exposures constrain the distortion map with much higher relative accuracy than external data.
  Astrometric solution takes these constraints; can achieve routinely accuracy of 0.1 pixel.

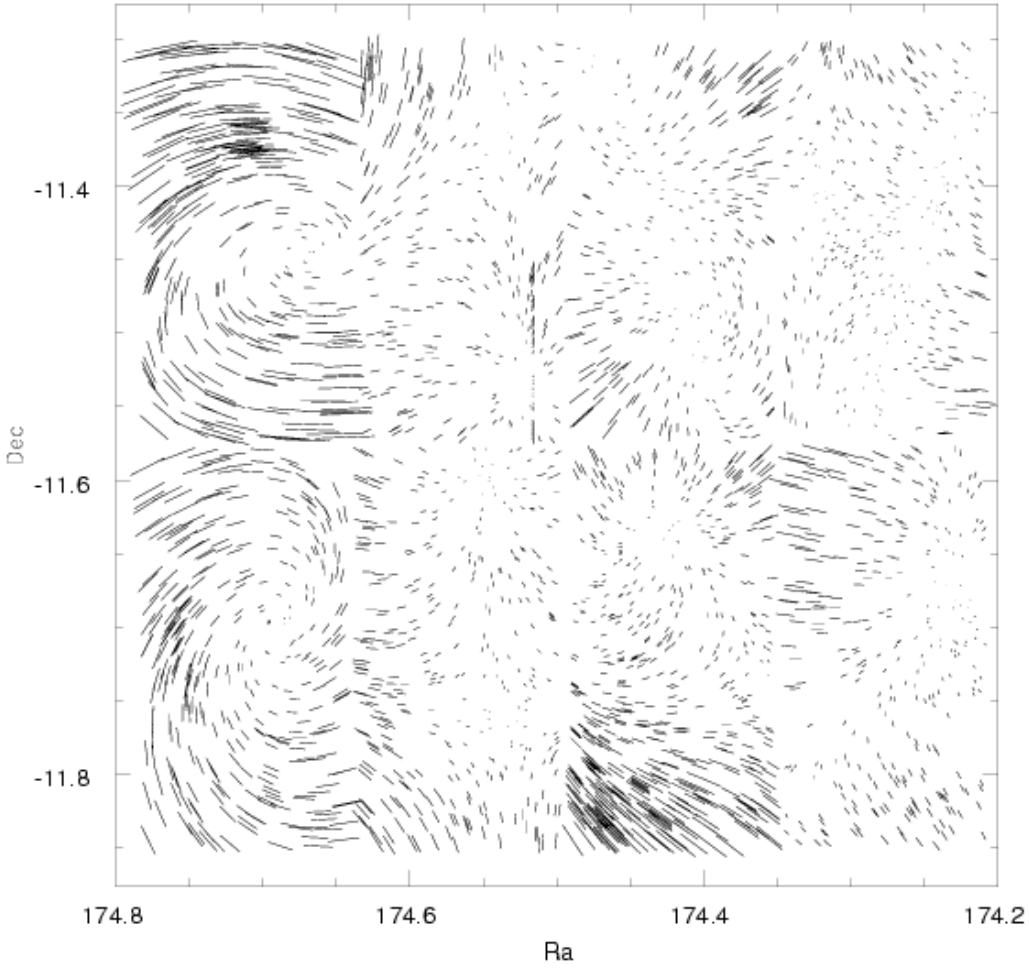

Geometric distortion of the WFI.
Difference of positions of stars as obtained from a simple translation, and a third-order astrometric correction obtained in the process of image reduction.
Maximum length of the sticks corresponds to about 6 pixels, or 1.″2

- Photometric solution: flatfielding yields accurate relative photometry across exposures;
  different exposures are tied together by brightness of joint objects, in particular across chip boundaries;
  absolute photometric calibration needs external data (e.g., standard star observations)

- Coaddition has to happen with sub-pixel accuracy: standard method is drizzling:
  new pixel frame is defined, onto which individual exposures are remapped, according to the overlap area between exposure pixel and drizzle pixel;
  coaddition onto the drizzle pixels, accounting for the noise properties of individual exposures (including masks, of course)

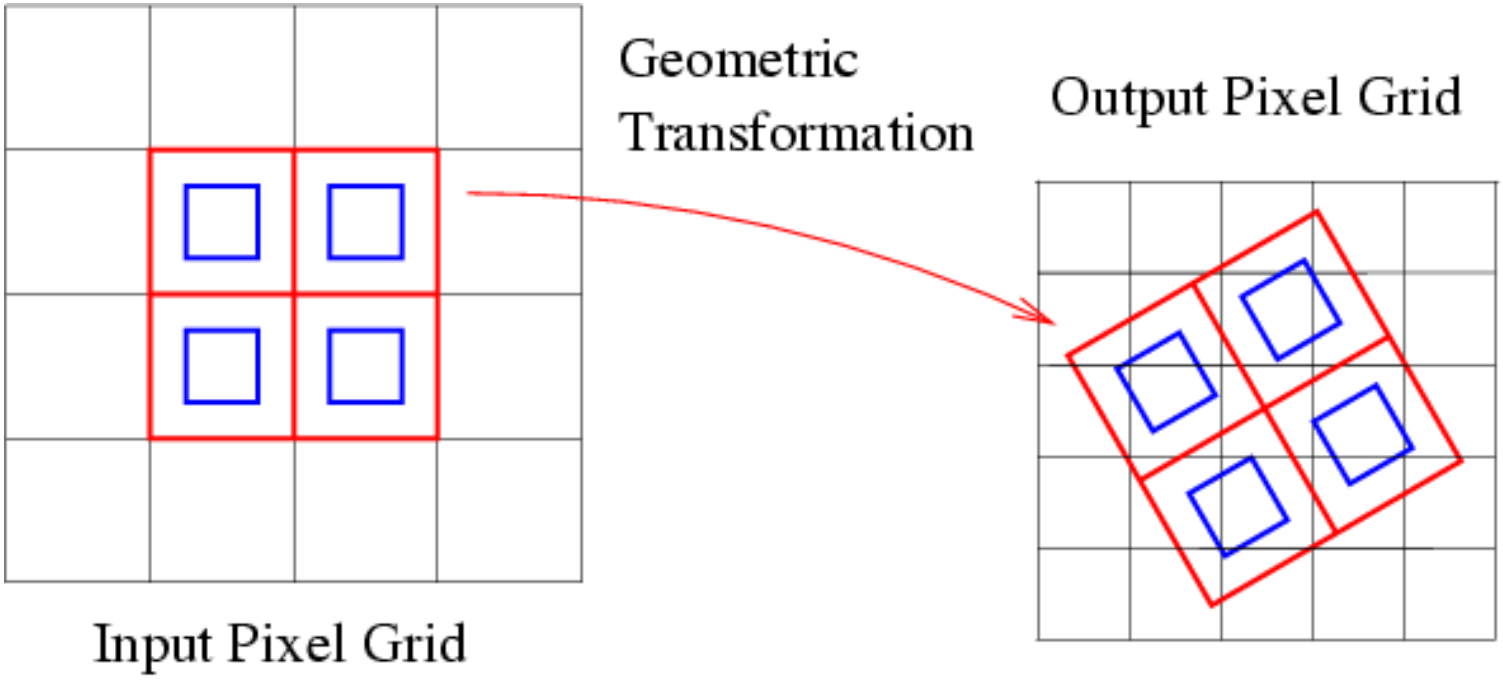

Principle of drizzling in the process of coaddition

Result of coaddition: science frame, plus a weight map (which contains information on pixel noise – spatially varying, owing to masks, CCD gaps, bad pixel, etc.)

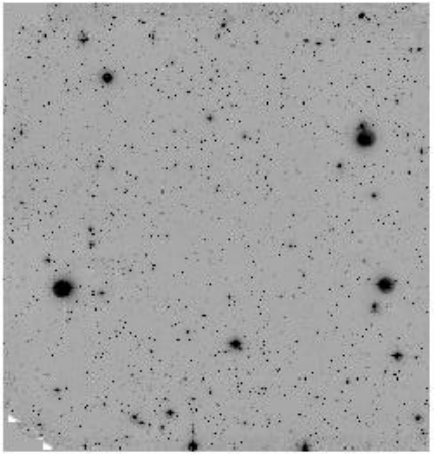

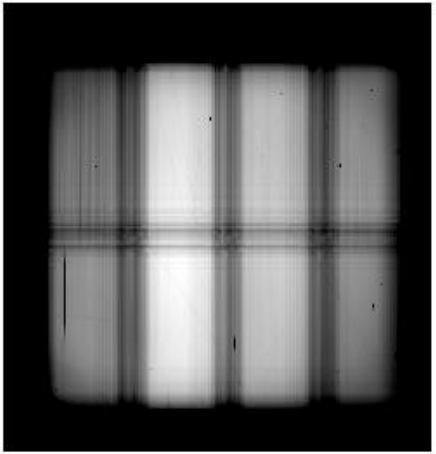

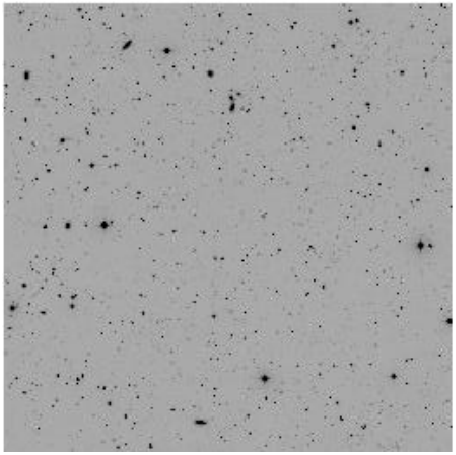

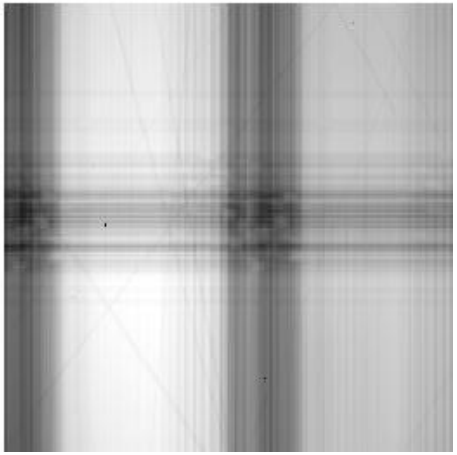

Image analysis

Major steps here include

- Identification of sources; this is done with by-now standard software, like SExtractor;
  identfies regions where n connected pixels are x-σ above the noise;
  problems: overlapping sources, splitting one source into several components;
- measuring the shape of the sources (the 'theorists way' doesn't exactly work);
- account for the convolution with the point-spread function (PSF);
- obtain shear estimates.

Special image analysis tools have been developed for weak lensing.

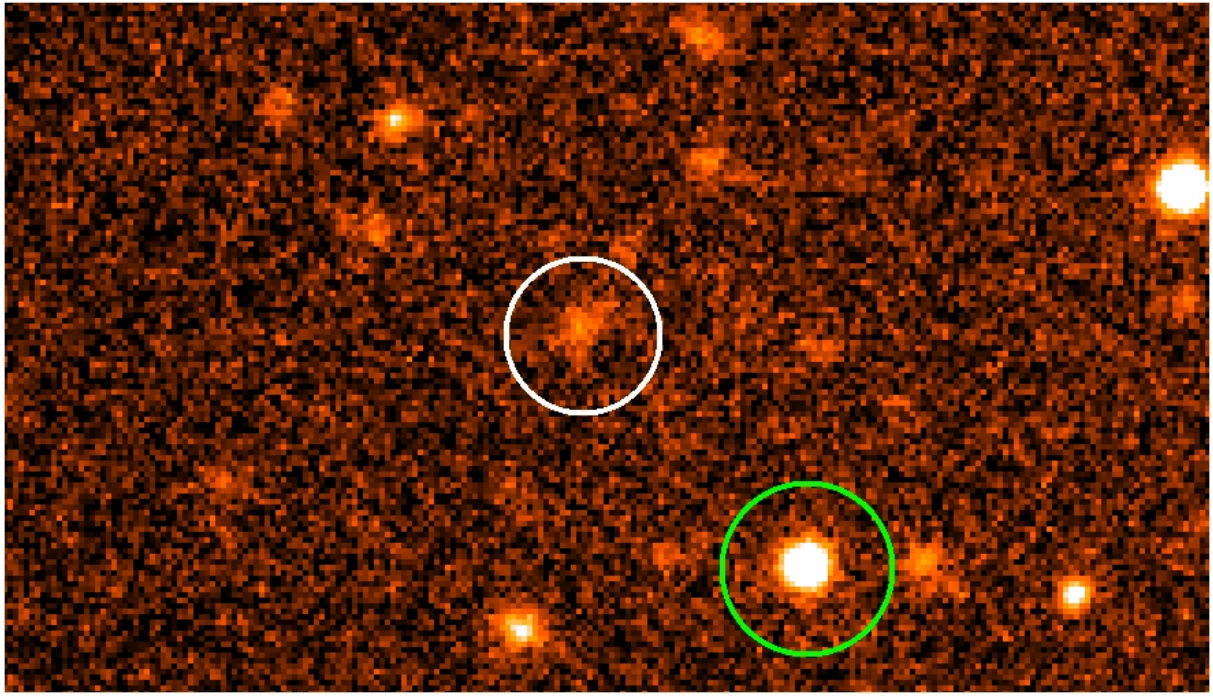

Green: star, used to measure the PSF

White: typical galaxy which is used for the shear analysis

These galaxies are faint, noisy and not remotely ellipses!

The point-spread function

Atmospheric turbulence smears images,

$$I^{\rm obs}(\boldsymbol{\theta}) = \int {\rm d}^2\vartheta \; I(\boldsymbol{\vartheta})\, P(\boldsymbol{\theta} - \boldsymbol{\vartheta}) \; ; \tag{28}$$

at excellent sites, and excellent telescopes, seeing (i.e., FWHM of PSF) has median of $\sim 0\farcs7$–$\sim 0\farcs8$;

recall: typical faint galaxies considerably smaller than this!

Effects of PSF:

- Smearing: the PSF makes elliptical images rounder;
- an anisotropic part of the PSF introduces image ellipticities, mimicing a shear.

PSF anisotropies due to tracking error, wind shake, image coaddition;
the image coaddition has to be done with $\sim 1/10$ pixel accuracy, to not introduce artificial PSF anisotropies in coadded image.

PSF anisotropy of several percents typical; if not corrected for, effect can be larger than the shear to be measured;

smearing by the PSF reduces ellipticity, if not corrected for, too low shear values would be obtained;

effects of the PSF (convolution) depends on the size of galaxy images: bigger ones are less affected than smaller ones.

The PSF can be measured at the position of stars (point sources);
if PSF smooth function of position, it can be interpolated between stellar images (or fitted by a low-order polynomial);

Potential problem: if PSF jumps between chips in multi-chip cameras, then coaddition produces PSF jumps on coadded frame (not a problem for WFI)!

Another problem: pixelization!

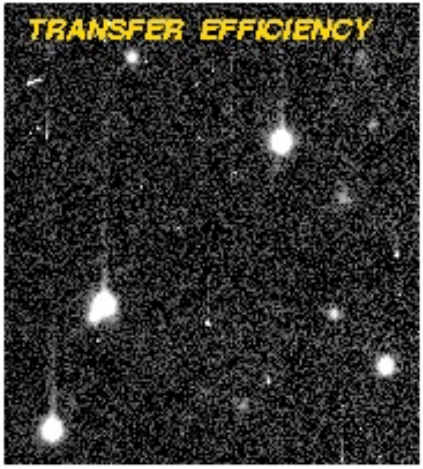

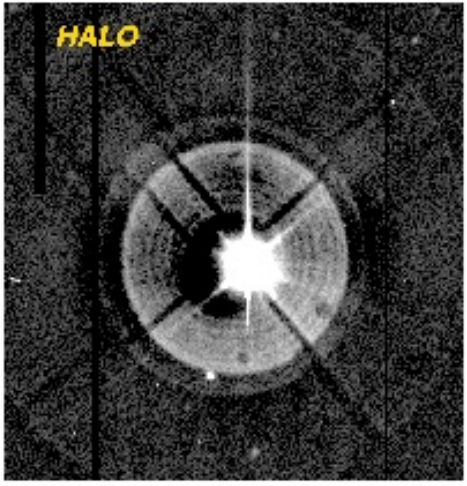

Reality is not always a nice place to be ...

The KSB scheme

Specific software developed to deal with these issues; most in use:
K(aiser)S(quires)B(roadhurst) method, or its implementation IMCAT.

Outline is as follows:

- Measure second brightness moments; the theorist's definition

$$Q_{ij} = \frac{\int \mathrm{d}^2\theta \, q_I[I(\boldsymbol{\theta})] \, I \, (\theta_i - \bar{\theta}_i) \, (\theta_j - \bar{\theta}_j)}{\int \mathrm{d}^2\theta \, q_I[I(\boldsymbol{\theta})] \, I} \, , \quad i,j \in \{1,2\}$$

  is impractical, as the weight function depends on the noisy surface brightness I, also because galaxy images are not isolated; therefore one uses

$$Q_{ij} = \frac{\int \mathrm{d}^2\theta \, w(\boldsymbol{\theta} - \bar{\boldsymbol{\theta}}) \, I(\boldsymbol{\theta}) \, (\theta_i - \bar{\theta}_i) \, (\theta_j - \bar{\theta}_j)}{\int \mathrm{d}^2\theta \, w(\boldsymbol{\theta} - \bar{\boldsymbol{\theta}}) \, I(\boldsymbol{\theta})} \, , \quad i,j \in \{1,2\} \, ;$$

  where size of weight function w is adapted to size of galaxy image (for optimal S/N measurement);

With this definition, transformation between image and source brightness moments no longer simple!

- Use stars on image, measure their PSF anisotropy, characterized by its (complex) ellipticity q, and fit a low-order polynomial to this PSF
  $\Rightarrow$ this yields an estimate of q at all galaxy positions.

- Assume that shear and PSF anisotropy are small; then they both will have a small effect on measured ellipticity;
  linearize these effects and write

$$\boxed{\chi_\alpha^{\rm obs} = \hat{\chi}_\alpha^0 + P_{\alpha\beta}^{\rm sm} q_\beta + P_{\alpha\beta}^{g} g_\beta}\,, \quad \text{where} \tag{29}$$

  $\hat{\chi}^0$: ellipticity of source convolved with the isotropic part of the PSF; i.e., ellipticity measured in the absence of shear and PSF anisotropy;
  important to note that $\mathrm{E}(\hat{\chi}^0) = 0$, due to random orientation of sources;
  $P_{\alpha\beta}^{\rm sm}$: tensor which describes the response of the image ellipticity to the PSF anisotropy;
  $P_{\alpha\beta}^{g}$: tensor which describes the response of the image ellipticity to an applied shear.

- Both, $P^{\rm sm}_{\alpha\beta}$ and $P^{g}_{\alpha\beta}$ are calculated for each image individually;
  they depend on higher-order moments of the brightness distribution and the size of the PSF.

- Given that $\left\langle \chi^0 \right\rangle = 0$, an estimate of the (reduced) shear is provided by

$$\epsilon = (P^g)^{-1} \left(\hat{\chi}^{\rm obs} - P^{\rm sm} q \right) \ . \tag{30}$$

  If image size much smaller than PSF, $|P^g|$ can be very small, i.e., correction factor in (30) can be very large;
  large multiplication factor also for the image noise!
  If this factor is too large, better discard source, or strongly downweight.

KSB works:
Detailed simulations have shown that KSB method can measure shear with better than $\sim 5\%$ accuracy, provided optimized weighting (by S/N) of image ellipticities is adopted.

CORRECTION OF PSF ANISOTROPY FROM STARS

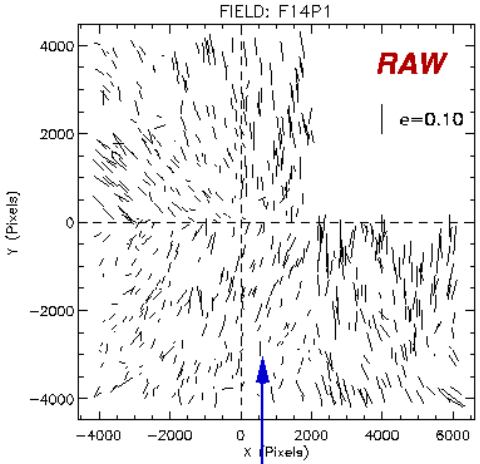

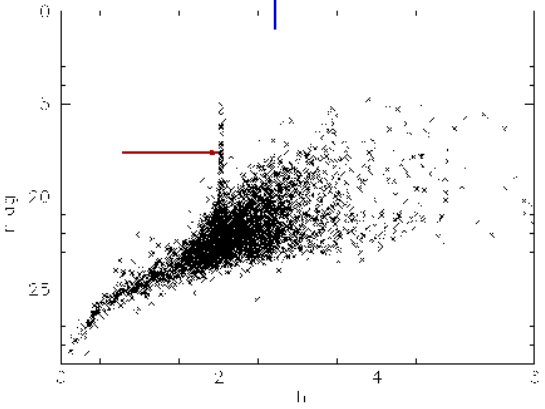

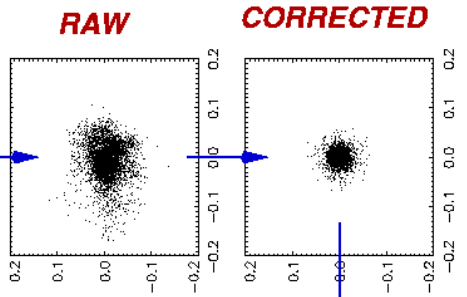

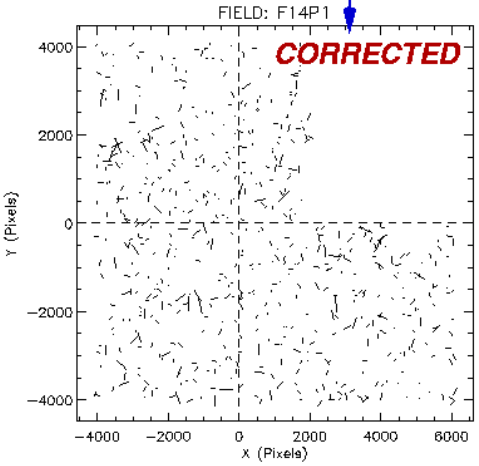

Alternative methods

Several different schemes for measuring shear have been developed, amongst them:

- shapelets: brightness profile of galaxy images and stars (PSF) described by a complete set of functions (shapelets);
  coefficients of these function for the PSF approximated as polynomial across field
- Lensfit: Bayesian approach to shape measurements
- Elliptical weight functions $w(\boldsymbol{\theta})$, fitted to image brightness
- one can construct simple kernel function K such that the convolution $K * P$ is round;
  has to be done locally, since PSF varies.

Several world-wide projects (STEP, GREAT08, GREAT10) for method comparison in blind tests have shown that shape measurements can be done to $\sim 2\%$ accuracy.

Shear observations from space

- A telecope in space is not bothered by atmosphere;
  should be ideal for shear measurements;
- weak lensing observations done by HST; PSF much smaller (diffraction limited, therefore also 'uglier'); pixel size smaller
- main problem of HST: FOV small, too few stars on image for accurate PSF measurement – time-stabiltity needs to be assumed (probably in principle OK, but breething ...) – mixed methods (PCA)
  CCD aging, CTE problems, cosmic rays plentyful!
- Powerful results obtained on clusters (where shear is $\sim$ 10%), but also for cosmic shear and galaxy-galaxy lensing.

Dark Matter in Clusters & Large-Scale Structure

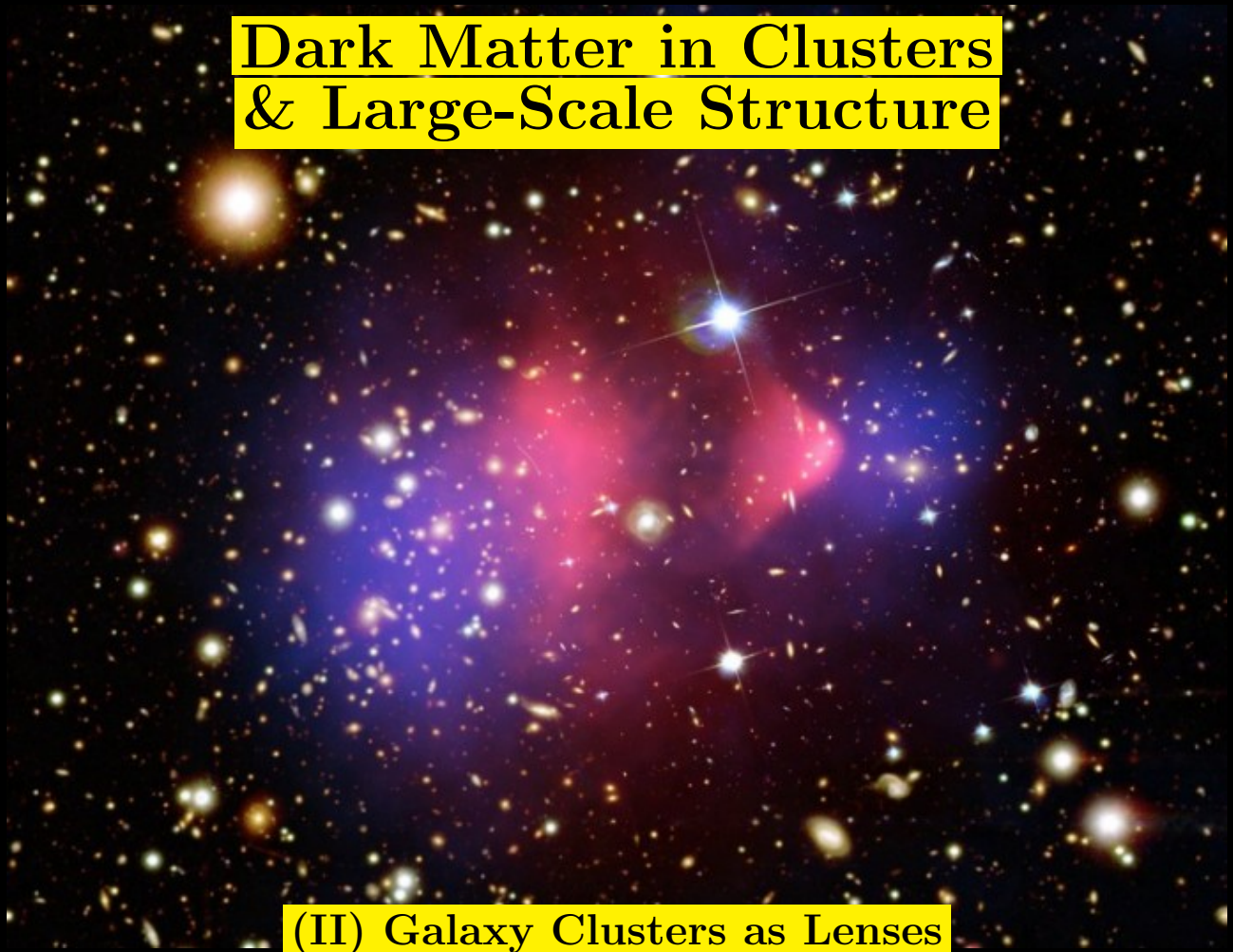

(II) Galaxy Clusters as Lenses

Properties of clusters of galaxies

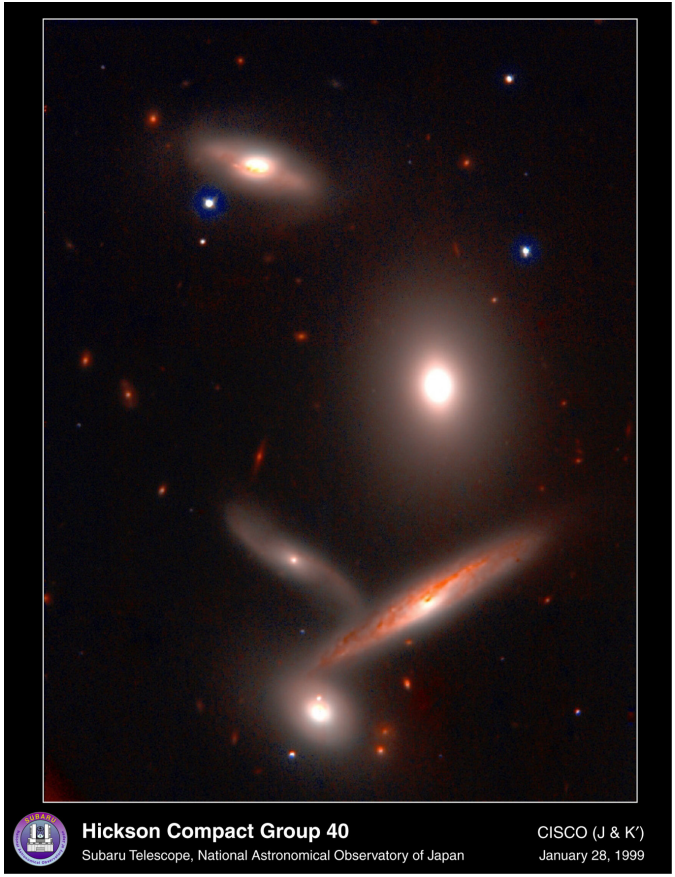

Introduction

Galaxies are not distributed randomly, but they cluster together;
regions of highest number density of galaxies are groups and clusters of galaxies;
first seen as overdensities projected on the sky;

our Milky Way is part of the Local Group (of which ~ 40 galaxies are known).

The compact group of galaxies HCG40

The Coma cluster, the nearest massive, regular cluster

General properties of clusters

- Clusters of galaxies contain tens to hundreds of bright galaxies;
- galaxy population dominated by early-type galaxies (E's and S0's);
- often a very massive cD galaxy at their center;
- wide range of morphology, from regular, compact clusters (often dominated by central cD galaxy) to bimodal distribution, or highly irregular morphology with strong substructure;
- X-ray and SZ-observations reveal the presence of a hot (several keV) intracluster medium (ICM);
- Mass balance: stars in cluster galaxies $\sim 3\%$, ICM $\sim 15\%$, rest ($\gtrsim 80\%$) is dark matter.

Hence, clusters are dominated by dark matter; mass determination done with three vastly different methods, as shown later.

Cosmological interest in clusters

- Clusters are most massive bound, virialized structures in the Universe;
- their structure is an important probe for cosmological models: hierarchical merging can be directly 'observed';
- Cold Dark Matter models predict 'universal' (NFW) density profile;
- their number density evolution probes the growth of the LSS: massive clusters are expected to be much rarer at high redshift;
- the abundance of clusters $n(M, z)$ probes the power spectrum of density fluctuations (in particular its normalization) and the cosmological growth function $D_+(z)$
  $\Rightarrow$ clusters therefore are a valuable cosmological tool

- baryon fraction in clusters believed to be the same as cosmological baryon fraction, $f_\mathrm{b} = \Omega_\mathrm{b}/\Omega_\mathrm{m}$;
  $f_\mathrm{b} \sim 0.15$ plus Ω_b from BBN $\Rightarrow \Omega_\mathrm{m} \sim 0.3$;
- they form signposts of the dark matter distribution in the Universe;
- act as laboratories for studying the evolution of galaxies and baryons in the Universe;
- Butcher–Oemler effect: fraction of blue galaxies in cluster larger at higher redshift $\Rightarrow$ clear sign of galaxy evolution in clusters;
- were the first objects where dark matter has been suspected (Zwicky 1933).

Strong lensing can probe mass distribution in inner part (within $\sim 2\theta_\mathrm{E}$), **weak lensing** at larger radii.

The mass of galaxy clusters

Three principal methods for determining the mass of galaxy clusters:

- from the motion of galaxies in clusters, assuming virial equilibrium, $2E_{\rm kin} + E_{\rm pot} = 0$;
- from the hot intra-cluster gas, visible in X-rays and SZ-effect, $\nabla P = -\rho_{\rm g}\,\nabla\Phi$;
- from gravitational lensing, weak and strong.

All three methods are complementary; lensing yields line-of-sight projected density of clusters, in contrast to other methods;

on the other hand, those rely on equilibrium (and symmetry) conditions; e.g., virial method on virial equilibrium (cluster is dynamically relaxed); anisotropy of orbit distribution.

Distant Galaxy Cluster
MS1054-0321

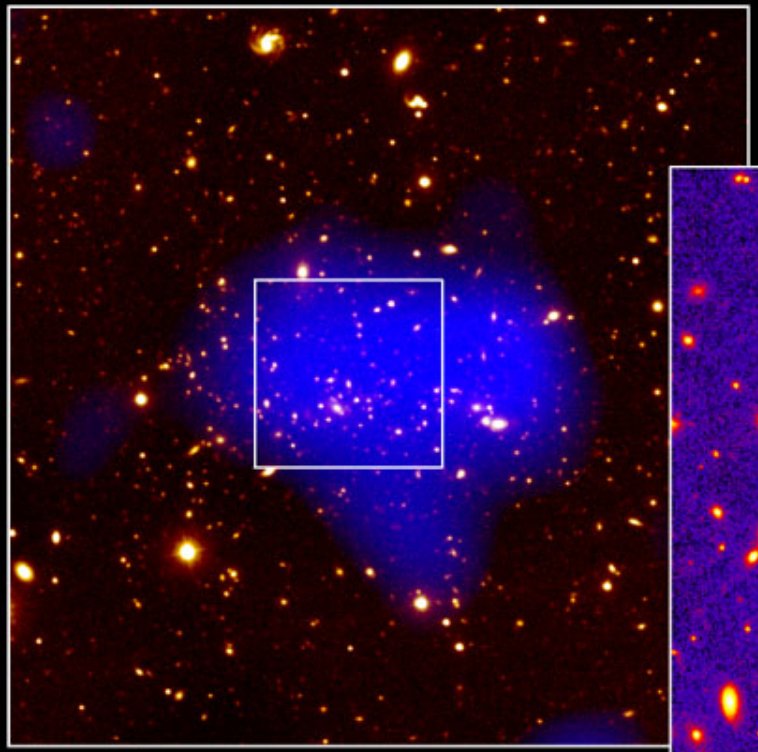

Ground + X-ray

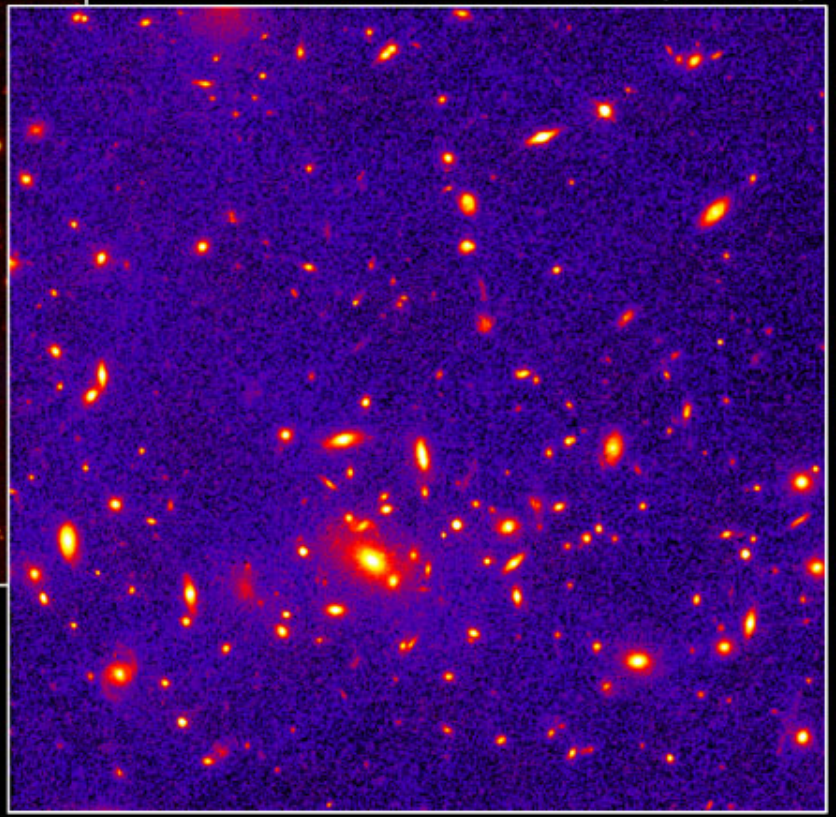

HST • WFPC2

PRC98-26 • August 19, 1998
STScI • OPO
M. Donahue (ST ScI) and NASA

Luminous arcs & multiple images

Luminous arcs & multiple images

- Giant arcs in clusters are highly distorted and magnified images of background galaxies;
- clusters thus act as 'natural telescope'; many of the most distant galaxies have been found behind clusters;
- arcs and multiple images probe inner mass distribution in clusters, within a few $\theta_{\rm E}$

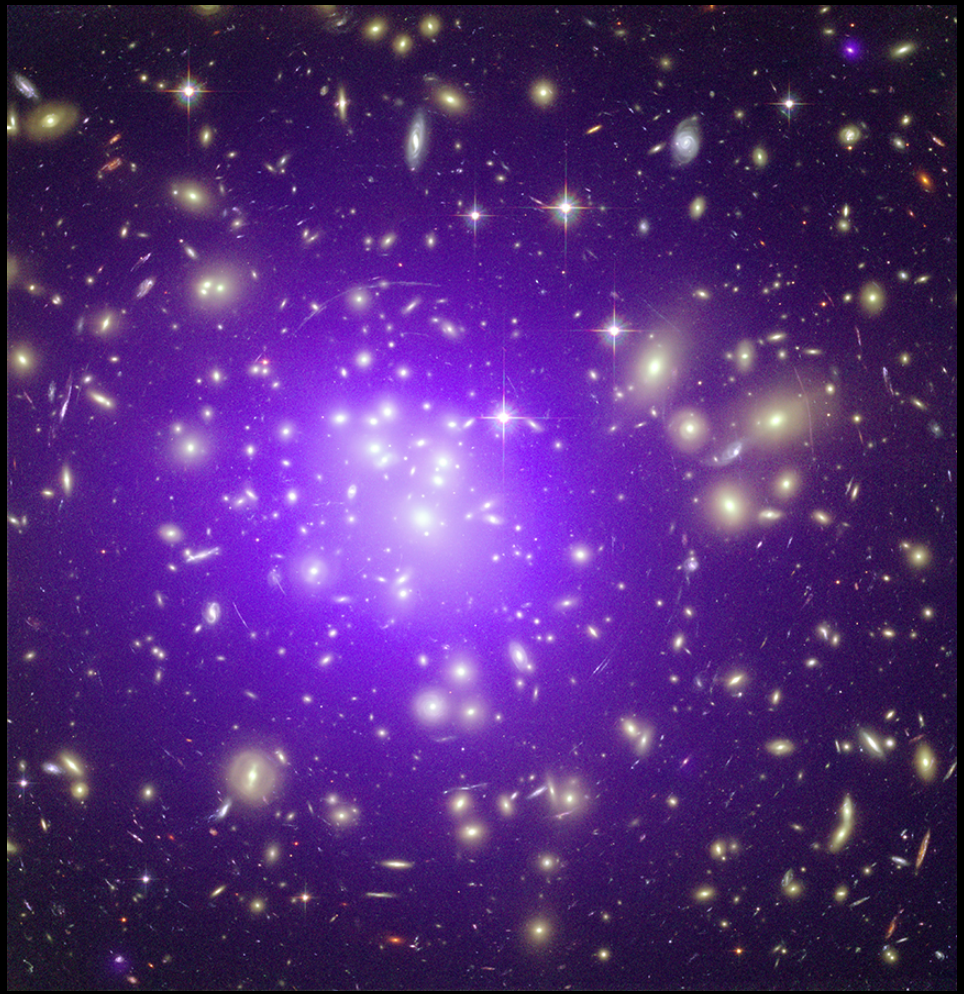

A1689, perhaps the strongest lensing cluster known, observed with the ACS onboard HST;

X-ray emission from Chandra superposed;

a huge number of arcs can be seen; a strong lensing analysis of this image has yet to be done, though;
A1689 also is a strong weak lensing cluster.

Galaxy Cluster Abell 1689 Details

Hubble Space Telescope • Advanced Camera for Surveys

NASA, N. Benitez (JHU), T. Broadhurst (The Hebrew University), H. Ford (JHU), M. Clampin (STScI), G. Hartig (STScI), G. Illingworth (UCO/Lick Observatory), the ACS Science Team and ESA • STScI PRC03-01b

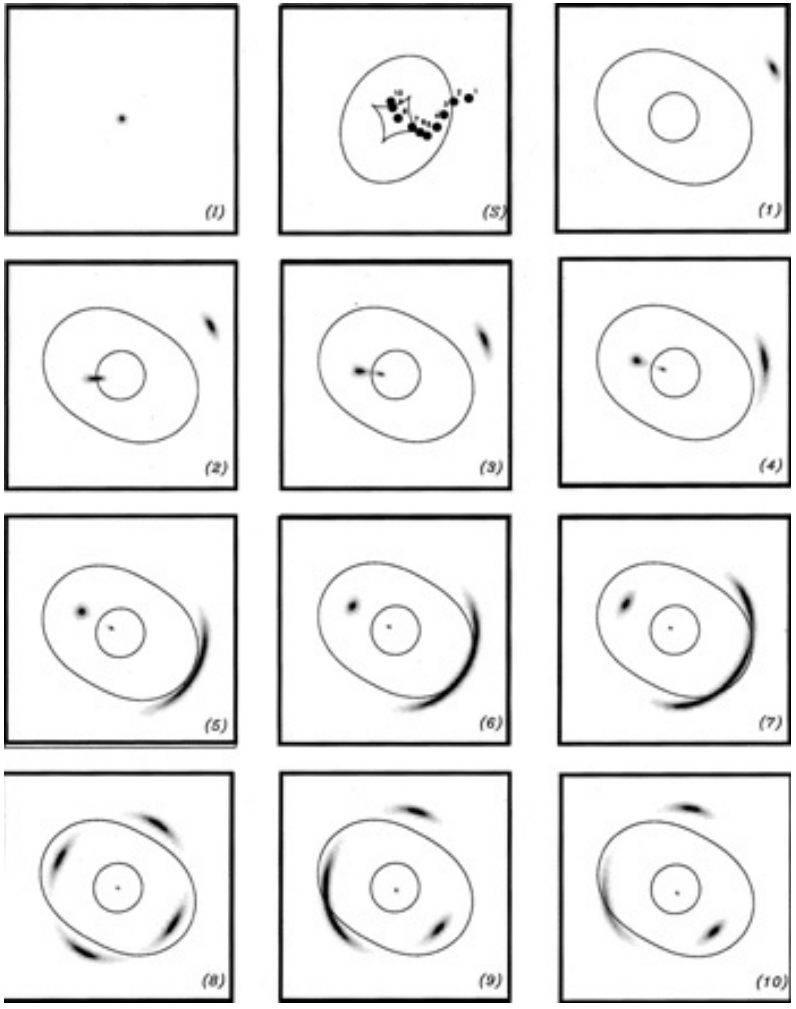

Geometries of arcs and multiple images as expected from an 'elliptical' lens;

essentially, all these configurations have been found in various clusters;
note: most prominent arcs occur near the major axis of the lens
note: radial arcs expected near inner (radial) critical curve, tangentially oriented arcs near outer (tangential) critical curve.

Fort & Mellier (1994)

First go: $M(\leq \theta_{\rm E})$

Giant arcs occur where distortion (and magnification) is very large;

to first approximation, assuming spherical mass distribution, location of arc from cluster center (BCG) yields Einstein radius of cluster;

therefore, assuming $\theta_{\rm arc} \approx \theta_{\rm E}$, it yields the mass inside the arc radius,

$$M(\theta_{\rm arc}) \approx \pi \, (D_{\rm d} \, \theta_{\rm arc})^2 \, \Sigma_{\rm cr} \; . \tag{31}$$

This estimate not very accurate, perhaps good to $\sim$ 40%; depends on level of asymmetry and substructure;

likely to overestimate masses, since arcs preferentially occur along major axis of clusters;

sometimes, center of cluster not readily identified!

Detailed modelling

If several arcs are present, and/or multiple images, detailed modelling can be done;

proceeds in interactive way: first, multiple images have to be identified;

simple (plausible) mass models are then assumed, parameters fixed by matching the multiple images, and requiring the distortion at the arcs to be strong and in correct orientation;

this model predicts further multiple images; can be checked for (HST imaging *very* important) through morphology and color;

new, refined model $\Rightarrow$ further predictions $\Rightarrow$ further refinements etc.;

such model have predictive power and can be trusted in detail; accuracy of mass estimates sometimes a few percent;

yield mass distribution in the inner part of clusters where strong lensing features occur;

redshift of arcs *very* useful – these can also be predicted.

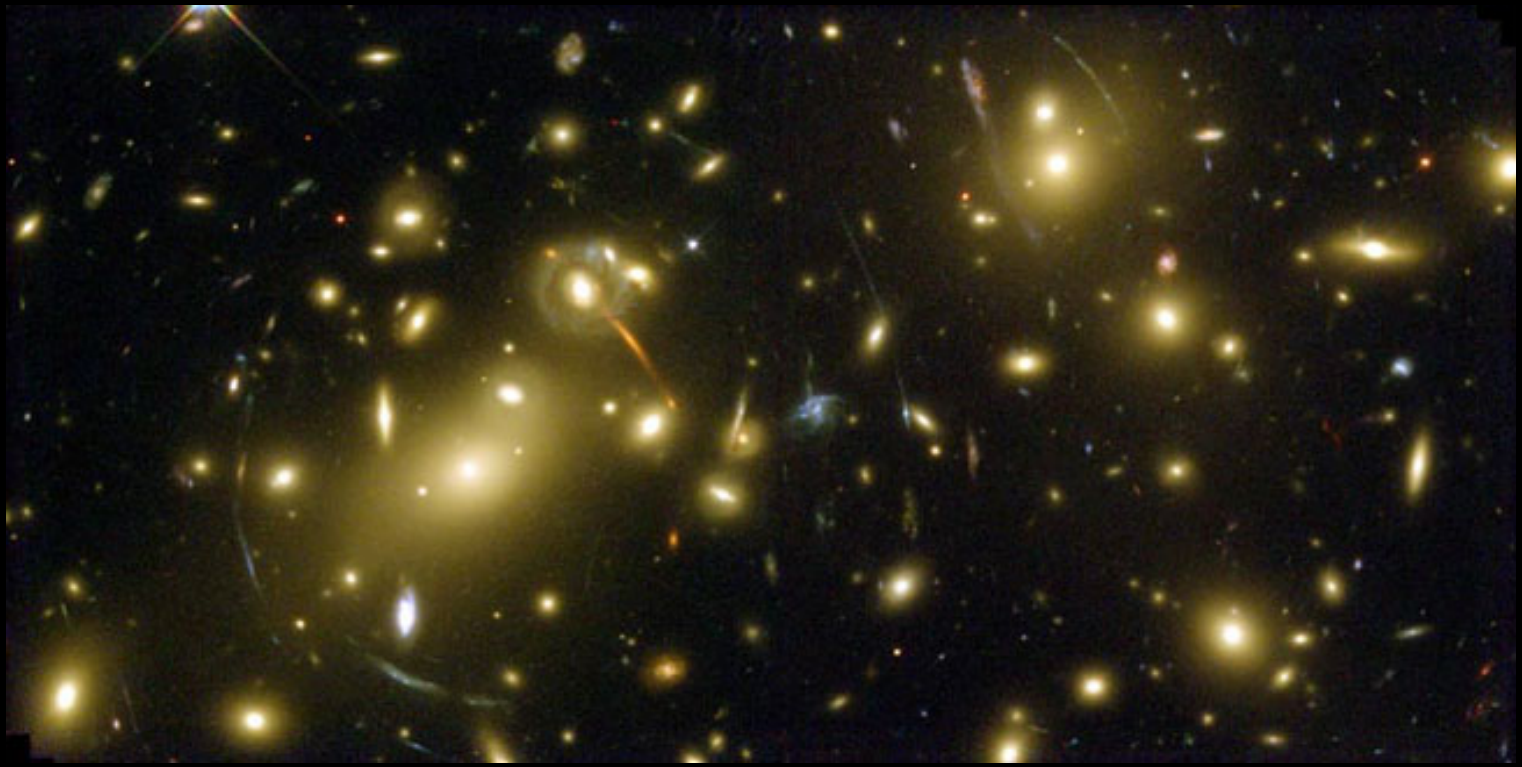

The cluster Abell 2218 is one of the ‘showcases’ of the Hubble Space Telescope.

The cluster RXJ1347 is the most X-ray luminous cluster known;

it is also very massive, as seen from the arcs;

it is less spectacular than A1689, since it has $z_{\rm d} = 0.45$ – fewer background galaxies; also, it is more regular – less substructure, fewer strong lensing features.

Results from strong lensing

- Mass in cluster center much more concentrated than predicted by X-ray observations – otherwise arcs would not occur;
  $\Rightarrow$ inner region of clusters 'complicated', cooling flows, other baryonic effects;
  'core radii' of $\sim 100\,\mathrm{kpc}$ can be excluded;

- often strong substructure seen in central part of clusters, or bimodality, as in A370;

- orientation of dark matter appears to follow closely orientation of the light in the cD galaxy;
  growth of cD closely related to cluster potential?

- Do cluster follow the NFW 'universal' density profile?
  In order to probe mass profile in the very inner part, radial arcs are very useful;
  not many known yet;
  that has changed with the ACS cluster survey; but only few results yet available

Mass reconstruction of galaxy clusters

- Weak lensing yields an estimate of the local (reduced) shear;
- shear $\gamma = (\psi_{11} - \psi_{22})/2 + \mathrm{i}\psi_{12}$ and surface mass density $\kappa = \nabla^2\psi/2$ both are second partial derivatives of the deflection potential ψ;
- hence, κ and γ are linearly related;
- it is therefore possible to derive the surface mass distribution from the shear!
- This method works best for clusters of galaxies; we shall see it allows the construction of parameter-free mass maps.

The Kaiser–Squires inversion

Since

$$\psi(\boldsymbol{\theta}) = \frac{1}{\pi} \int_{\mathbb{R}^2} \mathrm{d}^2\theta' \, \kappa(\boldsymbol{\theta}') \, \ln|\boldsymbol{\theta} - \boldsymbol{\theta}'| \; ,$$

and $\gamma = (\psi_{11} - \psi_{22})/2 + \mathrm{i}\psi_{12}$, one has

$$\begin{aligned} \gamma(\boldsymbol{\theta}) \;&=\; \frac{1}{\pi} \int_{\mathbb{R}^2} \mathrm{d}^2\theta' \, \mathcal{D}(\boldsymbol{\theta} - \boldsymbol{\theta}') \, \kappa(\boldsymbol{\theta}') \; , \quad \text{with kernel} \\ \mathcal{D}(\boldsymbol{\theta}) \;&\equiv\; \frac{\theta_2^2 - \theta_1^2 - 2\mathrm{i}\theta_1\theta_2}{|\boldsymbol{\theta}|^4} = \frac{-1}{(\theta_1 - \mathrm{i}\theta_2)^2} \; . \end{aligned} \tag{32}$$

Hence, γ is convolution of κ with kernel $\mathcal{D}$; in Fourier space this becomes a multiplication,

$$\hat{\gamma}(\boldsymbol{\ell}) = \pi^{-1} \hat{\mathcal{D}}(\boldsymbol{\ell}) \, \hat{\kappa}(\boldsymbol{\ell}) \quad \text{for} \quad \boldsymbol{\ell} \neq \mathbf{0} \; .$$

This can be inverted,

$$\hat{\kappa}(\boldsymbol{\ell}) = \pi^{-1} \hat{\gamma}(\boldsymbol{\ell}) \, \hat{\mathcal{D}}^*(\boldsymbol{\ell}) \quad \text{for} \quad \boldsymbol{\ell} \neq \mathbf{0} \; , \tag{33}$$

where

$$\hat{\mathcal{D}}(\boldsymbol{\ell}) = \pi \frac{\left(\ell_1^2 - \ell_2^2 + 2\mathrm{i}\ell_1\ell_2\right)}{|\boldsymbol{\ell}|^2}$$

was used (this implies $\mathcal{D}\mathcal{D}^* = \pi^2$).

Fourier back-transformation then yields

$$\kappa(\boldsymbol{\theta}) - \kappa_0 = \frac{1}{\pi} \int_{\mathbb{R}^2} \mathrm{d}^2\theta' \, \mathcal{D}^*(\boldsymbol{\theta} - \boldsymbol{\theta}') \, \gamma(\boldsymbol{\theta}') \tag{34}$$

Constant κ_0 occurs since $\boldsymbol{\ell} = \mathbf{0}$-mode undetermined;
physical reason: uniform κ yields no shear.

κ must be real
$\Rightarrow$ imaginary part of integral should be zero

$$\Rightarrow \quad \boxed{\kappa(\boldsymbol{\theta}) - \kappa_0 = \frac{1}{\pi} \int_{\mathbb{R}^2} \mathrm{d}^2\theta' \, \mathcal{R}\mathrm{e}\left[\mathcal{D}^*(\boldsymbol{\theta} - \boldsymbol{\theta}') \, \gamma(\boldsymbol{\theta}')\right]} \, . \tag{35}$$

This is due to the fact that the two shear components are not independent – we'll come back to that!

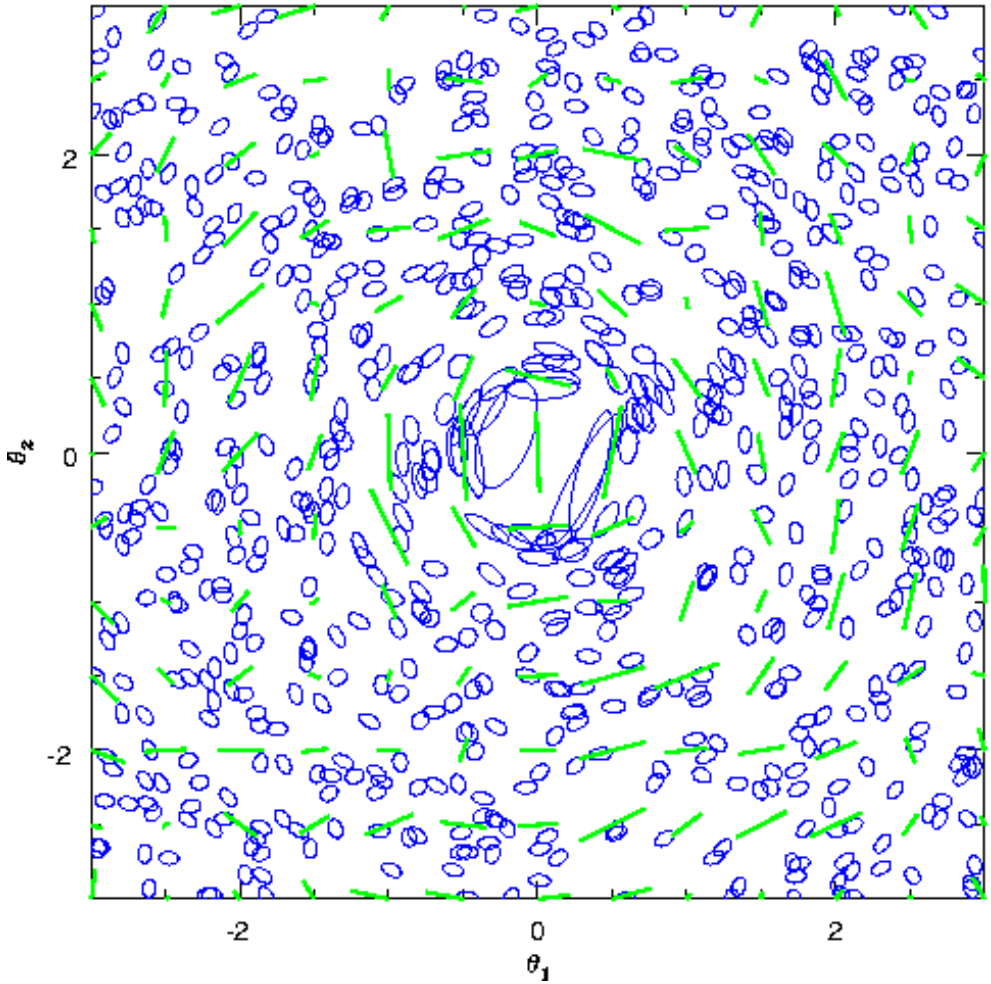

Schematic view of cluster mass reconstruction from weak lensing:

ellipticities of bg. galaxies are locally averaged, yields shear estimate (sticks)

then, smoothed shear field $\Rightarrow$ smoothed mass map

From C. Seitz, dissertation (1996)

Hence, if γ can be measured, κ can be determined!

Difficulties with Kaiser & Squires inversion

$$\kappa(\boldsymbol{\theta}) - \kappa_0 = \frac{1}{\pi} \int_{\mathbb{R}^2} \mathrm{d}^2\theta' \, \mathcal{R}\mathrm{e} \left[\mathcal{D}^*(\boldsymbol{\theta} - \boldsymbol{\theta}') \, \gamma(\boldsymbol{\theta}') \right] \ .$$

- γ can at best be estimated at discrete points (galaxy images) – smoothing required $\rightarrow$ finite resolution of mass maps
- not the shear γ, but only the reduced shear g can be determined from galaxy ellipticities
- integral extends over $\mathbb{R}^2$, data available only on finite field
- the additive constant, or as explained soon, an undetermined constant; originated from the *mass-sheet degeneracy*

κ from the reduced shear g

Noting that the reduced shear $g = \gamma/(1-\kappa)$ can be obtained from the ellipticity of images, one can write:

$$\kappa(\boldsymbol{\theta}) - \kappa_0 = \frac{1}{\pi} \int_{\mathbb{R}^2} \mathrm{d}^2\theta' \, \left[1 - \kappa(\boldsymbol{\theta}')\right] \, \mathcal{R}\mathrm{e}\left[\mathcal{D}^*(\boldsymbol{\theta} - \boldsymbol{\theta}') \, g(\boldsymbol{\theta}')\right] \; ; \tag{36}$$

this integral equation can be solved by iteration – converges quickly.

The unfortunate mass-sheet degeneracy

For a given source and lens redshift:

The mass distributions $\kappa(\boldsymbol{\theta})$ and, for all λ,

$$\kappa_\lambda(\boldsymbol{\theta}) := \lambda\kappa(\boldsymbol{\theta}) + (1-\lambda)$$

yield **the same** image configurations, magnification ratios, image shapes!

Magnification depends on λ, $\mu_\lambda = \mu/\lambda^2$ – but unmeasurable without information about the source (or source population)

[Time-delay affected, $(H_0\,\Delta t)_\lambda = \lambda(H_0\,\Delta t)$]

Radial slope of density profile affected

Invariant: (Mass inside) Einstein radius, angular structure (e.g., ellipticity)

Thus:

To determine slope of mass profile, absolute masses (away from the Einstein radius), Hubble constant, mass-sheet degeneracy must first be broken!!

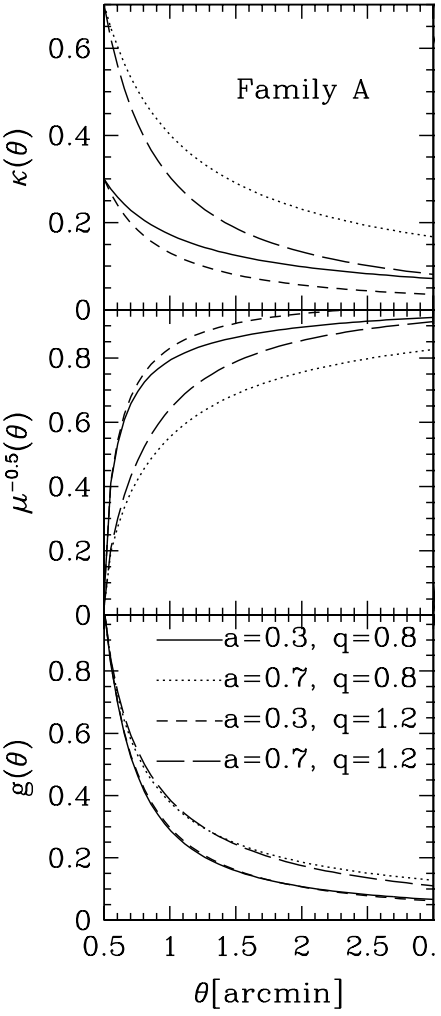

Illustration of mass-sheet degeneracy:

Four different mass distributions (top – all local power laws) lead to pairwise almost degenerate weak lensing observable g (bottom).

Magnification information can break this degeneracy, but requires very accurate external calibration.

Schneider et al. (2000)

How to break the mass-sheet degeneracy

- Assume a parametrized mass model (e.g., power law, or NFW, for κ)
- Assume $\kappa \to 0$ (or $\kappa \to \kappa_{\rm NFW}$) for large separation from lens center
- Use independent mass probes – e.g., stellar dynamics in galaxies
- Assume 'mass follows light' on average, for clusters
- Have independent information about source size or luminosity (e.g., fundamental plane)
- Employ statistical distribution of source properties (e.g., number counts for large-scale cluster lensing)
- MSD can be broken if sources at vastly different (and known) redshifts are lensed by the same mass concentration (e.g., multiple arc systems in clusters)

These methods are 'more or less' successful ...
MSD remains the **largest obstacle** for model-independent accurate results.

For galaxy lenses, stellar dynamical techniques have been most successful.

Finite-field inversions

or: Getting κ from a shear measurement on a finite data field.

Those start from

$$\nabla\kappa = \begin{pmatrix} \gamma_{1,1} + \gamma_{2,2} \\ \gamma_{2,1} - \gamma_{1,2} \end{pmatrix} \equiv \boldsymbol{u}_\gamma(\boldsymbol{\theta}) \ , \tag{37}$$

a *local* relation between shear and surface mass density;

can be easily derived from definitions of κ and γ in terms of ψ_{ij}.

A similar relation can be derived in terms of reduced shear,

$$\nabla K(\boldsymbol{\theta}) = \frac{-1}{1 - g_1^2 - g_2^2} \begin{pmatrix} 1 - g_1 & -g_2 \\ -g_2 & 1 + g_1 \end{pmatrix} \begin{pmatrix} g_{1,1} + g_{2,2} \\ g_{2,1} - g_{1,2} \end{pmatrix} \equiv \boldsymbol{u}_g(\boldsymbol{\theta}) \ , \tag{38}$$

where

$$K(\boldsymbol{\theta}) \equiv \ln[1 - \kappa(\boldsymbol{\theta})] \ . \tag{39}$$

Here, $\kappa < 1$ assumed; otherwise we're in the strong lensing regime anyway.

These equations can be integrated, by formulating them as a von Neumann problem on the data field $\mathcal{U}$:

$$\nabla^2\kappa = \nabla\cdot\boldsymbol{u}_\gamma \quad \text{with} \quad \boldsymbol{n}\cdot\nabla\kappa = \boldsymbol{n}\cdot\boldsymbol{u}_\gamma \quad \text{on} \quad \partial\mathcal{U}\ ; \tag{40}$$

$\boldsymbol{n}$: outward-directed normal on the boundary of $\mathcal{U}$.

Analogous equation holds for K in terms of g; numerical solution fast, using over-relaxation.

Solution unique, up to additive constant (MSD!!).

Formulation equivalent to minimization of the action

$$\int_{\mathcal{U}} \mathrm{d}^2\theta\ |\nabla\kappa(\boldsymbol{\theta}) - \boldsymbol{u}_\gamma(\boldsymbol{\theta})|^2\ ; \tag{41}$$

foregoing relation derived as Euler's equation of the variational principle.

These parameter-free mass reconstructions have been applied to quite a number of clusters – a tool to make dark matter distribution 'visible'.

Inverse methods

Optimized technique: maximum-likelihood fit of data:

'Parameterize' lens by potential ψ on grid and minimize

$$-\ln \mathcal{L} = \sum_{i=1}^{N_\mathrm{g}} \frac{|\epsilon_i - g\left(\boldsymbol{\theta}_i, \{\psi_n\}\right)|^2}{\sigma_i^2\left(\boldsymbol{\theta}_i, \{\psi_n\}\right)} \tag{42}$$

w.r.t. to these values; to avoid overfitting, one need regularization; entropy regularization seems best suited.

Only with inverse methods can strong lensing constraints be included ('stong and weak lensing united').

Note: it is *essential* to put ψ on a grid, not κ:
from κ on a finite field, the shear cannot be predicted;
also, relation between ψ and γ local!

Examples

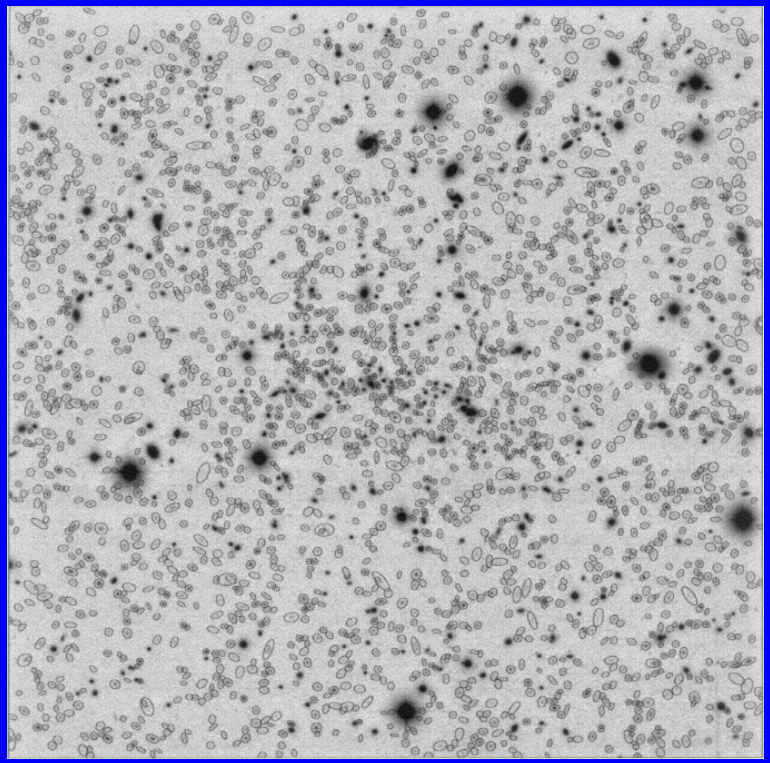

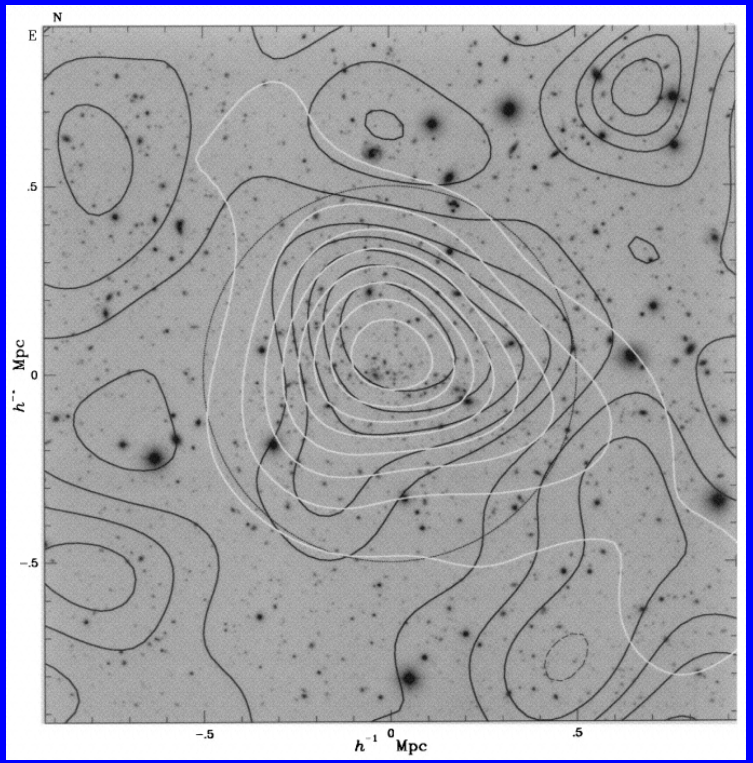

Left: Ground-based image of MS1054−03; on this $7'.5 \times 7'.5$ image, about 2400 galaxy ellipticities are measured; right: mass reconstruction (black), compared to light distribution (white) – from Luppino & Kaiser (1997)

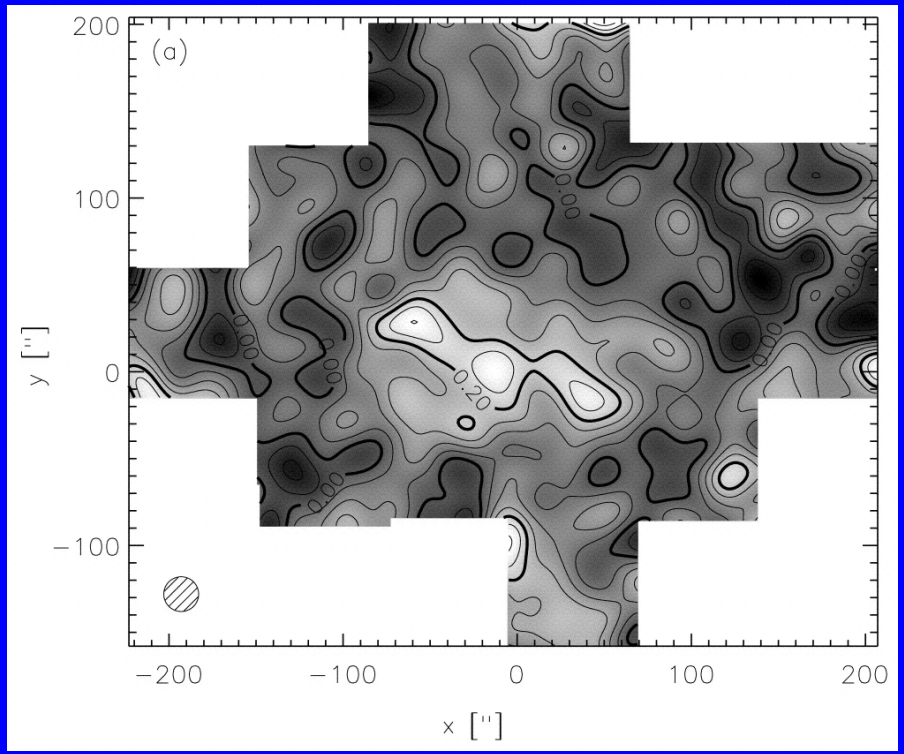

Mass construction of the same cluster, from an HST mosaic (Hoekstra et al. 2000);

clearly, substructure can be seen, cluster appears to consist of three central components;

not unexpected, clusters at these high redshifts are in the process of their formation through repeated mergers;

Multiple components also seen in galaxy distribution in this cluster;
this cluster also shows high fraction of merging galaxies.

Dark matter filament connecting clusters

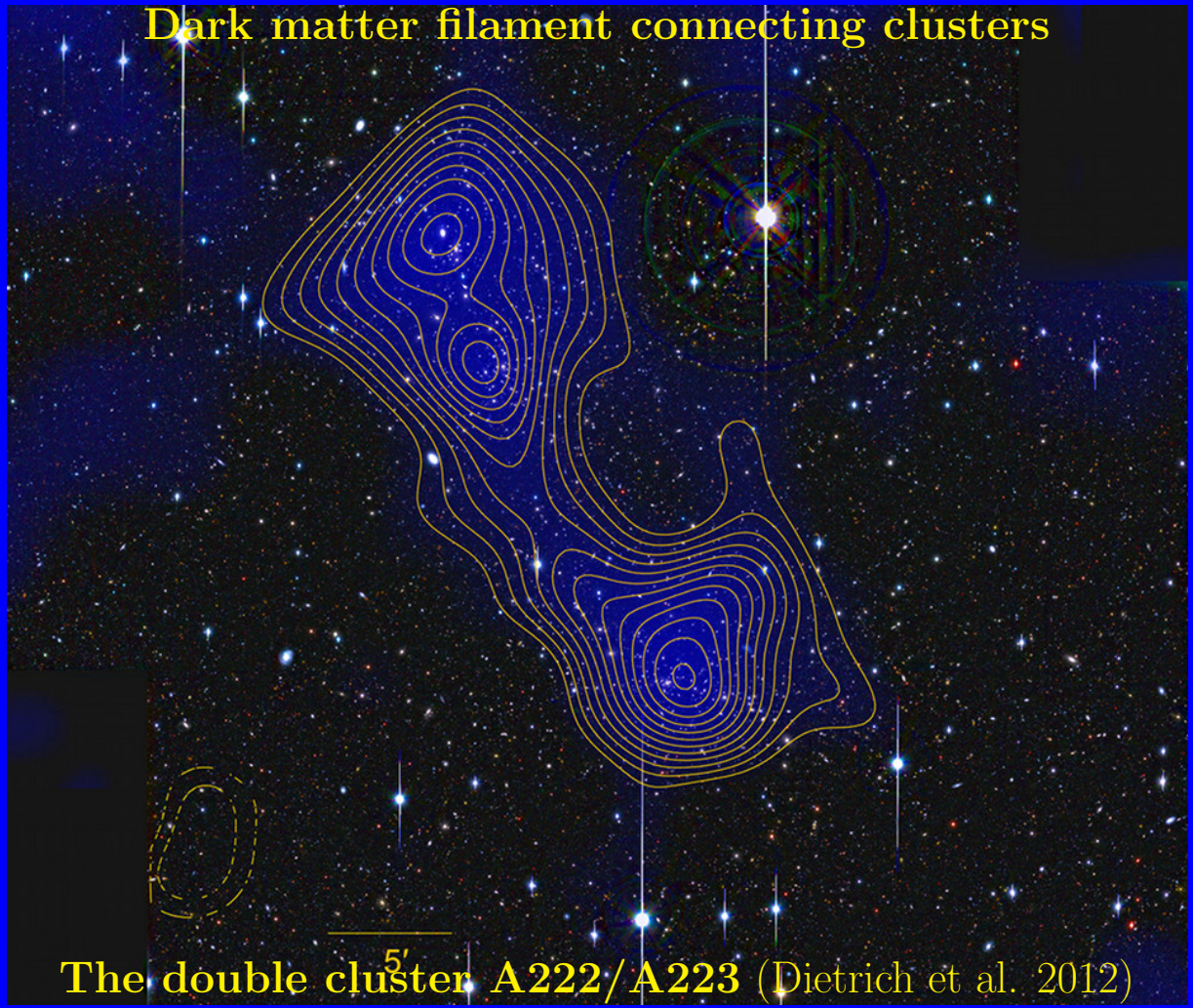

The double cluster A222/A223 (Dietrich et al. 2012)

The mean density profile of clusters

Umetsu et al. (2011a, b) studied 5 (4) strong lensing clusters using shear + magnification bias (number counts) + strong lensing:

Mass profiles of these 5 clusters:

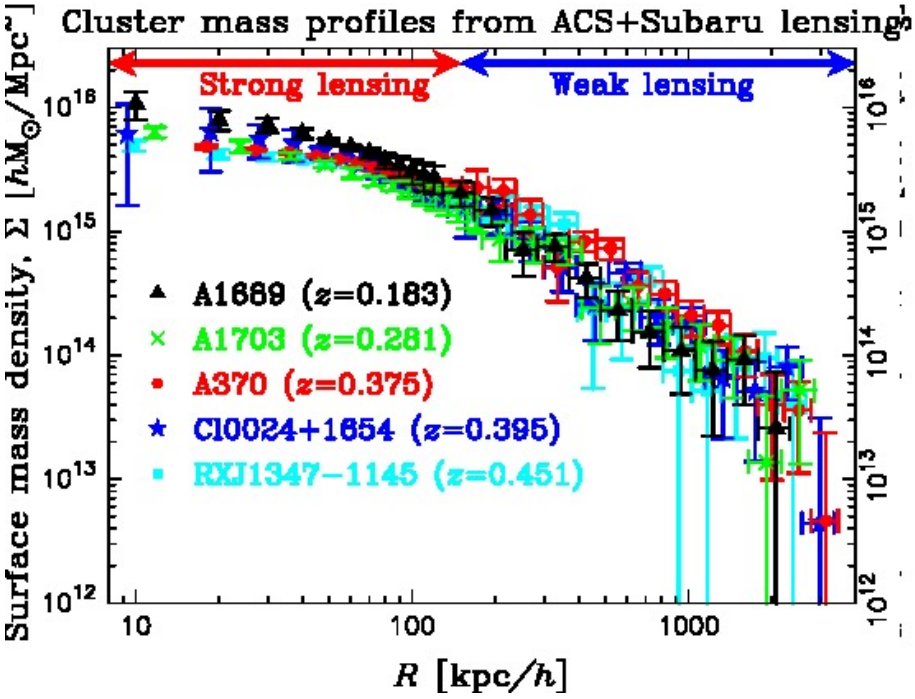

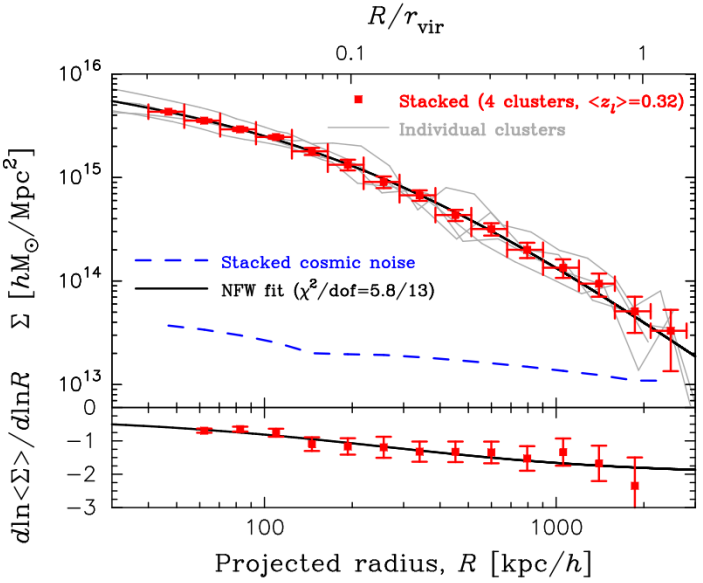

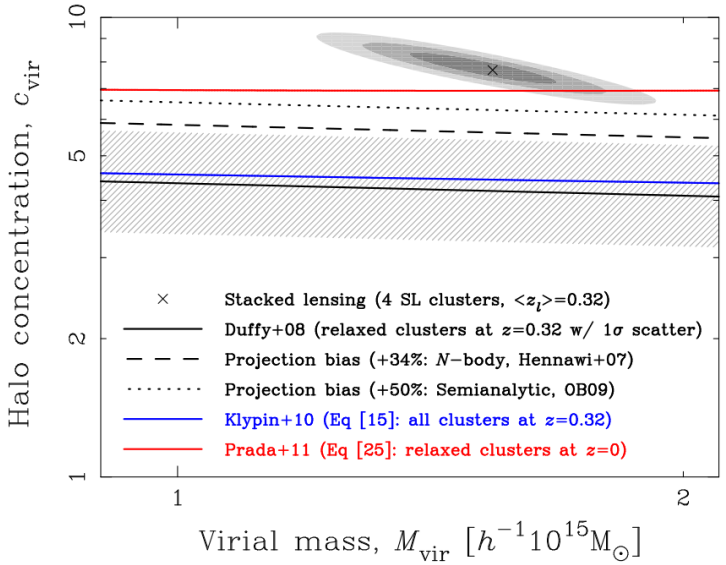

- NFW-profile fits remarkably well! Too well?
- Mean concentration parameter is $c \approx 7.7$, slightly higher that expected in 3-D, from DM-only simulations
- c biased high due to strong lensing selection

Oguri (2011) used 28 clusters from Sloan Giant Arcs Survey; shear only

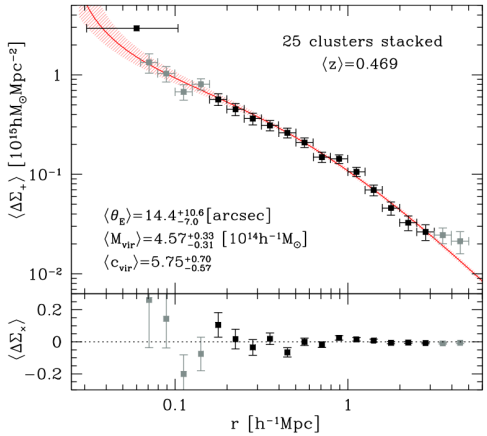

all clusters

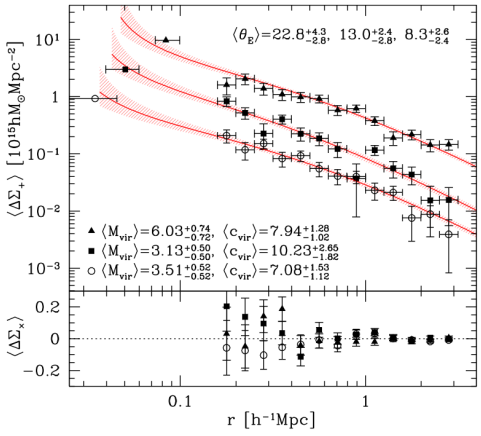

$\theta_{\rm E}$ bins

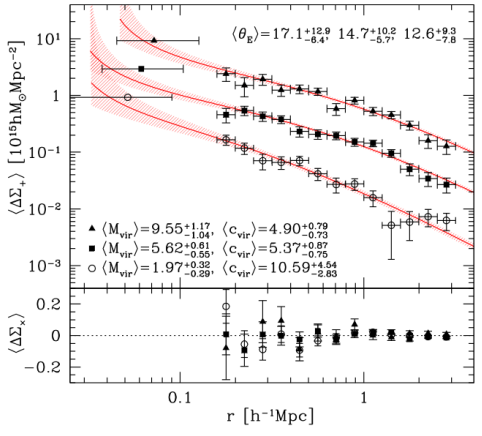

$M_{\rm vir}$ bins

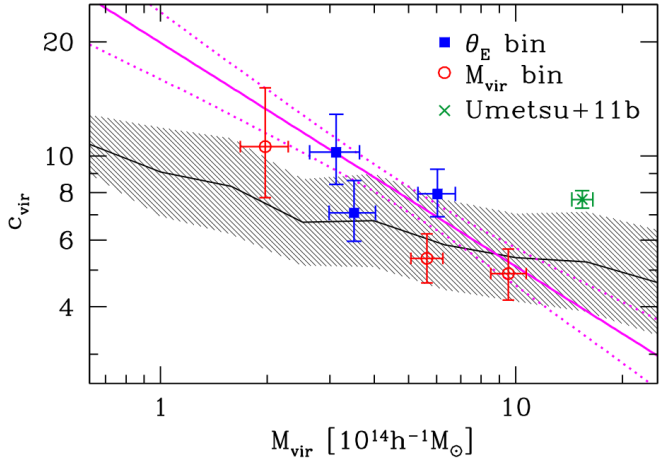

NFW-concentration,
compared to expectations including selection bias

How unique are these mass profiles?

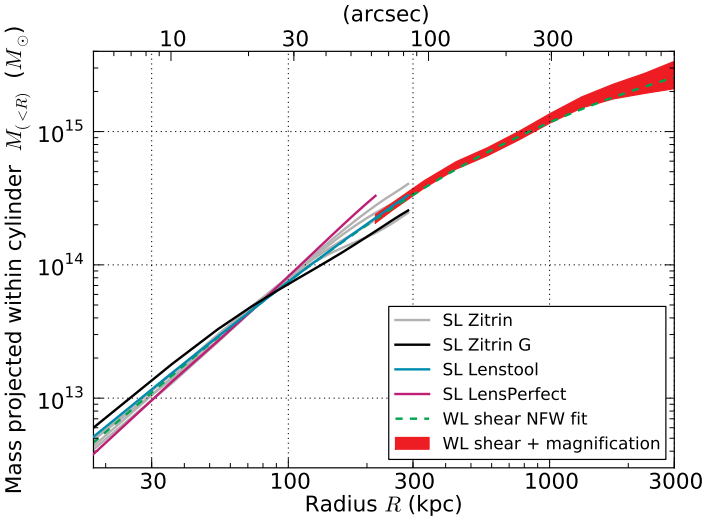

Projected enclosed mass in A2261 for different methods to get mass model (Coe et al. 2012)

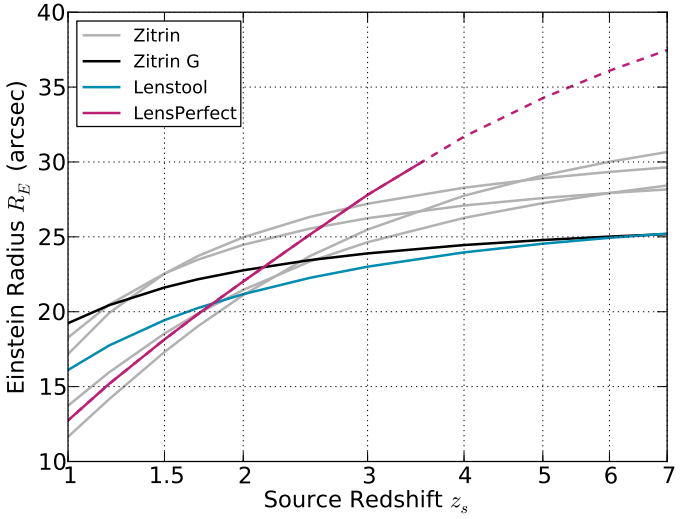

Einstein radius as function of source redshift in A 2261, obtained from different models (Coe et al. 2012)

Differences show mass-sheet degeneracy at work!

Too many too massive clusters?

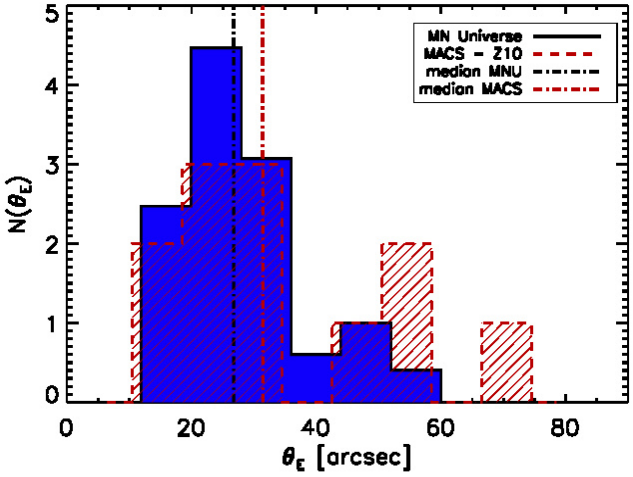

Distribution of Einstein radii from MareNostrum simulations and from 12 $z > 0.5$ MACS clusters (Meneghetti et al. 2011)
Too large a discrepancy?

Also: high $M_{\rm vir}$ for high-z clusters

Arc statistics

BUT

- Definition of ‘Einstein radius’ problematic

MACS J0717.5+3745
($z = 0.546$)
critical curves
for $z_s \sim 2.5$

Zitrin et al. (2009)

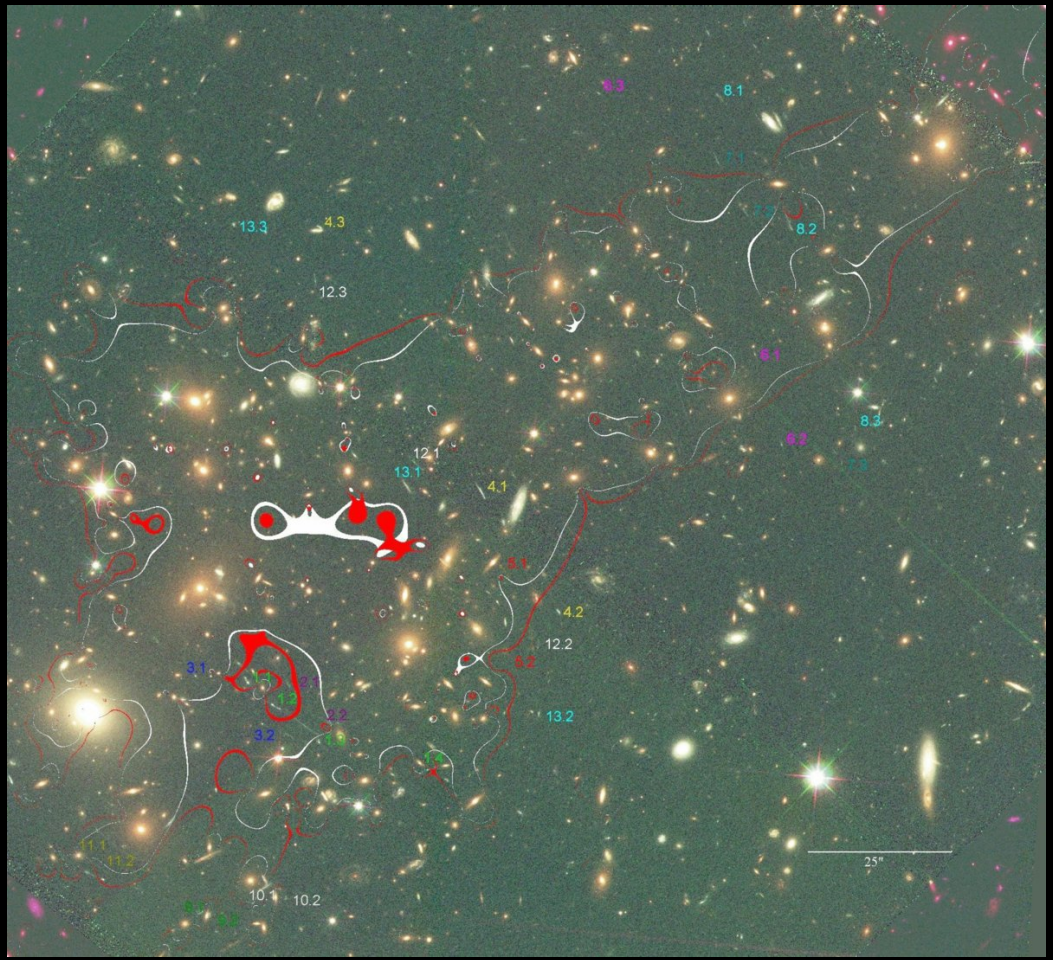

BUT

- Definition of 'Einstein radius' problematic
- Line-of-sight matter density (random projections) can strongly enhance lensing strength
- Strong lensing of clusters (significantly) affected by baryonic matter
- Selection bias – projection of triaxial or strongly asymmetric clusters
- Often, too few redshifts of strongly lensed sources known (in particular critical for high-z clusters)
- Do we really know the 'mass'-spectrum at the extreme end?
- How to properly compare observations with model predictions (*a posteriori* statistics)?

Clusters are dominated by collisionless matter:

The Bullet Cluster is a pair of colliding galaxy clusters (Clowe et al. 2006)

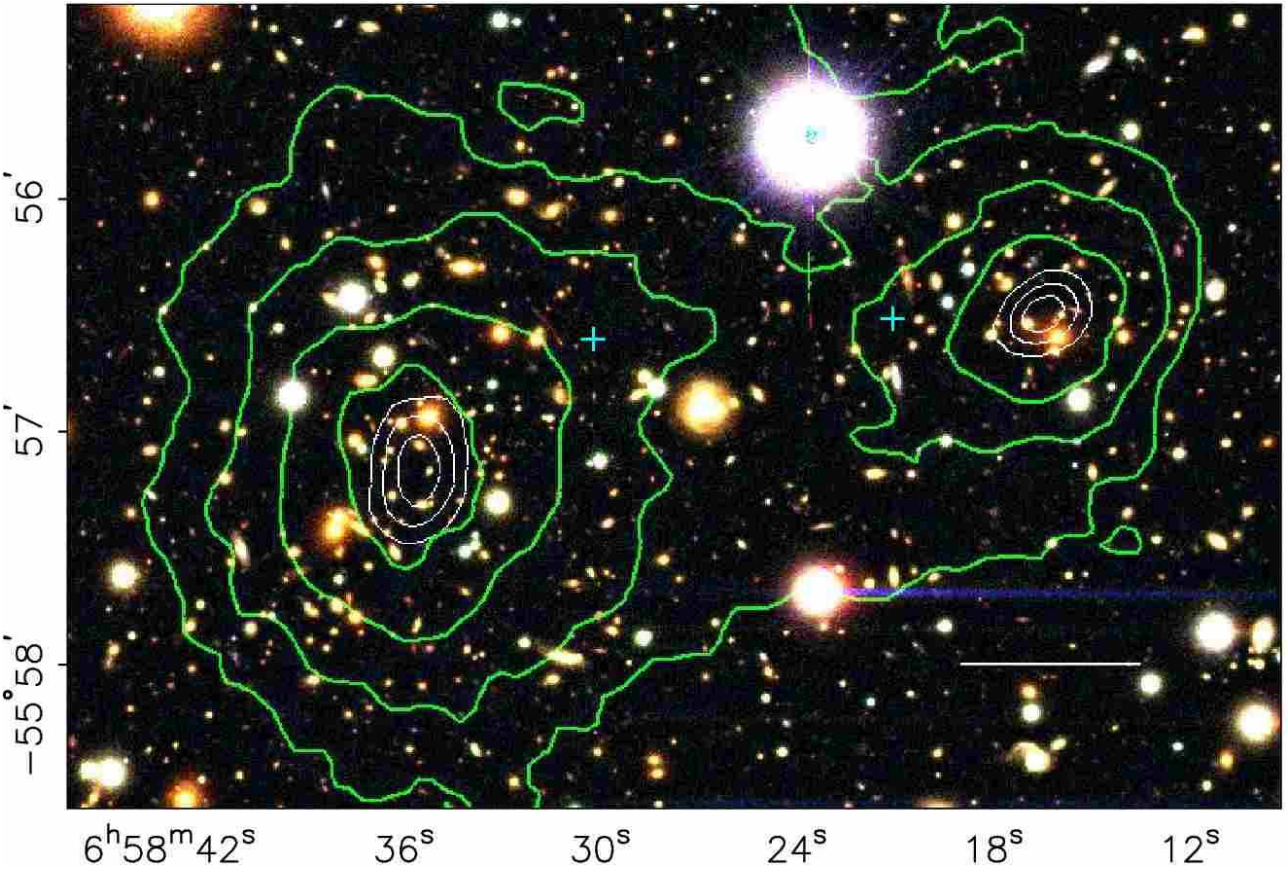

X-ray emission from the bullet cluster

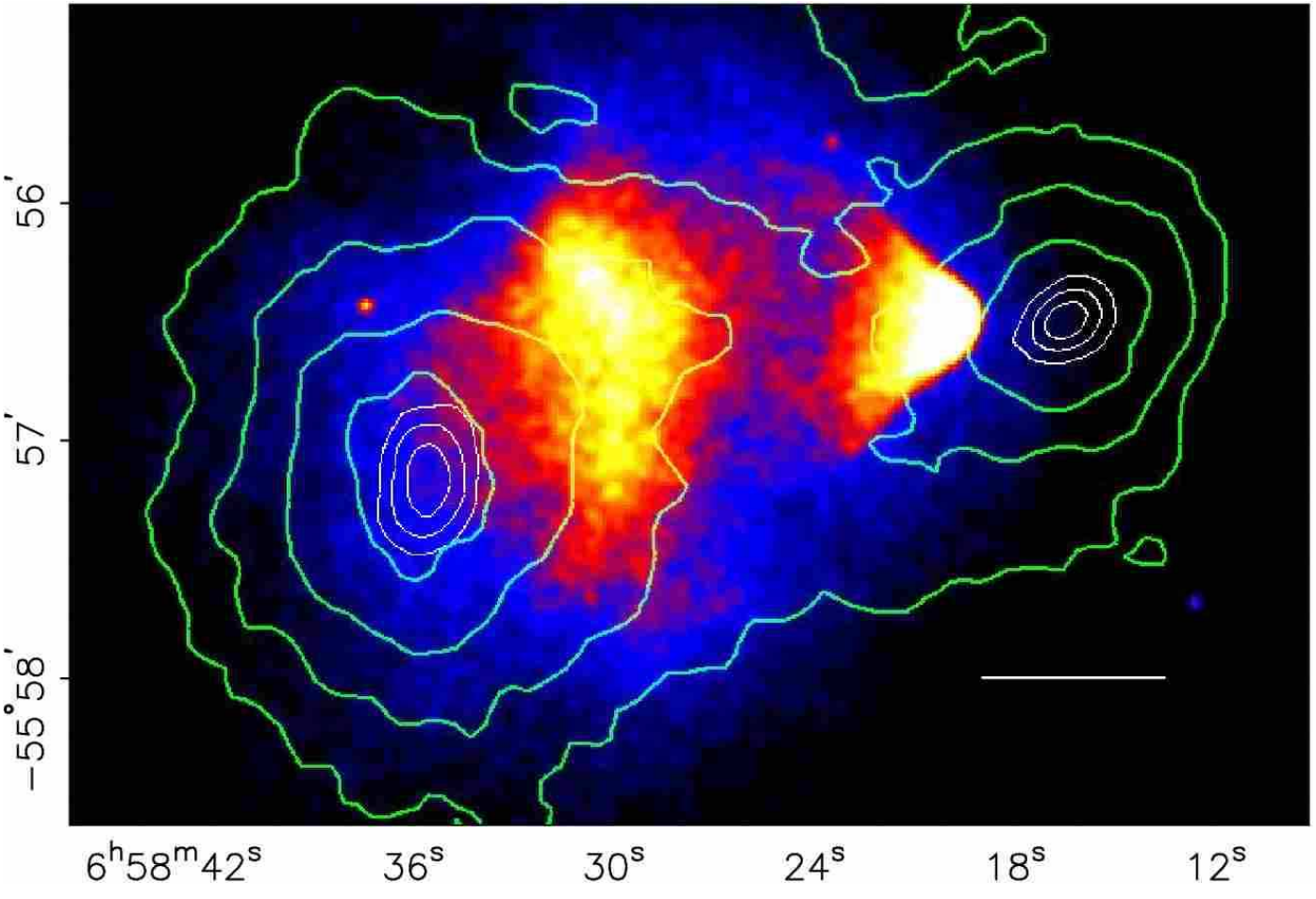

- Lensing shows that most of the mass is located near the galaxies,
- and not centered on the gas, which is displaced by the collision.
- $\Rightarrow$ Most of the mass in this cluster pair must behave collisionless, like galaxies.
- Most of the mass is dark matter – the bullet cluster can not be explained by changing the law of gravity without invoking collisionless dark matter.
- The bullet cluster is not the only case where this clear distinction can be made...

The cluster MACS J0025.4−1222 ($z = 0.59$)

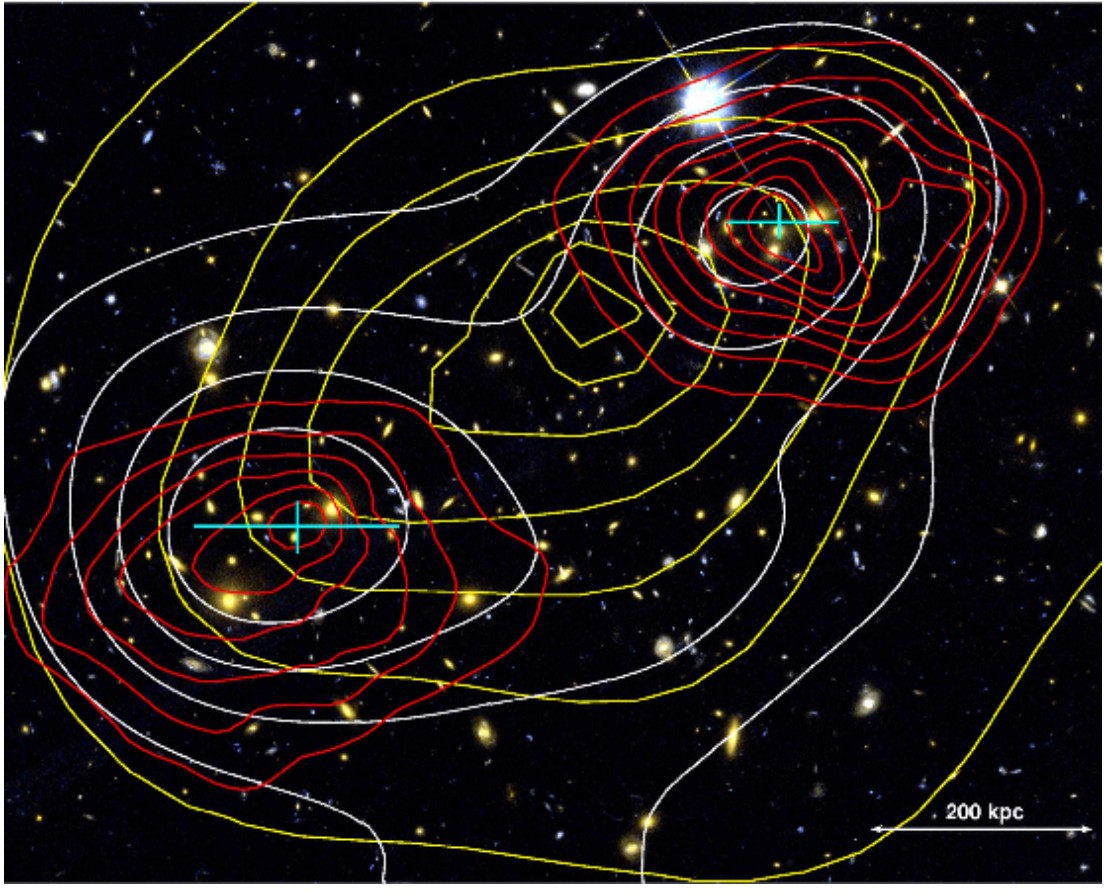

(Bradac et al. 2008)

red:
surface mass density;

yellow:
X-ray emission;

white:
smoothed optical light.

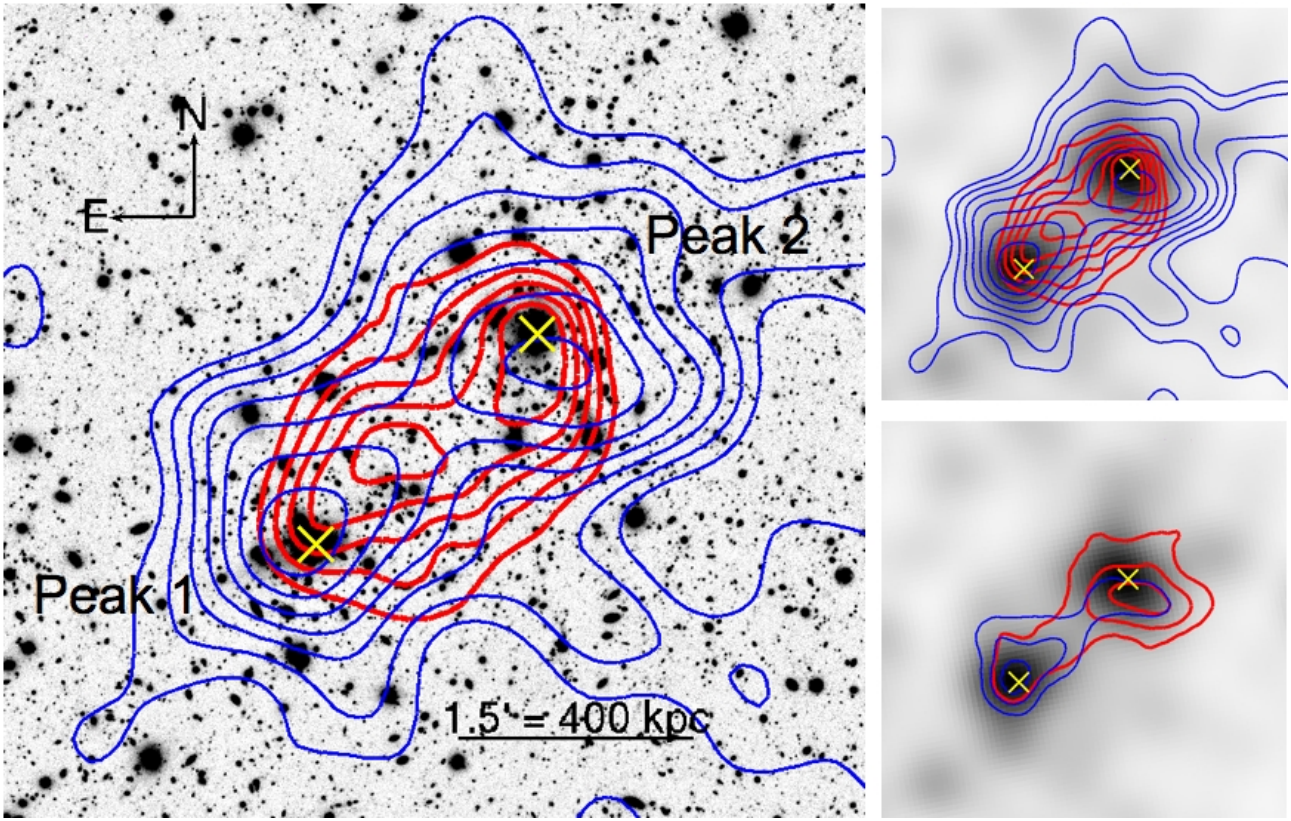

A1758N (Ragozzine & Clowe 2011)
Blue: mass reconstruction; red: X-ray emission

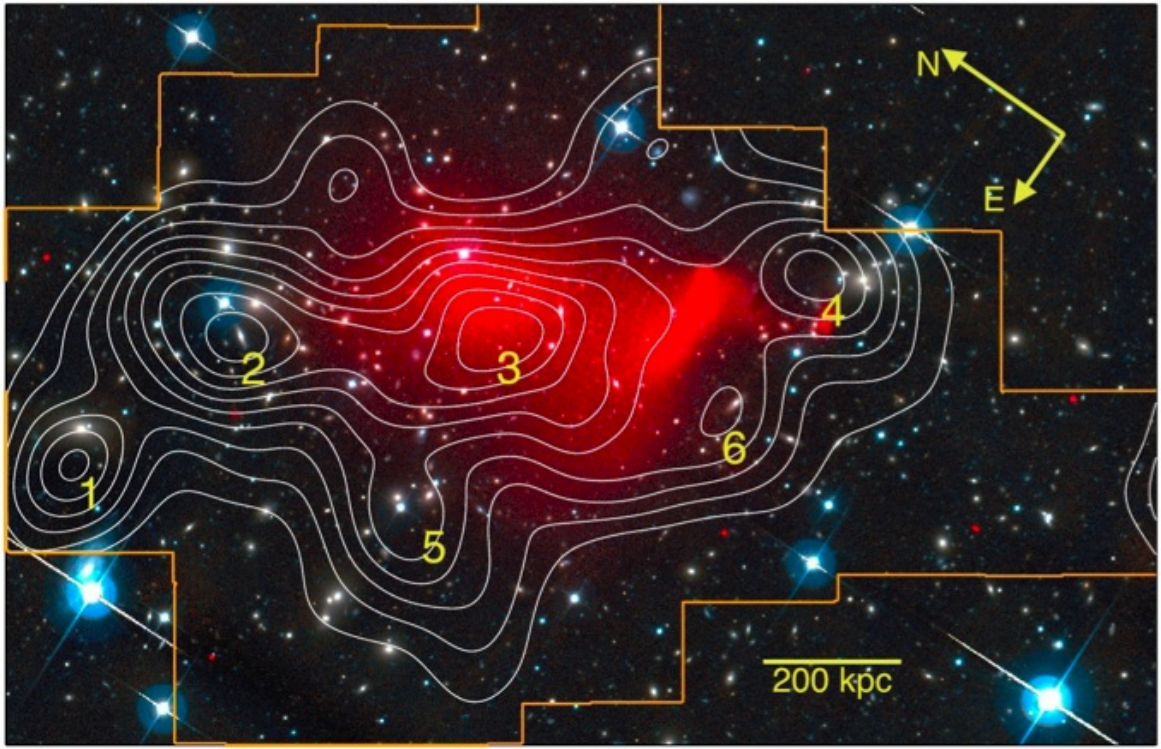

Jee et al. (2012): Abell 520 shows complicated structure in mass (contours) and X-ray emission (red shades)

Results

- Mass reconstruction of clusters using weak lensing has by now become routine.
- Overall, projected mass distribution quite similar to projected galaxy distribution and shape of X-ray emission, for clusters that appear relaxed.
- Many clusters are unrelaxed, in particular our beloved strong lensing clusters.
- Mass-sheet degeneracy hampers model-free determination of virial mass of clusters; however, once physical parametrization employed (such as NFW-profile), profile parameters can be determined quite accurately.
- Radial mass profile compatible with NWF profile.
- Dark matter filament connecting pairs of clusters.
- Clusters contain collisionless dark matter – Bullet clusters.

Aperture mass

Definition

In weak lensing regime, $\kappa \ll 1$, mass-sheet degeneracy corresponds to adding uniform κ_0;

if $U\left(|\boldsymbol{\theta}|\right)$ is a compensated weight function with

$$\int \mathrm{d}\theta\, \theta\, U(\theta) = 0\ ,$$

then the *aperture mass*

$$M_{\rm ap}(\boldsymbol{\theta}_0) = \int \mathrm{d}^2\theta\, \kappa(\boldsymbol{\theta})\, U(|\boldsymbol{\theta} - \boldsymbol{\theta}_0|) \tag{43}$$

is independent of κ_0.

$M_{\rm ap}(\boldsymbol{\theta}_0)$ is a mass map filtered with a zero-total weight function (think of U as a Mexican hat-like filter).

The useful property of $M_{\rm ap}$ is due to the following:

One can derive from (37) that $M_{\rm ap}$ can be written directly in terms of the shear,

$$\boxed{M_{\rm ap}(\boldsymbol{\theta}_0) = \int \mathrm{d}^2\theta\, Q(|\boldsymbol{\theta}|)\, \gamma_{\rm t}(\boldsymbol{\theta};\boldsymbol{\theta}_0)}\,, \tag{44}$$

where we have defined (as before) the *tangential component* $\gamma_{\rm t}$ of the shear relative to the point $\boldsymbol{\theta}_0$, and

$$Q(\theta) = \frac{2}{\theta^2}\int_0^\theta \mathrm{d}\theta'\; \theta'\, U(\theta') - U(\theta)\;. \tag{45}$$

Hence, $M_{\rm ap}$ can be directly obtained from the shear data, i.e., the ellipticities of galaxy images.

One can thus search for mass overdensities directly from the shear ('shear peaks'), without first doing a mass reconstruction.

Note: If U has finite support, Q has finite support
$\Rightarrow$ Aperture mass can be calculated on finite data field.

Mass detection of clusters

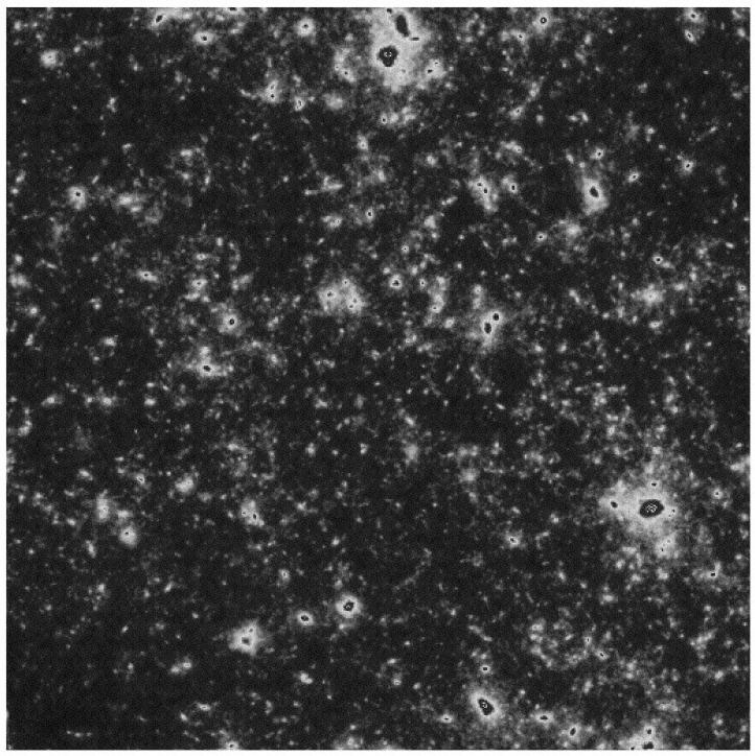

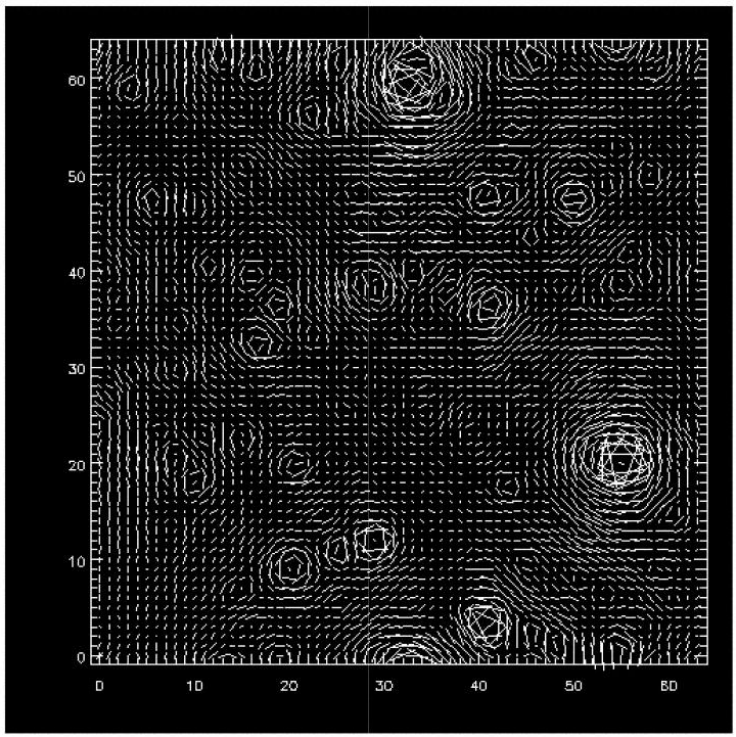

Projected mass distribution of the LSS (left) and shear field (right; from Jain et al 2000). Mass concentrations correspond to circular patterns of tangentially oriented shears.

Results

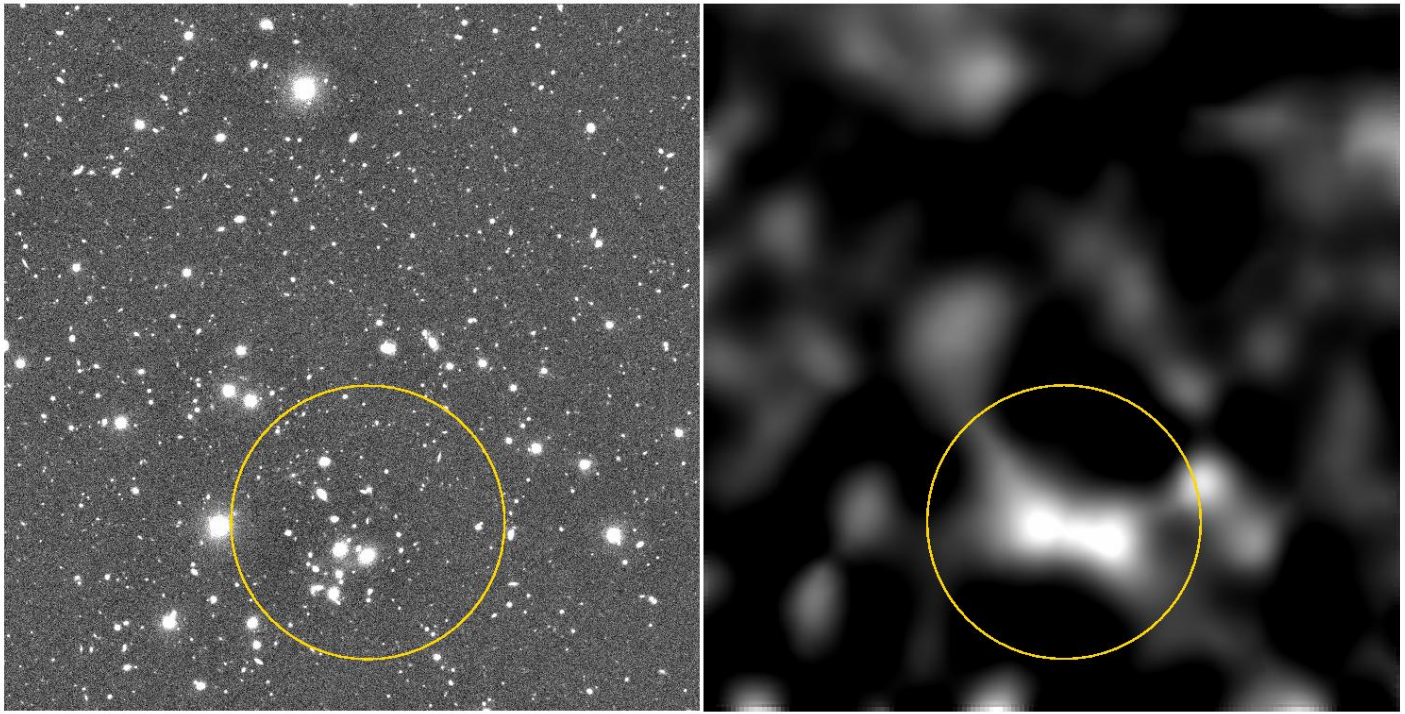

One cluster found in an empty-field pointing with the FORS1/VLT; left is optical image, right is mass reconstruction;

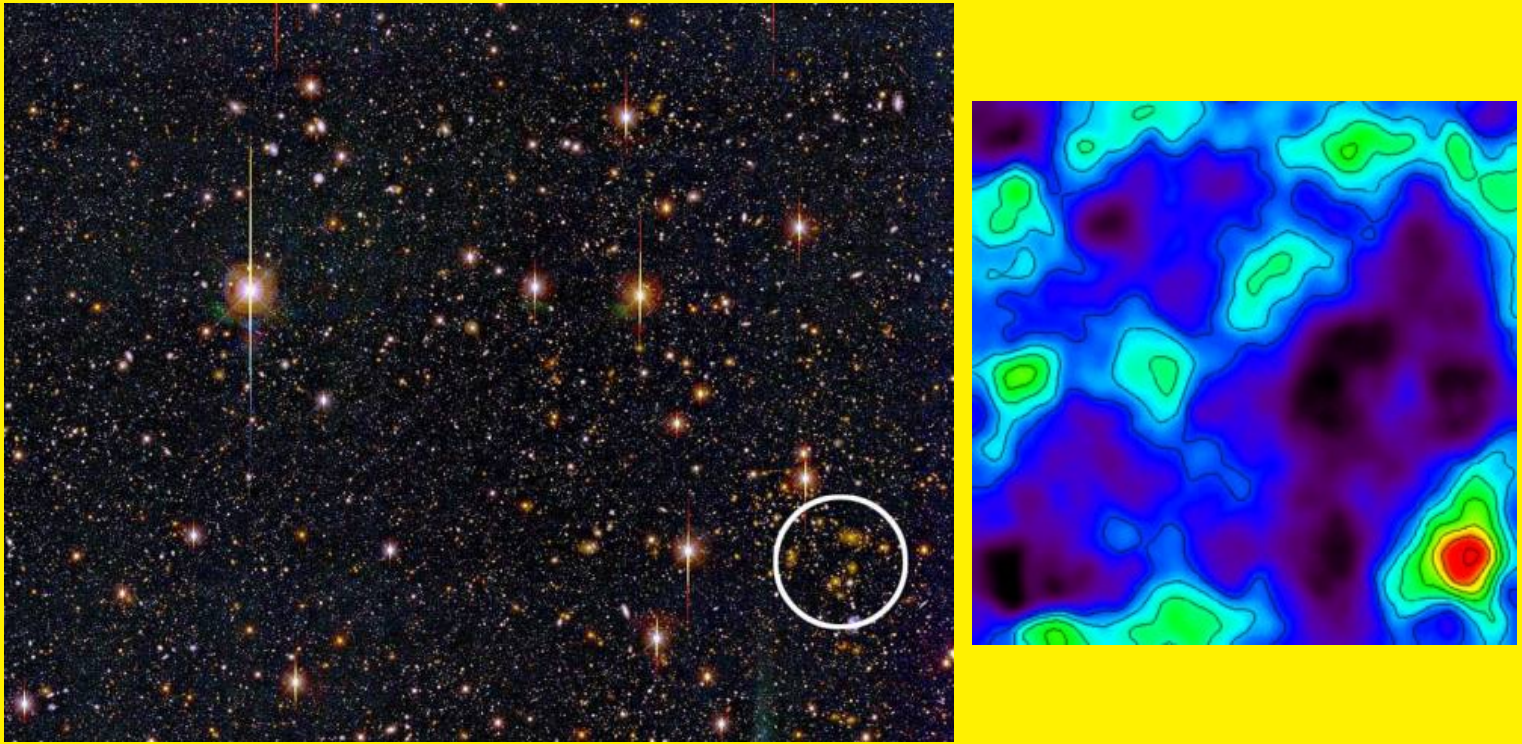

Left: BTC image of a blank field, right: mass reconstruction, showing the presence of a (mass-selected) cluster – spectrocopically verified to be at $z = 0.276$ (Wittman et al. 2001)

By now, hundreds of cluster candidates found by lensing have been published; however, only few of them spectroscopically confirmed;

known clusters rediscovered by blind lensing search;

very powerful method to search for dark matter halos, independent of baryonic properties (which determine luminosities);

abundance can be directly compared to ray-tracing simulations through the LSS – no intermediate step (e.g., halo selection, mass determination) necessary!

Therefore, clean probe of cosmology;

in particular, statistics probes mean density profile of clusters and equation-of-state of dark energy;

can use the same data sets as the ones obtained for cosmic shear surveys.

Dark Matter in Clusters & Large-Scale Structure

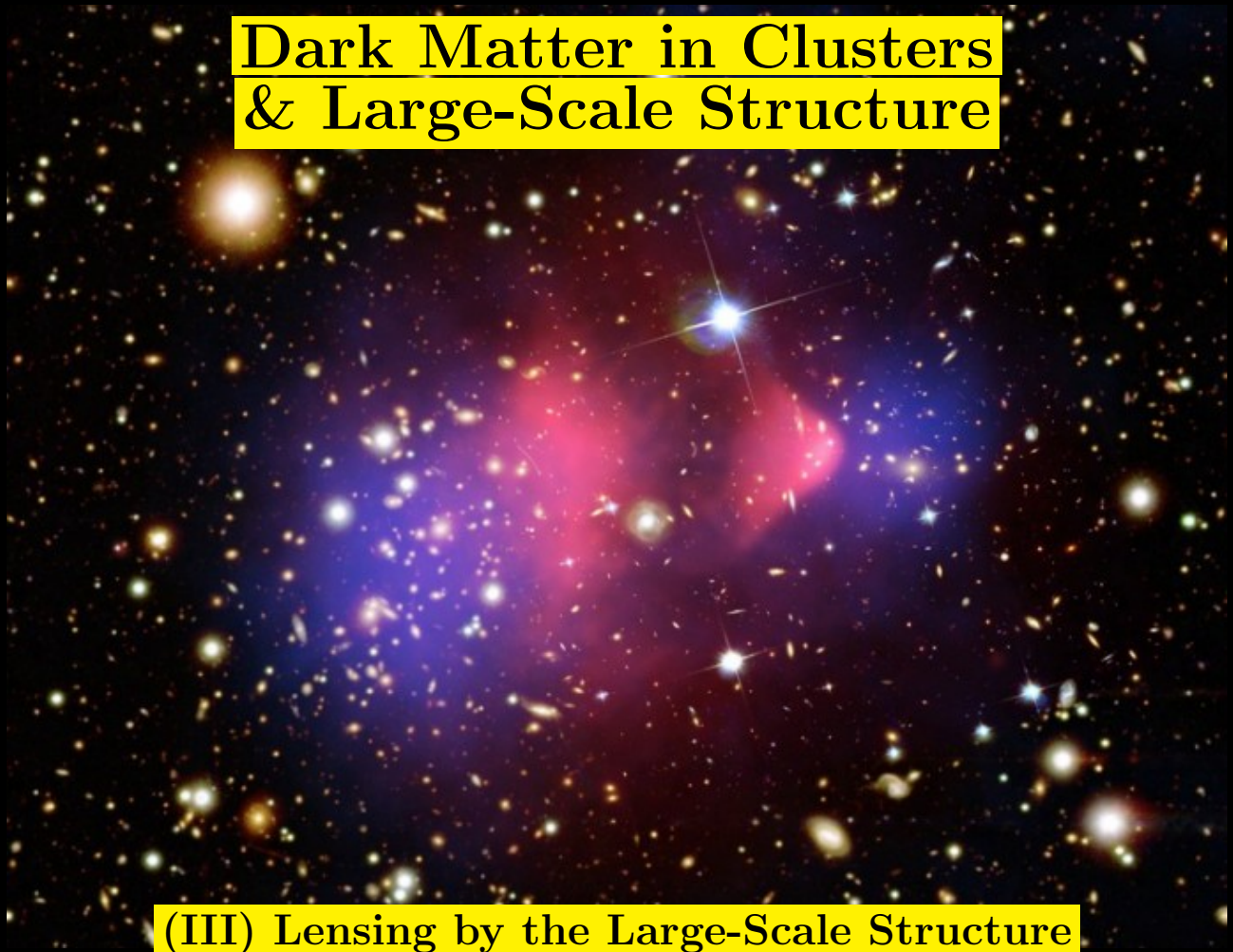

(III) Lensing by the Large-Scale Structure

Large-scale structure lensing: theory

Light bundles propagating through the Universe are continuously deflected and distorted by the gravitational field of the inhomogeneous mass distribution – the LSS;

the distortion causes shape distortions of images of distant galaxies; the statistics of the distortions reflect the statistical properties of the LSS.

Cosmic Shear deals with the investigation of this connection, from the measurement of the correlated image distortion to the inference of cosmological information from this distortion field.

In contrast to 'ordinary' lensing, here the light deflection does not occur in a 'lens plane' but by a 3-d matter distribution; needs different description.

DEFLECTION OF LIGHT RAYS CROSSING THE UNIVERSE, EMITTED BY DISTANT GALAXIES

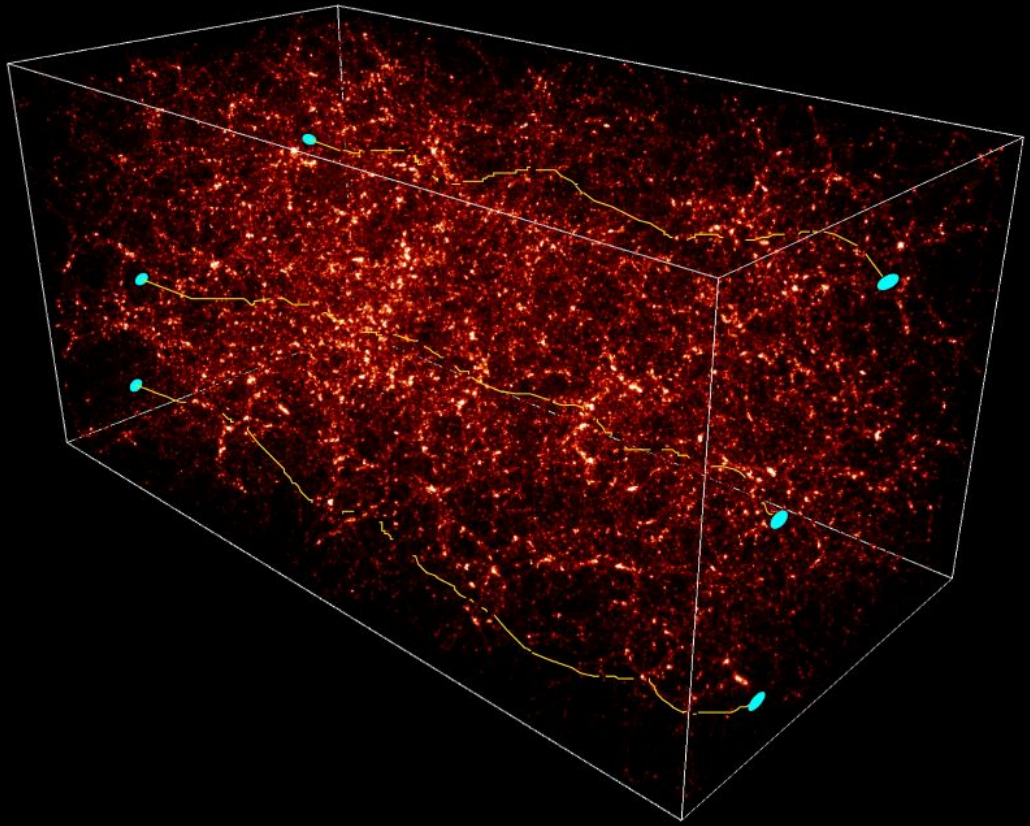

SIMULATION: COURTESY NIC GROUP, S. COLOMBI, IAP.

Light propagation in an inhomogeneous Universe

The governing equation for the propagation of thin light bundles through arbitrary space-times is the equation of geodesic deviation,

$$\frac{\mathrm{d}^2\boldsymbol{\xi}}{\mathrm{d}\lambda^2} = \mathcal{T}\,\boldsymbol{\xi}\;, \tag{46}$$

where $\boldsymbol{\xi}$ is the proper transverse separation of two neighboring light rays, λ the affine parameter, and $\mathcal{T}$ is the *optical tidal matrix* which describes the influence of space-time curvature on the propagation of light;
$\mathcal{T}$ can be expressed directly in terms of the Riemann curvature tensor.

For the case of a weakly inhomogeneous Universe, the tidal matrix can be explicitly calculated in terms of the Newtonian potential – and by that simplifies considerably.

Write the slightly perturbed metric of the Universe as

$$\mathrm{d}s^2 = a^2(\tau)\left[\left(1+\frac{2\Phi}{c^2}\right)c^2\mathrm{d}\tau^2 - \left(1-\frac{2\Phi}{c^2}\right)\left(\mathrm{d}\chi^2 + f_K^2(\chi)\mathrm{d}\omega^2\right)\right]\ ; \qquad (47)$$

χ: comoving radial distance;
a: scale factor, normalized to unity today;
τ: conformal time, $\mathrm{d}t = a\ \mathrm{d}\tau$;
$f_K(\chi)$: comoving angular diameter distance; ($= \chi$ in a spatially flat model)
Φ: Newtonian potential.

With that form of the metric, the optical tidal matrix $\mathcal{T}$ can be calculated explicitly.

One then obtains the following result:

The **comoving** separation vector $\boldsymbol{x}(\boldsymbol{\theta}, \chi)$ between a ray separated by an angle $\boldsymbol{\theta}$ at the observer from a fiducial ray evolves according to

$$\frac{\mathrm{d}^2\boldsymbol{x}}{\mathrm{d}\chi^2} + K\,\boldsymbol{x} = -\frac{2}{c^2}\left[\nabla_\perp \Phi\left(\boldsymbol{x}(\boldsymbol{\theta}, \chi), \chi\right) - \nabla_\perp \Phi^{(0)}\left(\chi\right)\right] \;; \tag{48}$$

K: spatial curvature $= (H_0/c)^2\,(\Omega_\mathrm{m} + \Omega_\Lambda - 1)$;
$\nabla_\perp = (\partial/\partial x_1, \partial/\partial x_2)$ is transverse *comoving* gradient operator;
$\Phi^{(0)}(\chi)$: potential along fiducial ray.

Formal solution of transport equation obtained by method of Green's function:

$$\boldsymbol{x}(\boldsymbol{\theta}, \chi) = f_K(\chi)\boldsymbol{\theta} - \frac{2}{c^2}\int_0^\chi \mathrm{d}\chi'\, f_K(\chi - \chi')\left[\nabla_\perp \Phi\left(\boldsymbol{x}(\boldsymbol{\theta}, \chi'), \chi'\right) - \nabla_\perp \Phi^{(0)}\left(\chi'\right)\right] \tag{49}$$

Formal solution only, as the unknown $\boldsymbol{x}(\boldsymbol{\theta}, \chi)$ occurs on the right-hand side.

Remember,

$$\frac{\mathrm{d}^2 f_K(\chi)}{\mathrm{d}\chi^2} = -K\, f_K(\chi)\;.$$

Source at χ with distance $\boldsymbol{x}$ from fiducial light ray will be seen in the absence of lensing at angular separation $\boldsymbol{\beta} = \boldsymbol{x}/f_K(\chi)$;

hence, define the Jacobian matrix

$$\mathcal{A}(\boldsymbol{\theta}, \chi) = \frac{\partial \boldsymbol{\beta}}{\partial \boldsymbol{\theta}} = \frac{1}{f_K(\chi)} \frac{\partial \boldsymbol{x}}{\partial \boldsymbol{\theta}} \,, \tag{50}$$

and obtain

$$\mathcal{A}_{ij}(\boldsymbol{\theta}, \chi) = \delta_{ij} - \frac{2}{c^2} \int_0^\chi \mathrm{d}\chi' \, \frac{f_K(\chi - \chi') f_K(\chi')}{f_K(\chi)} \, \Phi_{,ik} \left(\boldsymbol{x}(\boldsymbol{\theta}, \chi'), \chi' \right) \, \mathcal{A}_{kj}(\boldsymbol{\theta}, \chi') \tag{51}$$

This equation still is exact (in limit of validity of weak-field metric).

Expand $\mathcal{A}$ in powers of Φ, and keep only up to linear term:

$$\mathcal{A}_{ij}(\boldsymbol{\theta},\chi) = \delta_{ij} - \frac{2}{c^2}\int_0^\chi \mathrm{d}\chi' \, \frac{f_K(\chi-\chi')f_K(\chi')}{f_K(\chi)}\,\Phi_{,ij}\left(f_K(\chi')\boldsymbol{\theta},\chi'\right) \ . \qquad (52)$$

Hence, to linear order, distortion obtained by integrating along the unperturbed ray;

if we define the potential

$$\psi(\boldsymbol{\theta},\chi) := \frac{2}{c^2}\int_0^\chi \mathrm{d}\chi' \, \frac{f_K(\chi-\chi')}{f_K(\chi)f_K(\chi')}\,\Phi\left(f_K(\chi')\boldsymbol{\theta},\chi'\right) \qquad (53)$$

then $\mathcal{A}_{ij} = \delta_{ij} - \psi_{,ij}$, as in ordinary lens theory.

In this approximation, lensing by the 3-D matter distribution can be treated as an equivalent lens plane with deflection potential ψ, mass density $\kappa = \nabla^2\psi/2$, and shear $\gamma = (\psi_{,11} - \psi_{,22})/2 + \mathrm{i}\psi_{,12}$.

Cosmic shear: the principle

Next, we relate κ to density fluctuations δ in the Universe:

1. take 2-D Laplacian of ψ, and add the term $\Phi_{,33}$ in the integrand – that one vanishes through integration along line-of-sight;
2. make use of the 3-D Poisson equation in comoving coordinates

$$\nabla^2\Phi = \frac{3H_0^2\Omega_\mathrm{m}}{2a}\delta \tag{54}$$

to obtain

$$\kappa(\boldsymbol{\theta},\chi) = \frac{3H_0^2\Omega_\mathrm{m}}{2c^2}\int_0^\chi \mathrm{d}\chi' \frac{f_K(\chi')f_K(\chi-\chi')}{f_K(\chi)}\frac{\delta\left(f_K(\chi')\boldsymbol{\theta},\chi'\right)}{a(\chi')}\,. \tag{55}$$

Note: κ is proportional to Ω_m: lensing is sensitive to $\Delta\rho \propto \Omega_\mathrm{m}\,\delta$, not just to $\delta = \Delta\rho/\bar{\rho}$.

3. for a source redshift distribution with $p_z(z)\,\mathrm{d}z = p_\chi(\chi)\,\mathrm{d}\chi$, the effective surface mass density becomes

$$\begin{aligned}\kappa(\boldsymbol{\theta}) &= \int \mathrm{d}\chi\; p_\chi(\chi)\,\kappa(\boldsymbol{\theta},\chi) \\ &= \frac{3H_0^2\Omega_\mathrm{m}}{2c^2}\int_0^{\chi_\mathrm{h}} \mathrm{d}\chi\; g(\chi)\,f_K(\chi)\,\frac{\delta\left(f_K(\chi)\boldsymbol{\theta},\chi\right)}{a(\chi)} \end{aligned} \tag{56}$$

with

$$g(\chi) = \int_\chi^{\chi_\mathrm{h}} \mathrm{d}\chi'\; p_\chi(\chi')\frac{f_K(\chi'-\chi)}{f_K(\chi')}\;, \tag{57}$$

essentially the source-redshift weighted $D_\mathrm{ds}/D_\mathrm{s}$ for a density fluctuation at distance χ.

χ_h is the comoving horizon distance.

Power spectrum of cosmic shear

If $\hat{\kappa}(\boldsymbol{\ell})$ is Fourier-transform of $\kappa(\boldsymbol{\theta})$, then

$$\left\langle \hat{\kappa}(\boldsymbol{\ell})\,\hat{\kappa}(\boldsymbol{\ell}')\right\rangle = (2\pi)^2\,\delta_{\rm D}(\boldsymbol{\ell}+\boldsymbol{\ell}')\,P_\kappa(|\boldsymbol{\ell}|)\;, \tag{58}$$

where $P_\kappa(|\boldsymbol{\ell}|)$ is the **power spectrum** of κ.

It is related to the power spectrum of density fluctuations in the Universe by

$$P_\kappa(\ell) = \frac{9H_0^4\Omega_{\rm m}^2}{4c^4}\int_0^{\chi_{\rm h}}{\rm d}\chi\,\frac{g^2(\chi)}{a^2(\chi)}\,P_\delta\left(\frac{\ell}{f_K(\chi)},\chi\right)\;, \tag{59}$$

The power spectrum P_κ, if observable, can be used to constrain the 3-D power spectrum P_δ.

Different source populations [with different redshift distributions, and thus different $g(\chi)$] yield different projections of P_δ – more information: **'Cosmic shear tomography'**, **'3-D lensing'**.

Cosmology enters

- 'analytically' in $\chi(z)$, $p_z \to p_\chi$; prefactors H_0, Ω_m
- non-analytically in $P_\delta(k, \chi)$

or, put differently,

- geometrically (distance-redshift relation) and
- through structure growth.

There are useful analytic fitting formulae (Peacock & Dodds; Smith et al. for power spectrum; Scoccimarro & Couchman for bispectrum)

... but they are not sufficiently accurate for next generation of CS surveys.

Ray-tracing through LSS simulations seems to be the only way to achieve sufficiently accurate predictions for 3rd generation surveys.

Results from ray-tracing simulation

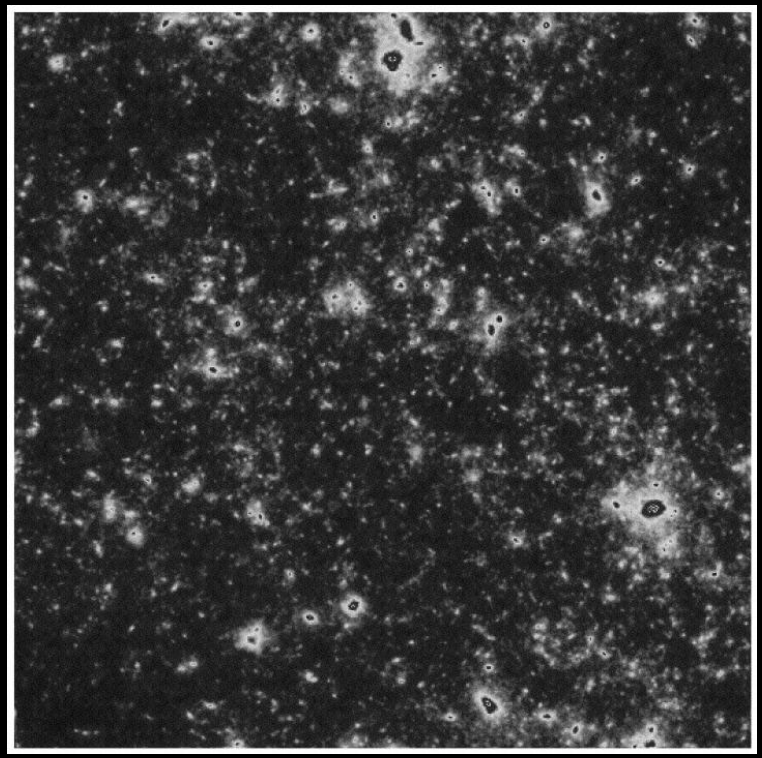

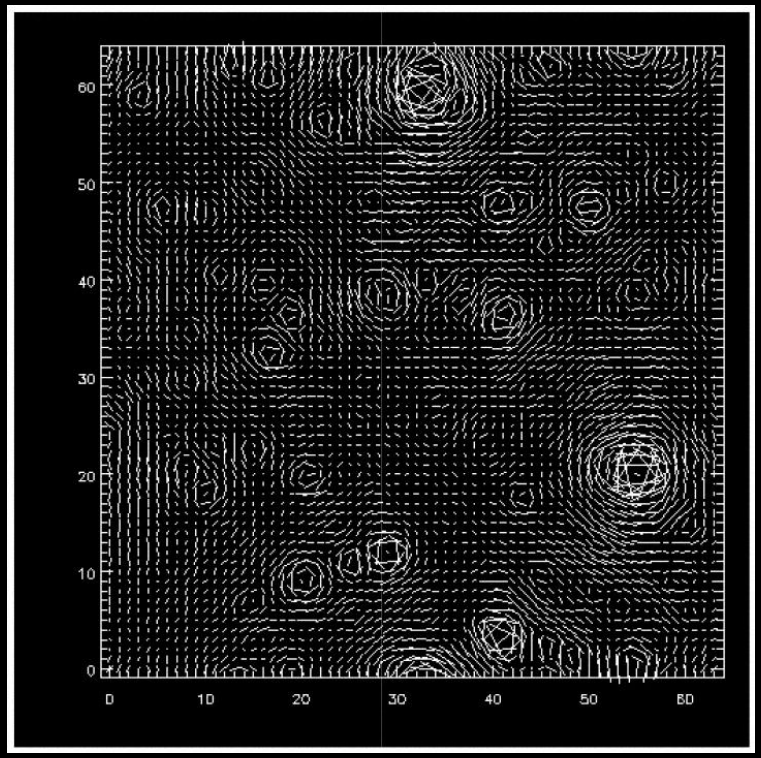

Projected matter density κ Shear field γ

from Jain, Seljak & White 2000

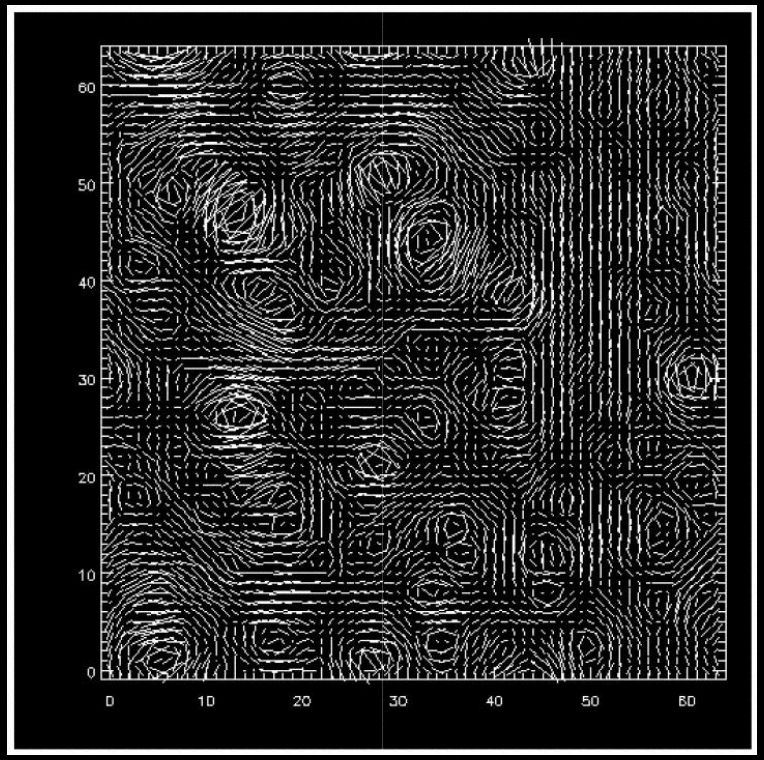

high-density Universe

$\Omega_{\rm m} = 1$

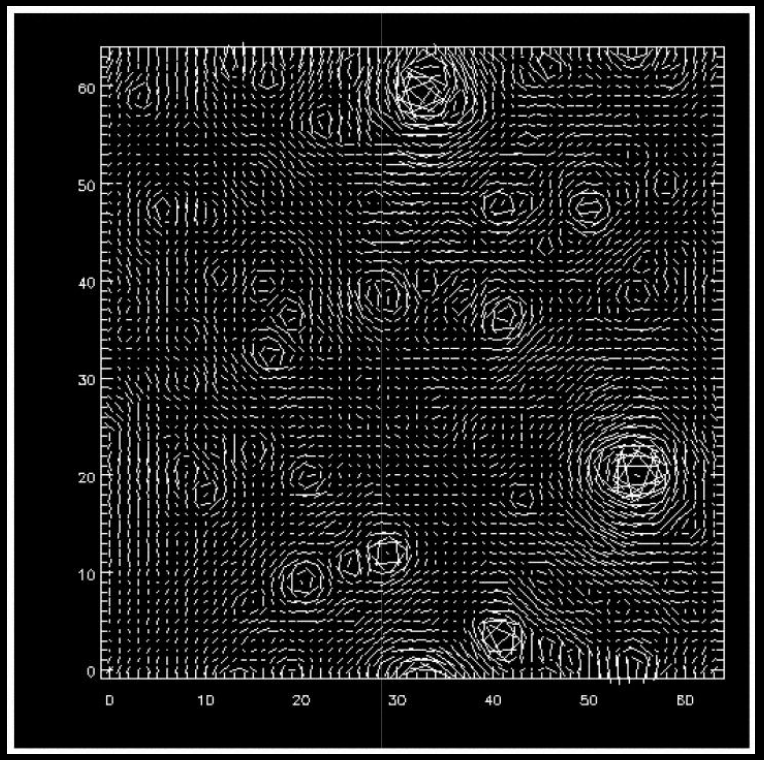

low-density Universe

$\Omega_{\rm m} = 0.3$

from Jain, Seljak & White 2000

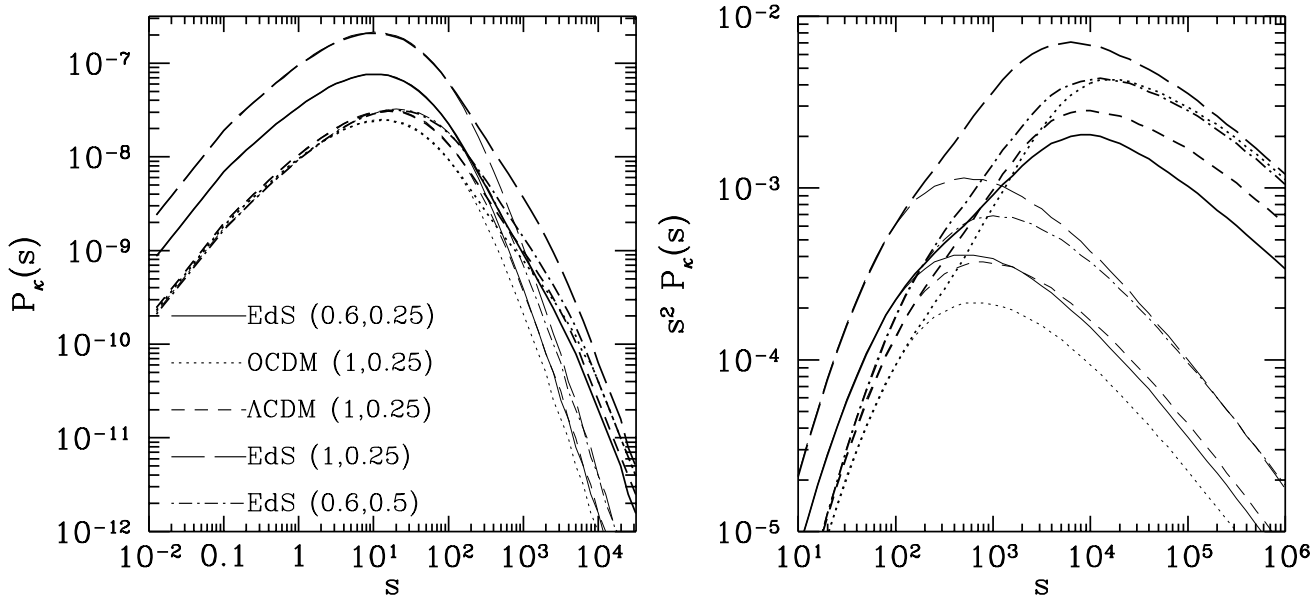

Power spectrum of projected density, $P_\kappa(\ell)$, and its dimensionless form, $\ell^2\,P_\kappa(\ell)$, for various cosmological models, characterized by $(\sigma_8, \Gamma_{\rm spect})$;

thin (thick) lines: linear (non-linear) evolution of the power spectrum;

peak occurs at around $\ell \sim 10^4$, corresponding to $\sim 1'$

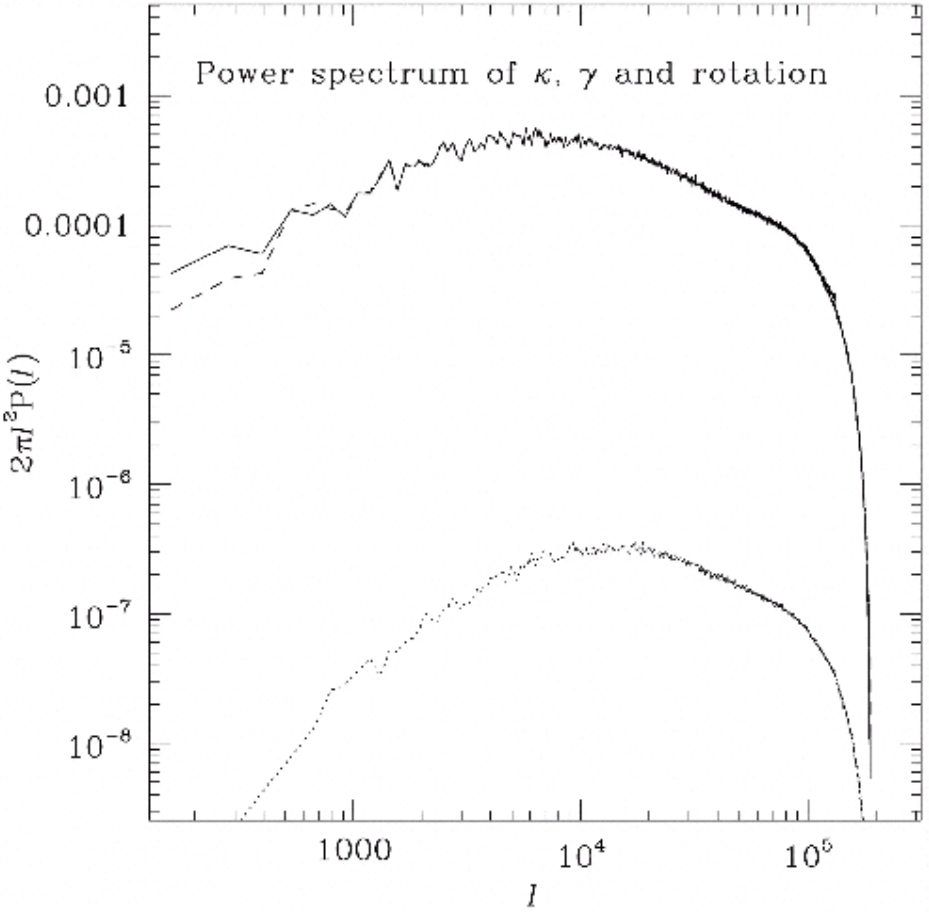

from Jain, Seljak & White (2000)

The foregoing expression is valid, *provided* the Born approximation can be employed and lens-lens-coupling neglected.
Correctly done in ray-tracing simulations!

rotational component seen to be smaller by 3 orders of magnitude; good *indication* that LL-coupling is not very important

Why cosmology from cosmic shear?

- Cosmic shear measures mass distribution at much lower redshifts ($z \lesssim 0.5$) and smaller physical scales [$R \sim 0.3h^{-1}(\theta/1')$Mpc] than CMB;
- Cosmic shear measures non-linearly evolved mass distribution and $P(k)$ at low z;
  in connection with CMB, gravitational instability picture can be tested directly;
- predictions far easier to make than for galaxy surveys – no issues of galaxy biasing;
- breaks degeneracies in parameter space from CMB;
- **most promising method for constraining e.o.s. of Dark Energy;**
- a new (and highly valuable) search method for density peaks (clusters);
- fully independent method!

Second-order cosmic shear measures

- Observable: shear two-point correlation functions $\xi_\pm(\theta)$.
- Other second-order statistics can (and should!!) be derived from them.

Consider pair of points (galaxy images); their separation direction φ is used to define the **tangential and cross-component** of the shear at these positions *for this pair*,

$$\gamma_{\rm t} = -\mathcal{R}{\rm e}\left(\gamma\,{\rm e}^{-2{\rm i}\varphi}\right)\ , \quad \gamma_\times = -\mathcal{I}{\rm m}\left(\gamma\,{\rm e}^{-2{\rm i}\varphi}\right)\ . \tag{60}$$

Then, the shear correlation functions are defined as

$$\begin{aligned}\xi_\pm(\theta) &= \langle\gamma_{\rm t}\gamma_{\rm t}\rangle \pm \langle\gamma_\times\gamma_\times\rangle\,(\theta)\ ,\\ \xi_\times(\theta) &= \langle\gamma_{\rm t}\gamma_\times\rangle\,(\theta)\ .\end{aligned}$$

Due to parity symmetry, $\xi_\times(\theta)$ expected to vanish.

Relation to power spectrum

From definition of $\xi_\pm$, one can show:

$$\xi_+(\theta) = \int_0^\infty \frac{\mathrm{d}\ell\,\ell}{2\pi}\,\mathrm{J}_0(\ell\theta)\,P_\kappa(\ell)\;; \tag{61}$$

$$\xi_-(\theta) = \int_0^\infty \frac{\mathrm{d}\ell\,\ell}{2\pi}\,\mathrm{J}_4(\ell\theta)\,P_\kappa(\ell)\;. \tag{62}$$

$\xi_\pm$ can be measured as follows: on a data field, select all pairs of faint galaxies with separation within $\Delta\theta$ of θ;

take the average $\langle\epsilon_{\mathrm{t}i}\,\epsilon_{\mathrm{t}j}\rangle$ over all pairs; since $\epsilon = \epsilon^{(\mathrm{s})} + \gamma(\boldsymbol{\theta})$, the expectation value of $\langle\epsilon_{\mathrm{t}i}\,\epsilon_{\mathrm{t}j}\rangle$ is $\langle\gamma_\mathrm{t}\gamma_\mathrm{t}\rangle\,(\theta)$, provided source ellipticities are uncorrelated.
Similarly for the cross-component.

The aperture mass

Consider circular aperture of radius θ; for a point inside the aperture, define tangential and cross-components of the shear relative to center of aperture (as before); define

$$M_{\rm ap}(\theta) = \int {\rm d}^2\vartheta \; Q(|\boldsymbol{\vartheta}|)\, \gamma_{\rm t}(\boldsymbol{\vartheta}) \; , \tag{63}$$

with Q: a weight function with support $\vartheta \in [0, \theta]$; e.g.,

$$Q(\vartheta) = \frac{6}{\pi\theta^2} \frac{\vartheta^2}{\theta^2} \left(1 - \frac{\vartheta^2}{\theta^2}\right) {\rm H}(\theta - \vartheta) \; .$$

Dispersion of $M_{\rm ap}(\theta)$ is related to power spetrum as

$$\left\langle M_{\rm ap}^2 \right\rangle (\theta) = \frac{1}{2\pi} \int_0^\infty {\rm d}\ell \; \ell \, P_\kappa(\ell) \, W(\theta\ell) \; , \tag{64}$$

with

$$W(\eta) := \frac{576 {\rm J}_4^2(\eta)}{\eta^4} \; , \tag{65}$$

Interrelations

These various 2-point statistics are interrelated:

1. $\xi_\pm \Leftarrow P_\kappa$ can be inverted to yield:

$$P_\kappa(\ell) = 2\pi \int_0^\infty \mathrm{d}\theta\, \theta\, \xi_+(\theta)\, \mathrm{J}_0(\ell\theta) = 2\pi \int_0^\infty \mathrm{d}\theta\, \theta\, \xi_-(\theta)\, \mathrm{J}_4(\ell\theta) \tag{66}$$

2. Take one of these and plug them into the other $\xi_\pm \Leftarrow P_\kappa$ relation:

$$\xi_+(\theta) = \xi_-(\theta) + \int_\theta^\infty \frac{\mathrm{d}\vartheta}{\vartheta} \xi_-(\vartheta) \left(4 - 12\frac{\theta^2}{\vartheta^2}\right) \;; \tag{67}$$

$$\xi_-(\theta) = \xi_+(\theta) + \int_0^\theta \frac{\mathrm{d}\vartheta\, \vartheta}{\theta^2} \xi_+(\vartheta) \left(4 - 12\frac{\vartheta^2}{\theta^2}\right) \;. \tag{68}$$

3. From (66), one can show that

$$\left\langle M_{\rm ap}^2 \right\rangle(\theta) = \int_0^{2\theta} \frac{\mathrm{d}\vartheta\, \vartheta}{\theta^2}\, \xi_+(\vartheta)\, T_+\left(\frac{\vartheta}{\theta}\right) = \int_0^{2\theta} \frac{\mathrm{d}\vartheta\, \vartheta}{\theta^2}\, \xi_-(\vartheta)\, T_-\left(\frac{\vartheta}{\theta}\right) \;. \tag{69}$$

with $T_\pm$ known functions.

Masking is an issue, even a serious one ....

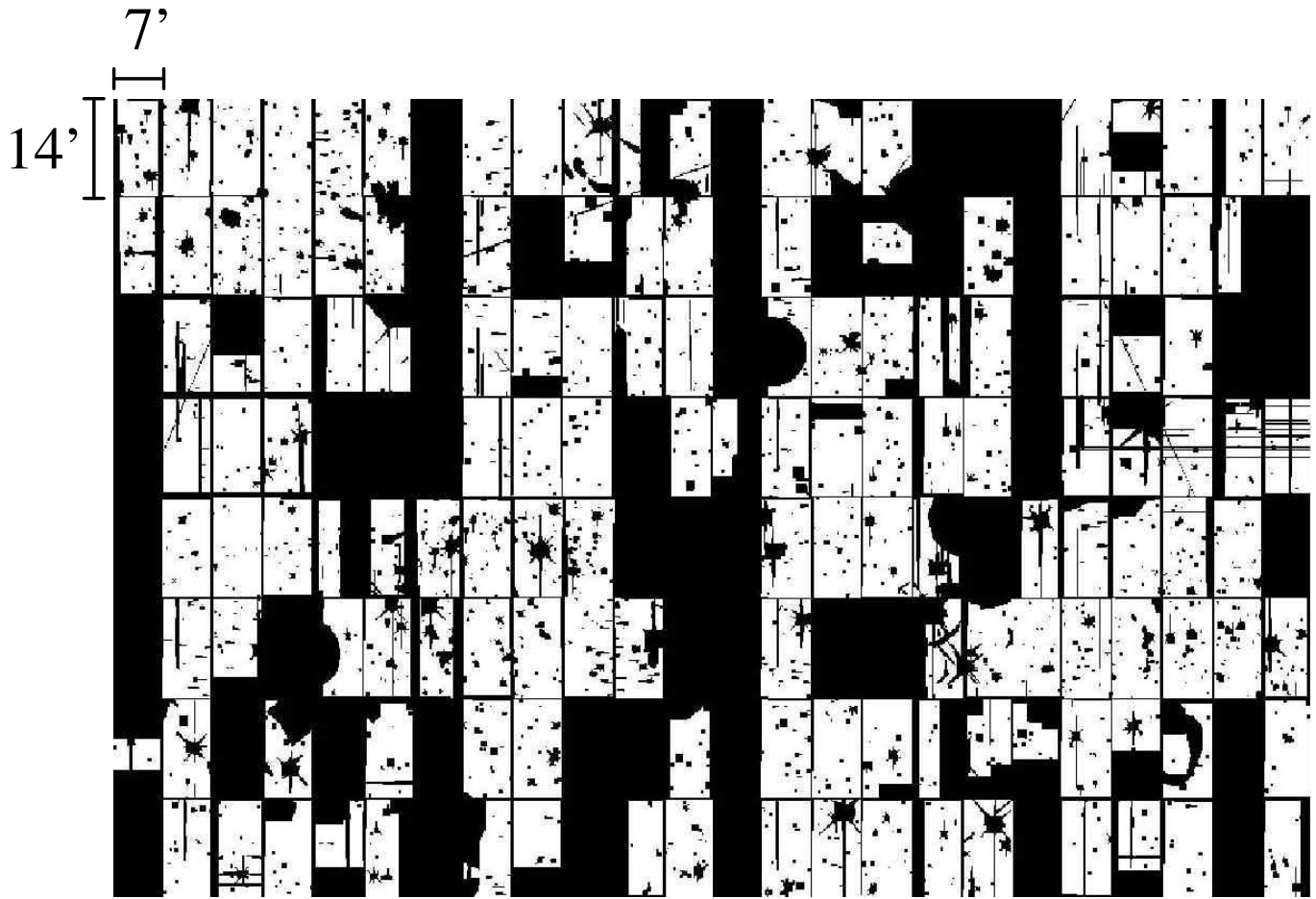

Expectations

Cosmic shear signal depends on

- cosmological model (Ω_m, Ω_Λ, Ω_ν, Γ, w),
- normalization σ_8 of the power spectrum,
- redshift distribution of the sources.

Measuring $\xi_\pm$ over a significant range of θ allows one to constrain these parameters;

measurement accuracy depends on number density of galaxies (that is, depth and quality of the images) and the solid angle covered:

Noise is combination of intrinsic ellipticity dispersion and cosmic variance.

E-modes, B-modes

In the derivation of the lens action of the LSS, we ended up with an equivalent surface mass density;

in particular, $\mathcal{A}$ then is a symmetric matrix;

shear (2-component quantity) then stems from this κ (1-component quantity);

$\Rightarrow$ the two shear components are not independent of each other!

Recall

$$\nabla\kappa = \begin{pmatrix} \gamma_{1,1} + \gamma_{2,2} \\ \gamma_{2,1} - \gamma_{1,2} \end{pmatrix} \equiv \boldsymbol{u}_\gamma(\boldsymbol{\theta}) \ ,$$

this implies $\nabla \times \boldsymbol{u}_\gamma \equiv 0$, a local relation between shear components.

This relation also present at the level of 2-point statistics:
One expects that

$$\int_0^\infty \mathrm{d}\theta\, \theta\, \xi_+(\theta) \mathrm{J}_0(\theta\ell) = \int_0^\infty \mathrm{d}\theta\, \theta\, \xi_-(\theta) \mathrm{J}_4(\theta\ell) \ , \tag{70}$$

since both are proportional to $P_\kappa(\ell)$.

$\Rightarrow$ The two correlation functions $\xi_\pm$ are not independent.

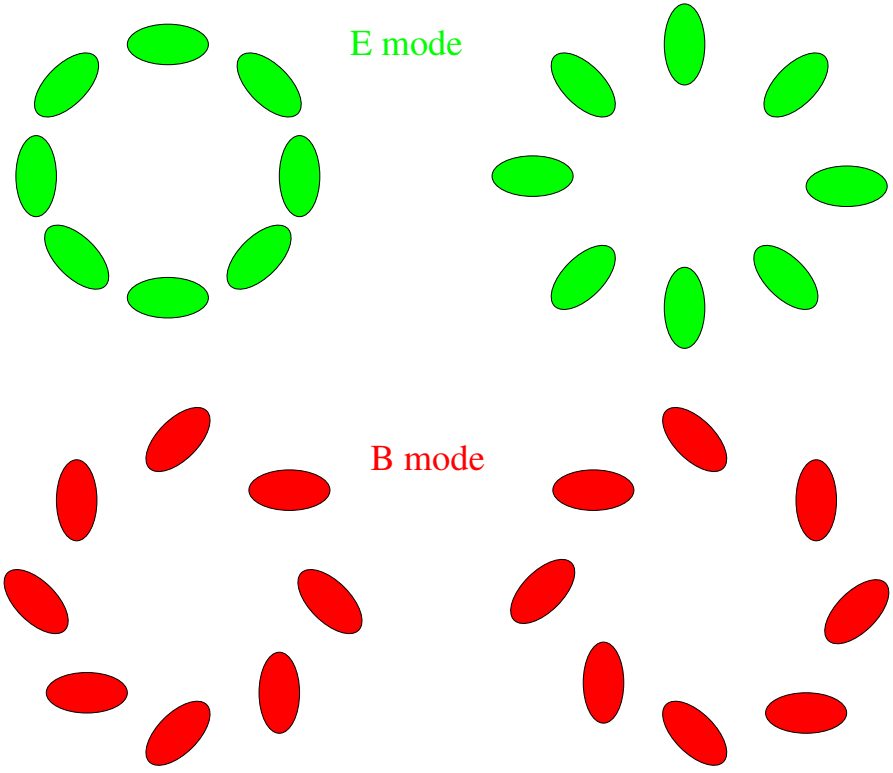

van Waerbeke & Mellier 2003

The observed shear field is not guaranteed to satisfy these relations, due to noise, remaining systematics, ...
however, there might be a 'shear' component present not due to lensing (by a single equivalent thin matter sheet κ).
Shear components which satisfy the foregoing relations are called E-modes; those which don't are B-modes.

One way to separate these modes locally: aperture statistics!

$\langle M_{\rm ap}^2(\theta)\rangle$ is sensitive *only* to E-modes;

if one defines in analogy

$$M_\perp(\theta) = \int \mathrm{d}^2\vartheta\; Q(|\boldsymbol{\vartheta}|)\,\gamma_\times(\boldsymbol{\vartheta})\;,$$

then $\langle M_\perp^2(\theta)\rangle$ is sensitive *only* to B-modes.

In general,

$$\left\langle\hat\gamma(\boldsymbol{\ell})\hat\gamma^*(\boldsymbol{\ell}')\right\rangle = (2\pi)^2\delta_{\rm D}(\boldsymbol{\ell}-\boldsymbol{\ell}')\,[P_{\rm E}(\ell)+P_{\rm B}(\ell)]\;,$$

containing both E- and B-modes.

$$\xi_+(\theta) = \int_0^\infty \frac{\mathrm{d}\ell\,\ell}{2\pi}\,\mathrm{J}_0(\ell\theta)\,[P_{\rm E}(\ell)+P_{\rm B}(\ell)]\;,$$

$$\xi_-(\theta) = \int_0^\infty \frac{\mathrm{d}\ell\,\ell}{2\pi}\,\mathrm{J}_4(\ell\theta)\,[P_{\rm E}(\ell)-P_{\rm B}(\ell)]\;.$$

This can again be inverted to yield:

$$P_{\rm E,B}(\ell) = \pi \int_0^\infty {\rm d}\theta\, \theta\, \left[\xi_+(\theta){\rm J}_0(\theta\ell) \pm \xi_-(\theta){\rm J}_4(\theta\ell)\right] \ .$$

Those can be combined to show that

$$\begin{aligned}
\left\langle M_{\rm ap}^2 \right\rangle(\theta) &= \frac{1}{2\pi}\int_0^\infty {\rm d}\ell\, \ell\, P_{\rm E}(\ell)\, W(\theta\ell) \\
&= \frac{1}{2}\int_0^{2\theta} \frac{{\rm d}\vartheta\, \vartheta}{\theta^2}\, \left[\xi_+(\vartheta)\, T_+(\vartheta/\theta) + \xi_-(\vartheta)\, T_-(\vartheta/\theta)\right] \ , \qquad (71) \\
\left\langle M_\perp^2 \right\rangle(\theta) &= \frac{1}{2\pi}\int_0^\infty {\rm d}\ell\, \ell\, P_{\rm B}(\ell)\, W(\theta\ell) \\
&= \frac{1}{2}\int_0^{2\theta} \frac{{\rm d}\vartheta\, \vartheta}{\theta^2}\, \left[\xi_+(\vartheta)\, T_+(\vartheta/\theta) - \xi_-(\vartheta)\, T_-(\vartheta/\theta)\right] \ , \qquad (72)
\end{aligned}$$

where, as before, $\qquad W(t) := \dfrac{576{\rm J}_4^2(t)}{t^4} \ .$

Note, $\left\langle M_{\rm ap}^2 \right\rangle$ depends only on E-modes, and $\left\langle M_\perp^2 \right\rangle$ only on B-modes!

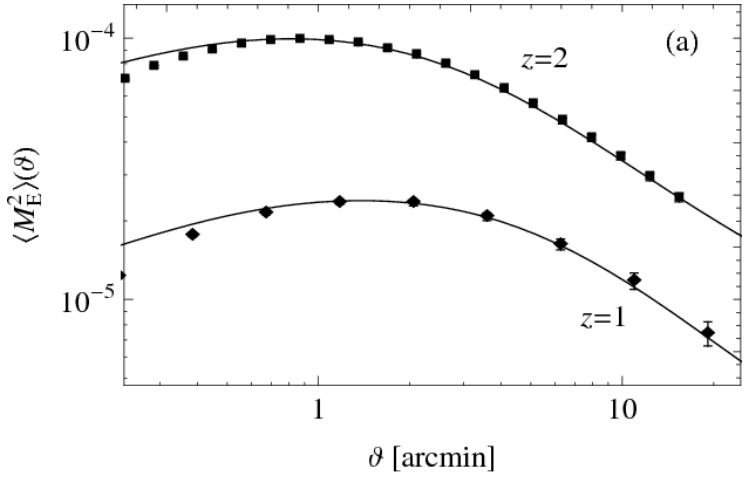

Ray-tracing prediction for E-/B-mode aperture dispersion;

based on Millennium Simulation;

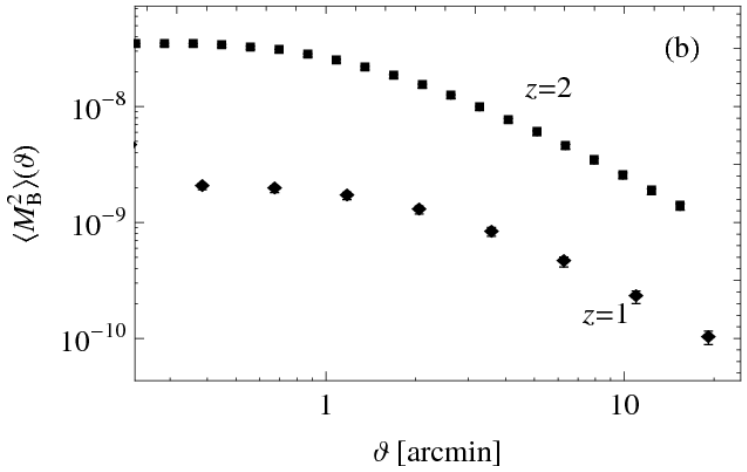

B-modes are so small as to be undetectable – hence, in observations, they should be compatible with zero;

from Hilbert et al. (2009).

COSEBIs

Complete Orthogonal Set of E-/B-mode Integrals, can be defined in terms of $\xi_\pm(\vartheta)$ for $\vartheta_{\rm min} \leq \vartheta \leq \vartheta_{\rm max}$.

Defined similarly as before,

$$E_n, B_n = \int_{\vartheta_{\rm min}}^{\vartheta_{\rm max}} {\rm d}\vartheta\, \vartheta\, \left[\xi_+(\vartheta)\, T_{n+}(\vartheta) \pm \xi_-(\vartheta)\, T_{n-}(\vartheta)\right] \ , \tag{73}$$

with weights $T_{n\pm}(\vartheta)$ chosen appropriately.

- COSEBIs yield E-/B-mode separation,
- contain the full information of the $\xi_\pm$ on finite interval,
- are **very** effective in data compression (only the first few modes contain significant cosmological information)!

Parameter estimate

Let $\mathbf{2}(\theta)$ be observed 2-pt shear statistics, like the 2PCF or the E_n;
that needs to be compared to corresponding statistics from cosmological model:
$\boldsymbol{p}$: set of parameters, e.g., $\Omega_\mathrm{m}, \Omega_\mathrm{DE}, H_0, \sigma_8, n_\mathrm{s}, \Omega_\mathrm{b}; w, w', \ldots$
models, fit formulae or simulations $\Rightarrow P_\delta(k;\boldsymbol{p})$
+ redshift distribution of sources $\Rightarrow P_\kappa(\ell,\boldsymbol{p})$
$\Rightarrow$ 2-pt.-stats. of shear,

$$\mathbf{2}(\theta) = \int \mathrm{d}\ell\; \ell\, W_{\mathbf{2}}(\ell\theta)\, P_\kappa(\ell;\boldsymbol{p})\;. \tag{74}$$

Parameters $\boldsymbol{p}$ estimated by maximizing likelihood

$$\mathcal{L}(\boldsymbol{p}) = \frac{1}{(2\pi)^{n/2}\sqrt{\det \mathrm{Cov}}}\, \exp\left(\frac{-\chi^2(\boldsymbol{p},\mathbf{2}^\mathrm{obs})}{2}\right)\; P_\mathrm{prior}(\boldsymbol{p})\;, \tag{75}$$

with

$$\chi^2(p, \mathbf{2}^{\rm obs}) = \sum_{ij} \left(\mathbf{2}_i(p) - \mathbf{2}_i^{\rm obs}\right) \, {\rm Cov}_{ij}^{-1} \, \left(\mathbf{2}_j(p) - \mathbf{2}_j^{\rm obs}\right) \ . \tag{76}$$

Cov: Covariance of the observables; rather difficult to obtain in general!

Either Gaussian approximation (analytic), or log-normal approximation (quite accurate!), or through simulations.

Additional cosmic shear statistics

- Higher-order correlations (3PCFs);
  probe non-Gaussian nature of density field,
  difficult to predict (8 functions with 3 arguments)
  not to mention covariance
- Peak statistics
  difficult to apply on data fields with gaps
  however, very sensitive probe

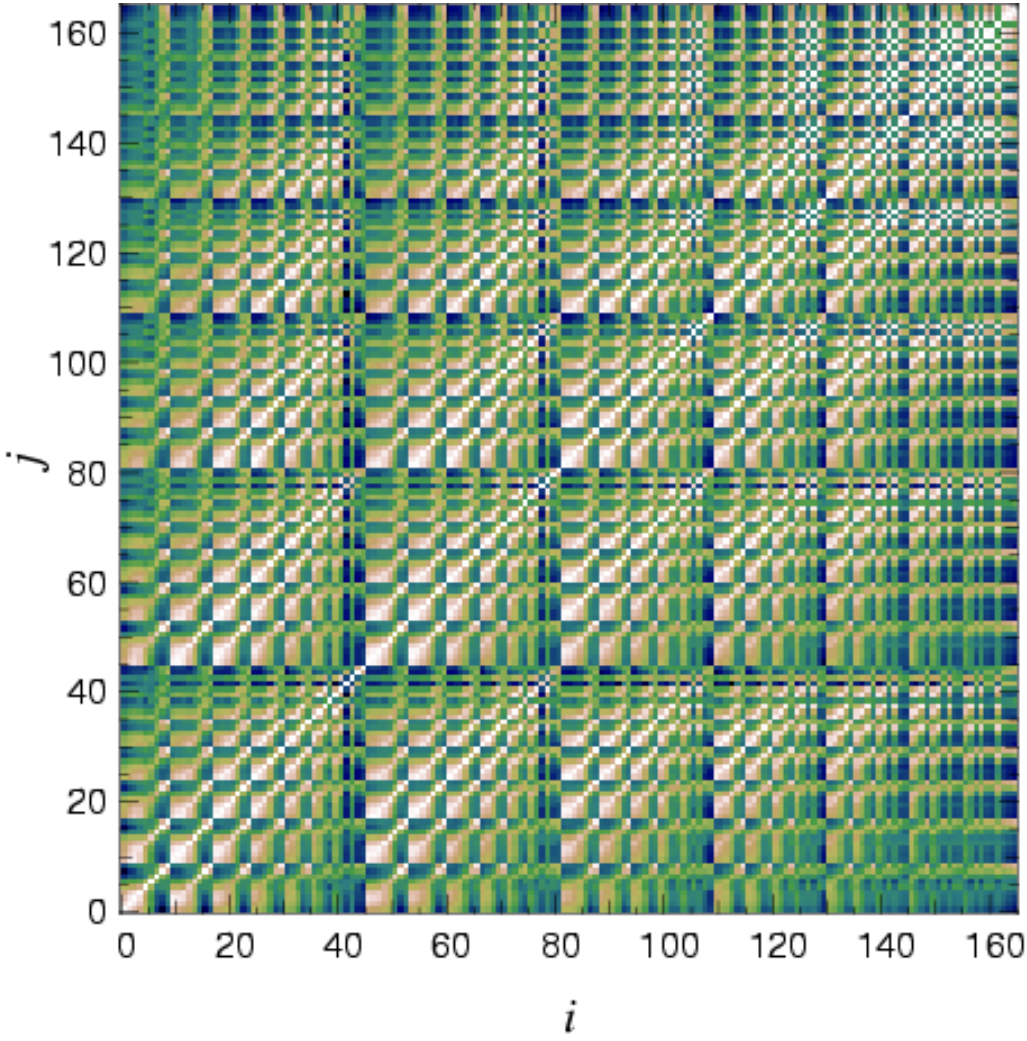

Covariance matrix of $\left\langle M_{\rm ap}^3 \right\rangle (\theta_1, \theta_2, \theta_3)$, for 9 bins in θ_i; relabeling was needed to display (and invert) the covariance matrix – difficult to invert, not diagonal-dominant ...
determined from ray-tracing simulations of T. Hamana, by patch-to-patch variance
from Kilbinger & Schneider (2005)

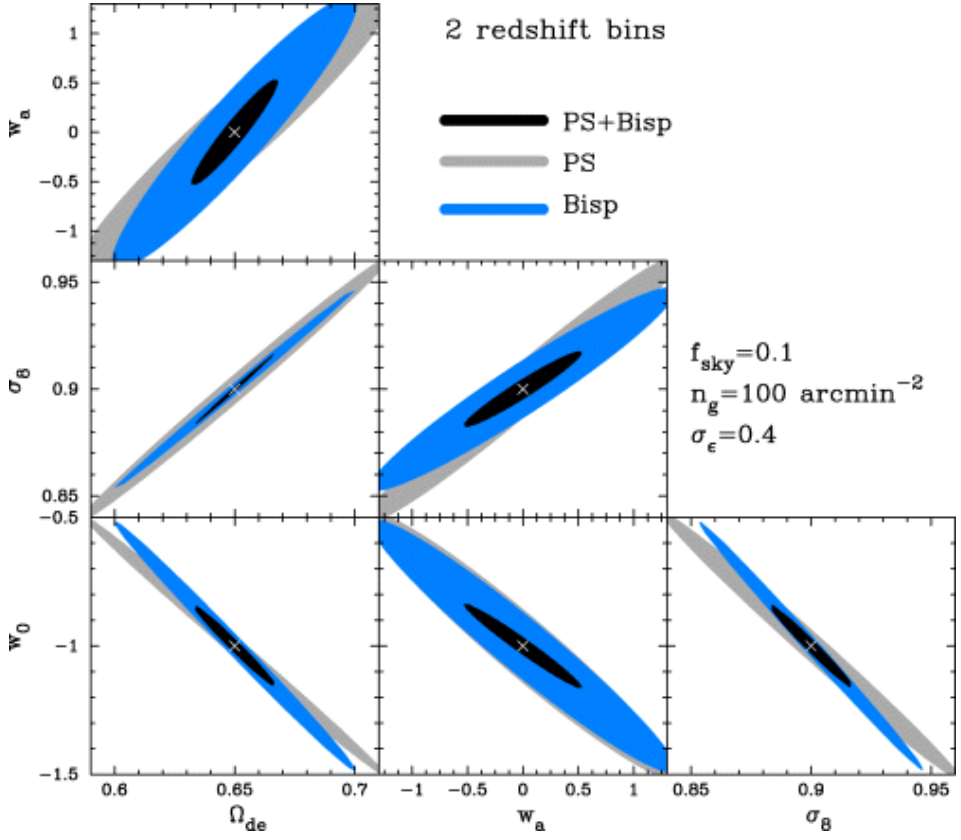

Higher-order shear statistics yield very valuable information;
here in combination with redshift slicing (just two z-bins)
simplified expressions for covariance matrices – 'Gaussian'.
from Takada & Jain (2004)

Large-scale structure lensing: results

In March 2000 ...

... four independent groups announced significant detection of cosmic shear:

- Bacon, Refregier & Ellis used 14 fields of $8' \times 16'$, from WHT;
- Kaiser, Wilson & Luppino used 6 fields of $30' \times 30'$, from UH8K at CFHT; total of ~ 120000 galaxies;
- van Waerbeke et al. used 8 fields from UH8K and CFH12K ($30' \times 45'$); total of ~ 170000 galaxies
- Wittman et al. used 3 fields of $43' \times 43'$ from BTC at CTIO; total of ~ 135000 galaxies.

In Nov. 2000, Maoli et al. announced cosmic shear measurement using 50 fields from VLT/FORS1 with $\sim 6'.5 \times 6'.5$, with a total of ~ 47000 galaxies

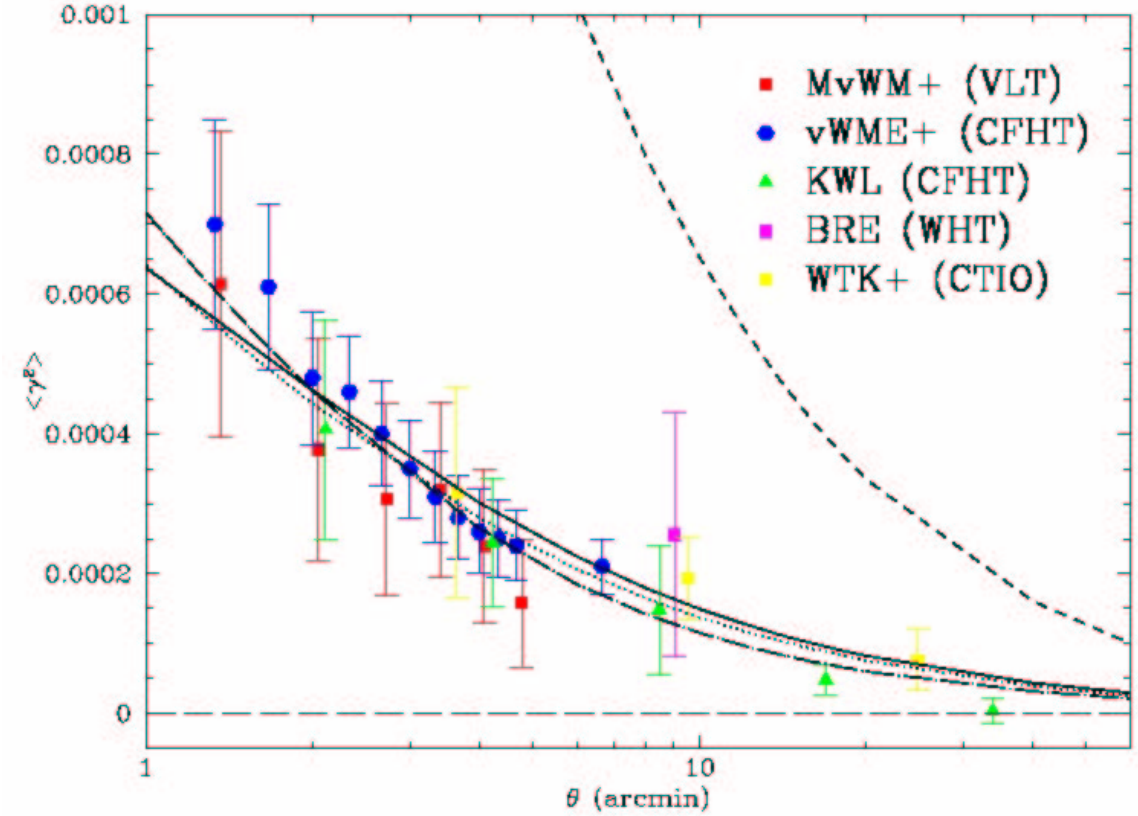
0.001
0.0008
0.0006
0.0004
0.0002
0
1
10
θ (arcmin)
<γ²>
MvWM+ (VLT)
vWME+ (CFHT)
KWL (CFHT)
BRE (WHT)
WTK+ (CTIO)

First conclusion: Cosmic shear measured

Results from

- 4 independent (and competing) teams,
- 4 telescopes,
- 5 cameras,
- independent data reductions,
- at least 2 independent ellipticity measurement schemes

agree remarkably well.

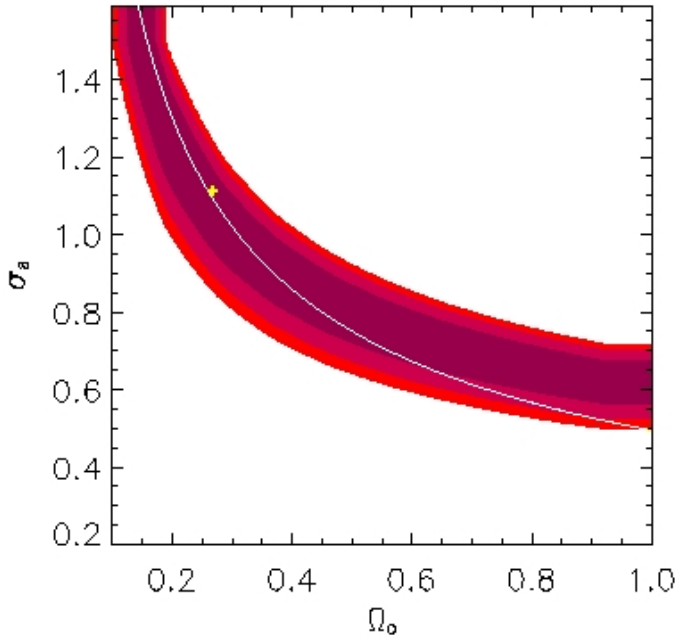

Constraints on $\Omega_{\rm m}$ and σ_8 from these five surveys;
best fit is $\Omega_{\rm m} = 0.26$, $\sigma_8 = 1.1$, but solution highly degenerate;
$\sigma_8 \sim 0.59\Omega_{\rm m}^{-0.47}$
very similar to constraint from cluster abundance (white curve)!

This is a non-trivial result:
cluster abundance depends on assumption of initial Gaussian random field, cosmic shear constraint is independent on this assumption.

Further surveys

- Additional surveys carried out afterwards – from ground and with HST
- Larger area $\Rightarrow$ better statistics
- Soon one started to worry more about systematics than statistics

Detection of B-modes

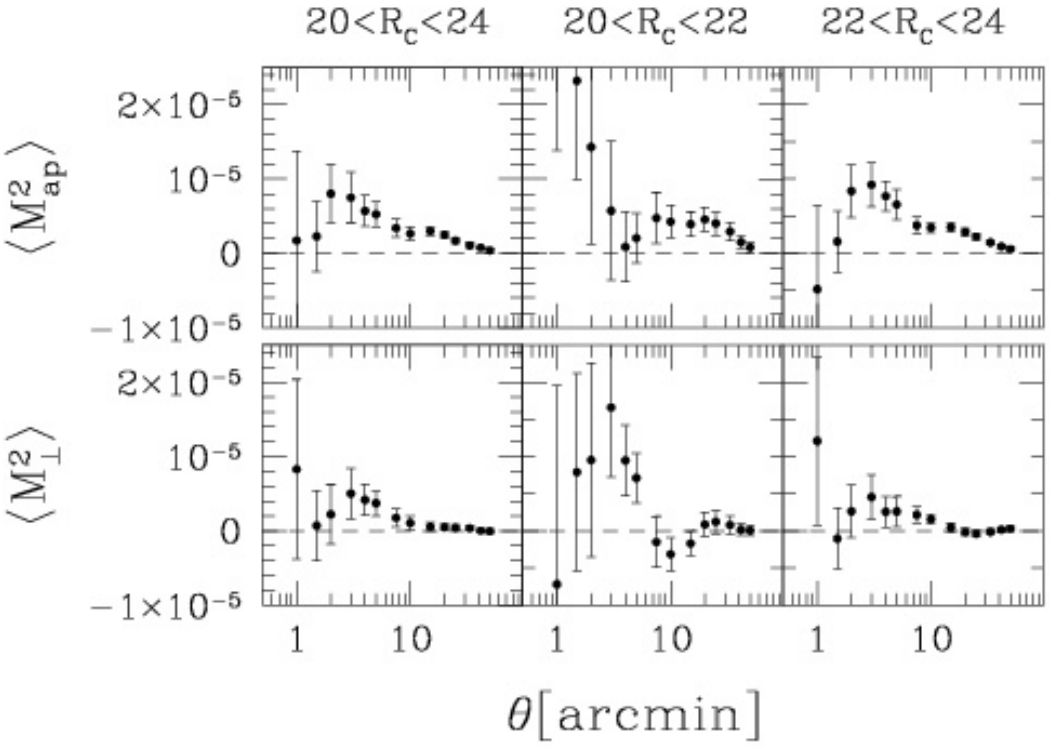

From the Red Cluster Sequence survey (Hoekstra et al. 2002)

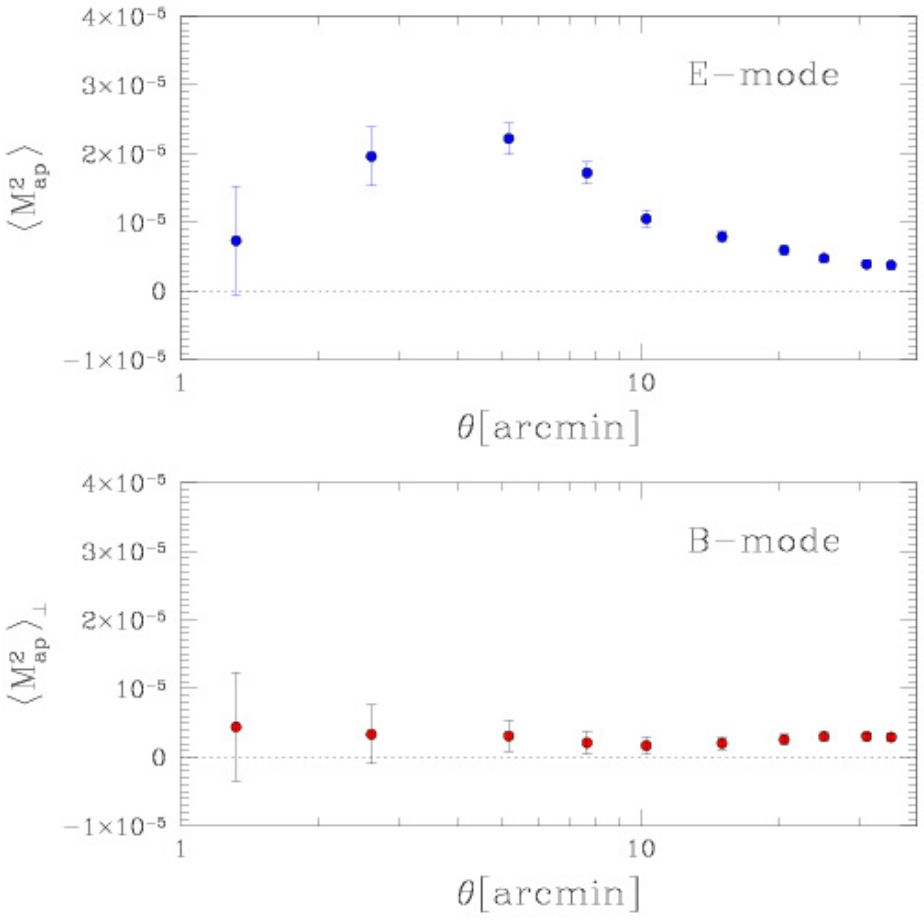

From the VIRMOS-DESCART survey; B-mode signal detected, though at smaller amplitude that E-mode signal;
in the analysis, amplitude of B-mode is added to error bars of the E-mode signal, to roughly account for this potential systematic error (van Waerbeke et al. 2002)
Note that $M_{\rm ap}(\theta)$ quickly decorrelates between different angular scales.

Table 1: Constraints on the power spectrum normalisation "σ_8" for $\Omega_m = 0.3$ for a flat Universe (from van Waerbeke et al. 2002)

ID	σ_8	Statistic	Field	$m_{\rm lim}$	CosVar	E/B	z_s	Γ
Maoli et al. 01	1.03 ± 0.05	$\langle\gamma^2\rangle$	VLT+CTIO+ WHT+CFHT	-	no	no	-	0.21
LVW et al. 01	0.88 ± 0.11	$\langle\gamma^2\rangle$, $\xi(r)$ $\langle M_{\rm ap}^2\rangle$	CFHT 8 sq.deg.	I=24	no	no (yes)	1.1	0.21
Rhodes et al. 01	$0.91^{+0.25}_{-0.29}$	$\xi(r)$	HST 0.05 sq.deg.	I=26	yes	no	0.9-1.1	0.25
Hoekstra et al. 01	0.81 ± 0.08	$\langle\gamma^2\rangle$	CFHT+CTIO 24 sq.deg.	R=24	yes	no	0.55	0.21
Bacon et al. 02	0.97 ± 0.13	$\xi(r)$	Keck+WHT 1.6 sq.deg.	R=25	yes	no	0.7-0.9	0.21
Refregier et al. 02	0.94 ± 0.17	$\langle\gamma^2\rangle$	HST 0.36 sq.deg.	I=23.5	yes	no	0.8-1.0	0.21
LVW et al. 02	0.94 ± 0.12	$\langle M_{\rm ap}^2\rangle$	CFHT 12 sq.deg.	I=24	yes	yes	0.78-1.08	0.1-0.4
Hoekstra et al. 02	$0.91^{+0.05}_{-0.12}$	$\langle\gamma^2\rangle$, $\xi(r)$ $\langle M_{\rm ap}^2\rangle$	CFHT+CTIO 53 sq.deg.	R=24	yes	yes	0.54-0.66	0.05-0.5
Brown et al. 02	0.74 ± 0.09	$\langle\gamma^2\rangle$, $\xi(r)$	ESO 1.25 sq.deg.	R=25.5	yes	no (yes)	0.8-0.9	-
Hamana et al. 02	$(2\sigma)0.69^{+0.35}_{-0.25}$	$\langle M_{\rm ap}^2\rangle$, $\xi(r)$	Subaru 2.1 sq.deg.	R=26	yes	yes	0.8-1.4	0.1-0.4
Jarvis et al. 02	$(2\sigma)0.71^{+0.12}_{-0.16}$	$\langle\gamma^2\rangle$, $\xi(r)$ $\langle M_{\rm ap}^2\rangle$	CTIO 75 sq.deg.	R=23	yes	yes	0.66	0.15-0.5

Cosmic shear from CFHTLS

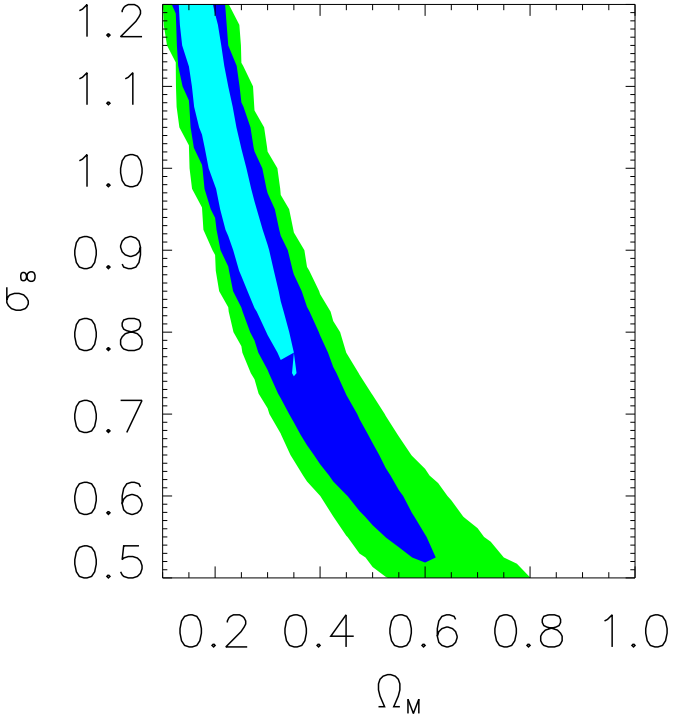

Semboloni et al. 2005

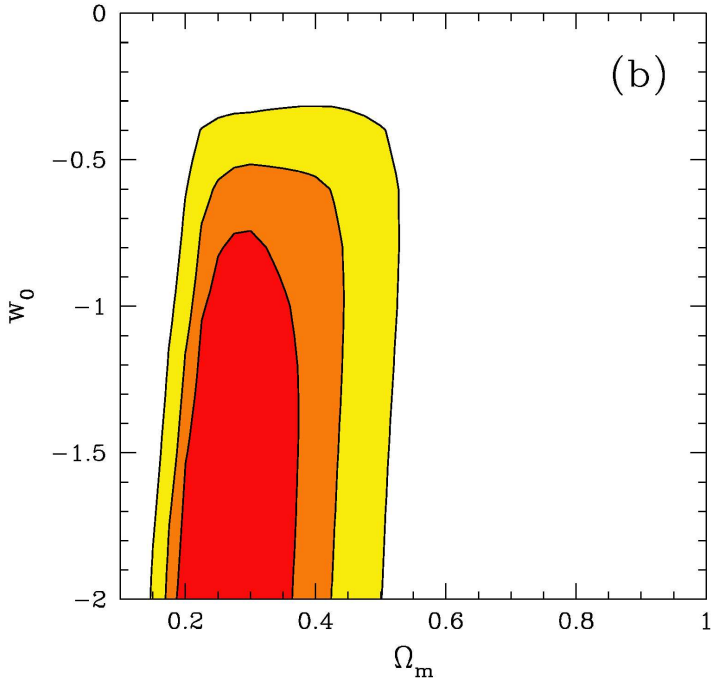

Hoekstra et al. 2005

Example: CTIO survey (Jarvis et al. 2005)

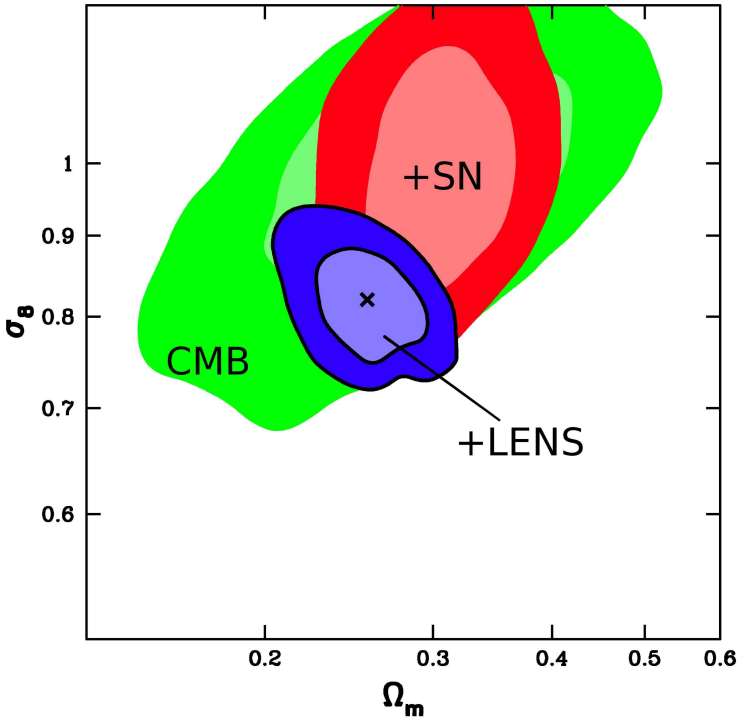

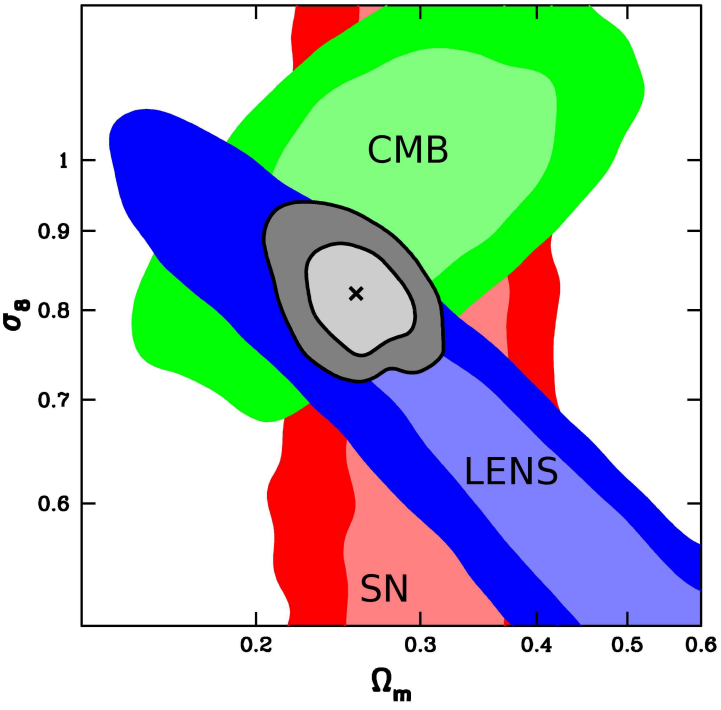

here, $w \equiv -1$

w left as free parameter:

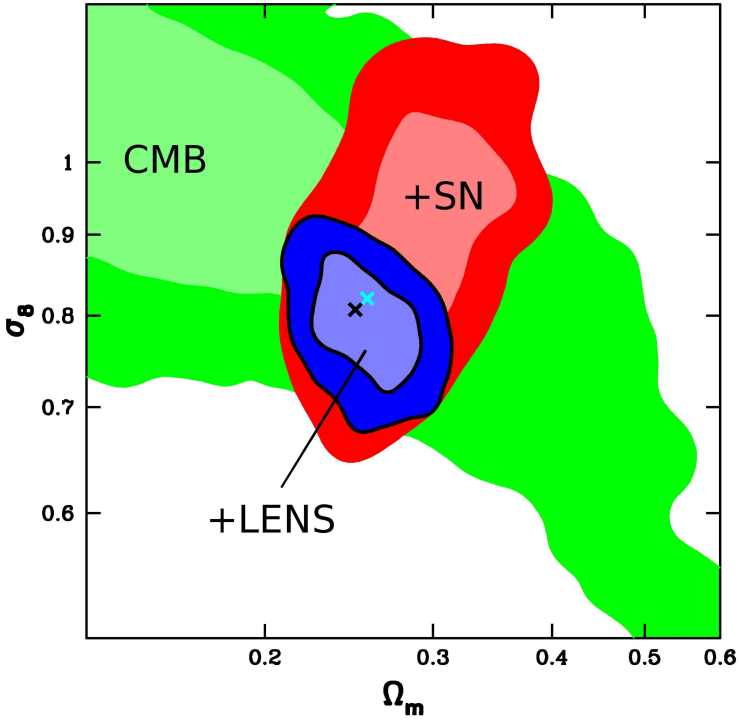

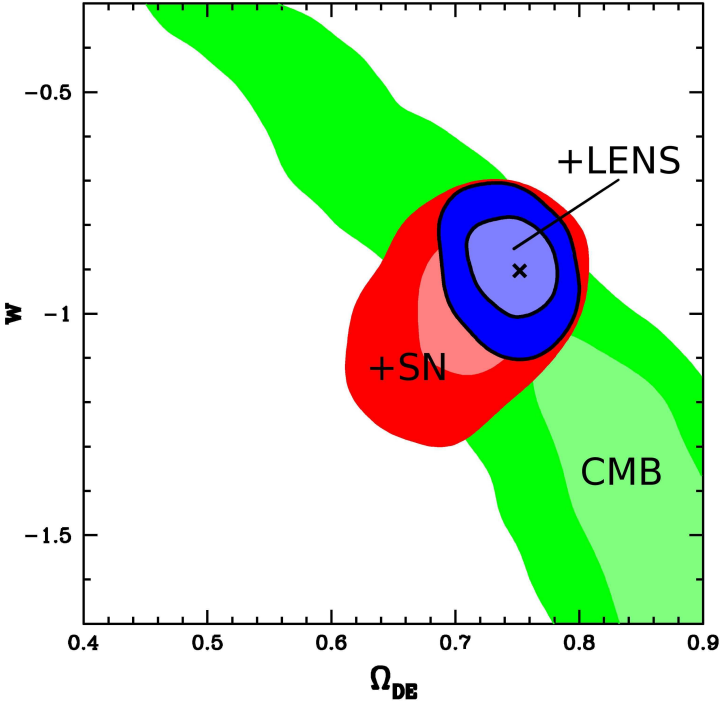

Example: GaBoDS survey (Hetterscheidt et al. 2005)

constraints obtained with two different cosmic shear statistics

small contours:
result from WMAP

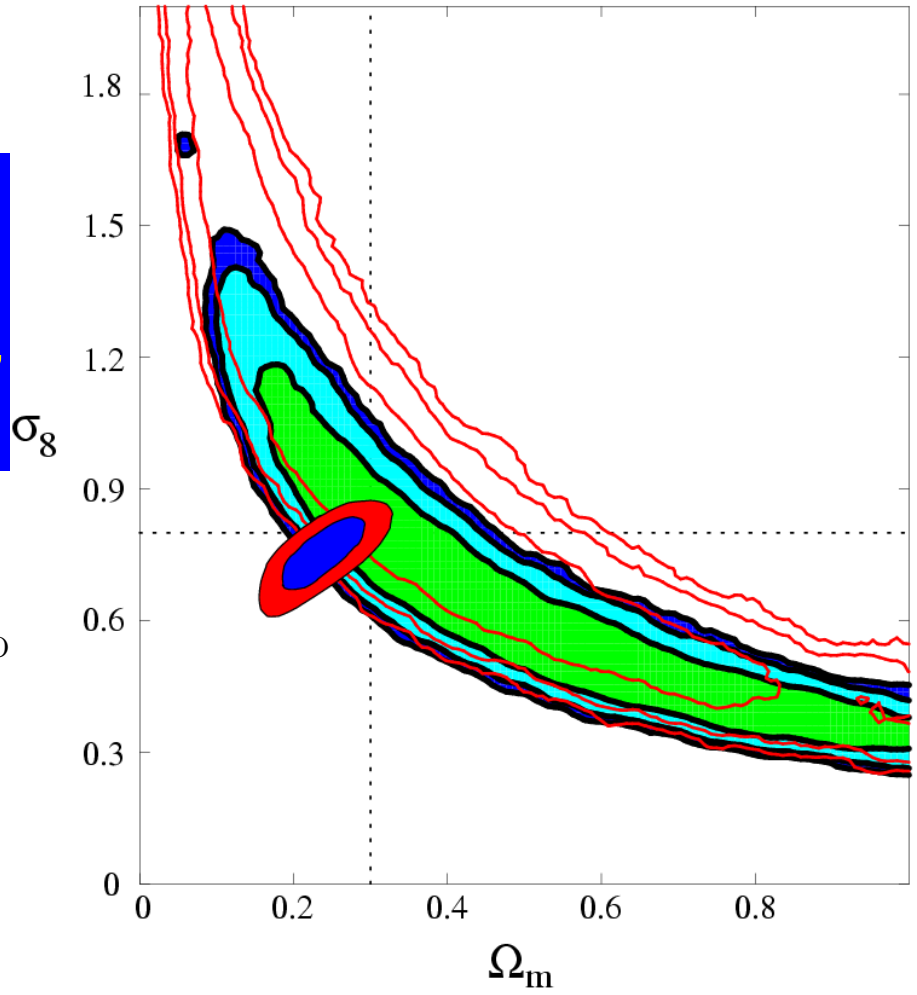

Determination of σ_8 ($\Omega_{\rm m} = 0.3$ assumed)

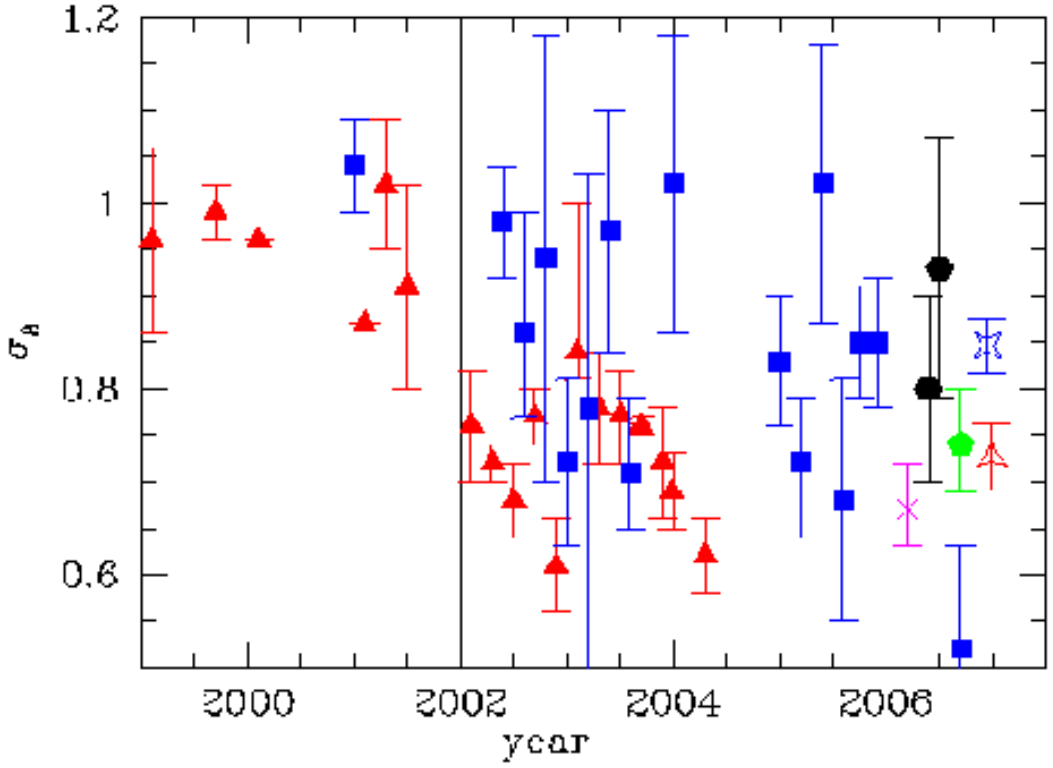

red: from clusters

blue: cosmic shear

black hexagon: GaBaDS

black pentagon: WMAP-3

from Hetterscheidt et al. (2006)

σ_8 is one of the worst determined cosmological parameter !

Systematics

Categories (subjective)

- **(A) Lot's of work been done, still some remains**

Systematics

Categories (subjective)

- **(A) Lot's of work been done, still some remains**
- **(B) Lot's of work to be done, but I don't lose sleep on it**

Systematics

Categories (subjective)

- **(A) Lot's of work been done, still some remains**
- **(B) Lot's of work to be done, but I don't lose sleep on it**
- **(C) I still don't lose sleep, but hope a few others do**

Systematics

Categories (subjective)

- **(A) Lot's of work been done, still some remains**
- **(B) Lot's of work to be done, but I don't lose sleep on it**
- **(C) I still don't lose sleep, but hope a few others do**
- **(D) Unless we get substantially more funding and a brand new great idea ...**

Systematics

Categories (subjective)

- **(A) Lot's of work been done, still some remains**
- **(B) Lot's of work to be done, but I don't lose sleep on it**
- **(C) I still don't lose sleep, but hope a few others do**
- **(D) Unless we get substantially more funding and a brand new great idea ...**
- **(E) Probably, $w \equiv -1$ anyway, and searching for life on Mars is a valuable career alternative**

Principle of shear estimate (KSB, Luppino & Kaiser '97)

$$\epsilon = (P^g)^{-1} \left(\hat{\epsilon}^{\rm obs} - P^{\rm sm} q\right) \ . \tag{77}$$

(A) PSF anisotropy correction

many methods proposed to get PSF anisotropy q – polynomial and rational function interpolation, PCA, correlation between different exposures;
good checks: B-modes, parity-violating modes ($\left\langle E^n B^{\rm odd}\right\rangle \equiv 0$), stellar ellipticity-shear correlations

(C) Smearing correction

several methods (KSB, shapelets); difficult to check;
self-calibration of data, e.g. through consistency;
for example one might use $\mathbf{4} \approx F(\mathbf{2}, \mathbf{3})$;
even now a 2% accuracy achievable (STEP)

(A) Intrinsic correlations and (C) shape–shear correlations

Let $\epsilon = \epsilon^{\rm s} + \gamma$, $z_1 \leq z_2$:

$$\begin{aligned}
\langle \epsilon_1 \epsilon_2^* \rangle &= \langle \epsilon_1^{\rm s} \epsilon_2^{\rm s*} \rangle \ : \text{intrinsic}, \ = 0 \text{ unless } z_1 \approx z_2 \\
&+ \langle \epsilon_1^{\rm s} \gamma_2^* \rangle \ : \text{hopefully}, \ = 0 \\
&+ \langle \gamma_1 \epsilon_2^{\rm s*} \rangle \ : \equiv 0 \\
&+ \langle \gamma_1 \gamma_2^* \rangle \ : \text{WANTED!}
\end{aligned}$$

(A): intrinsic correlations can be eliminated 'easily' with phot-z

(C): can be non-zero if ellipticity of light is affected by tidal field of environment; can be controlled, e.g., through z-dependence of signal

(A) Shear versus reduced shear

$$\langle \epsilon \rangle = \frac{\gamma}{1 - \kappa}$$

no real problem:
(a) approximate corrections are known analytically;
(b) automatically accounted for in ray-tracing simulations (needed anyway)

(C) Accuracy of predictions

good fitting formulae for $P_\delta(k,\chi)$, but not good enough for 3rd generation surveys;
no accurate model or fit for bispectrum;
no dark energy simulations yet;
N-body not good enough, baryons affect mass distribution on small scales;
accuracy of data will soon exceed accuracy of predictions (in particular true for 3rd-order statistics).

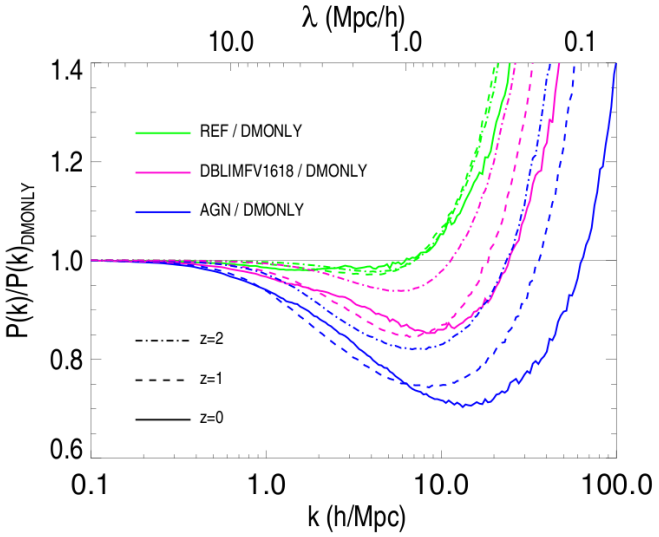

Higher-order statistics contains essential additional information, not yet included in most forecasts.

Theoretical predictions need to be improved (e.g., influence of baryons on power spectrum)

from Semboloni et al. (2011) based on OWL simulations.

⇒ **Extensive simulation effort required!** ⇐

Accuracy with which the power spectrum needs to be known (in the worst case) in order for systematics to be smaller than statistical (sampling variance) errors

from Huterer & Takada (2004)

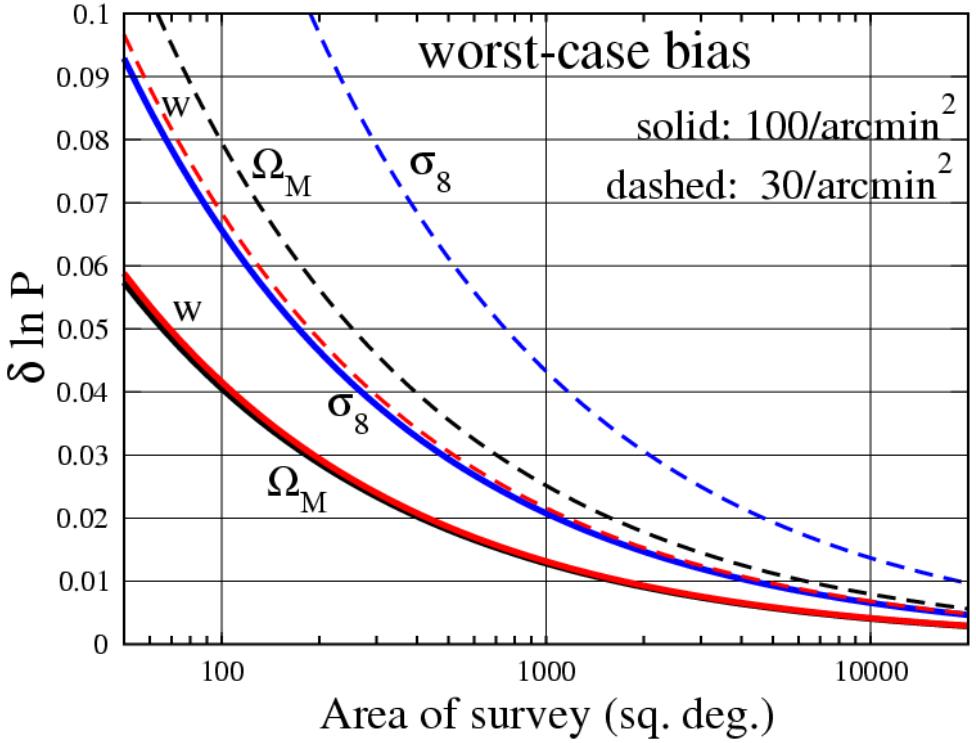

(B) Source clustering

more fg. galaxies in high-shear regions;
will affect 3PCF, and needs to be controlled by simulations.

(C) Foreground light masks, selection bias + strong lensing

centers of clusters & groups need to be 'masked out' due to bright galaxies and strong lensing effects (cf. center of A1689);
close pairs of images need to be eliminated due to blending, causes 'selection bias'
can be controlled partly by simulations

(B) (photometric) redshift estimates

requires accuracy, not precision:
not z of every galaxy needs to be determined very well, but statistical properties of z-distribution (mean, dispersion) in each bin must be known very accurately
but there is also self-calibration

Where are we now?

- Cosmic shear measured by several groups since 2000!
- Currently, systematics smaller than statistical uncertainty.
  New shear measurement techniques being developed.
  Methods to elimate intrinsic alignments are in place.
- Cosmic shear has yielded useful constraints on σ_8.
- CFHTLenS, deep ground-based, multi-color surveys over $170\,\mathrm{deg}^2$,
  with $n \sim 15\,\mathrm{arcmin}^{-2}$; $\langle z_\mathrm{s} \rangle \sim 0.9$;
- RCS2, shallower ground-based surveys over $\sim 900\,\mathrm{deg}^2$,
  with $n \sim 8\,\mathrm{arcmin}^{-2}$; $\langle z_\mathrm{s} \rangle \sim 0.6$;
- Space-based surveys over $\lesssim 2\,\mathrm{deg}^2$, with $n \sim 60\,\mathrm{arcmin}^{-2}$;
  $\langle z_\mathrm{s} \rangle \sim 1.2$ (COSMOS).

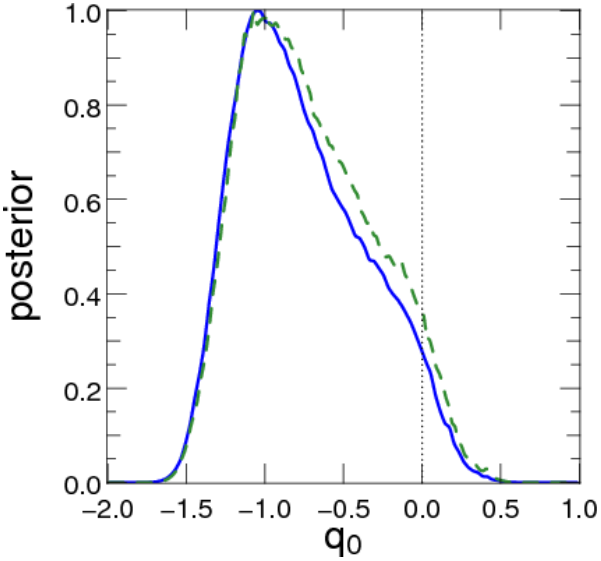

State of the art

From HST-COSMOS survey, independent evidence for cosmic acceleration
(from $\sim 1.5\,\mathrm{deg}^2$ of HST imaging – COSMOS)
EUCLID will cover 10^4-times the area !!!
Schrabback et al. (2010)

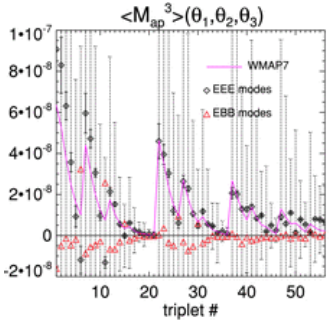

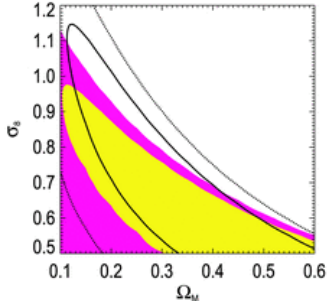

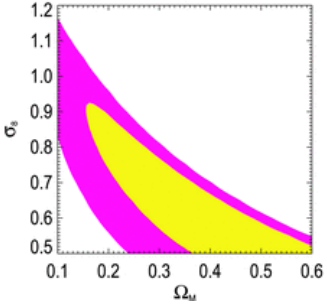

Semboloni et al. (2011)

Constraints from cosmic shear in
Ω_m-σ_8-plane
Here in combination with third-order cosmic shear measurements

Soon, oh soon....

will the results from CFHTLenS collaboration be published; they *greatly* improve over previous results, for cosmic shear, galaxy-galaxy lensing, ... stay tuned.

What comes next: The KiDS Survey

Kilo-Degree Survey (KiDS): a wide-field imaging survey,

carried out with new OmegaCAM@VST, a new 2.6-m telescope on Paranal

$1500\,\mathrm{deg}^2$ in 5 optical bands + suppl. 4 NIR bands (VISTA)
$\Rightarrow$ accurate photometric redshifts

2 mag. deeper that SDSS; $n \sim 12/\mathrm{arcmin}^2$, ongoing (since Sept. 2011)

... and DES and HSC

Dark Energy Survey: $5000\,\mathrm{deg}^2$ in 4 optical bands, to start in 2013.

HyperSuprimeCam@SUBARU: $1500\,\mathrm{deg}^2$ in 5 bands, 1 mag deeper than CFHTLS.

The future

- From space: Euclid (see Yannick Mellier's talk) – 10^4 times the COSMOS area!!!
- From the ground: After KiDS/VIKING, DES, HSC: LSST, 'ultimate ground-based astronomical imaging machine'
  ($\sim 20000\,\mathrm{deg}^2$, with $n \sim 30\,\mathrm{arcmin}^{-2}$; $\langle z_\mathrm{s} \rangle \sim 1.0$)

Conclusions

- Cosmic shear has yielded the first substantial cosmological constraints (mainly on σ_8)
- Weak lensing is **the** method to study the relation between galaxy and mass distribution
- Community has joined forces (e.g., STEP, GREAT08) and pushed succecssfully for a (near) all-sky multi-band imaging survey (Euclid) – with colossal breadth of applications
- (One of) the most promising method to study equation-of-state of dark energy
- Substantial efforts still needed – data reduction, shape measurements, modeling, simulations, statistical analysis, ...

Dark Matter in Clusters & Large-Scale Structure

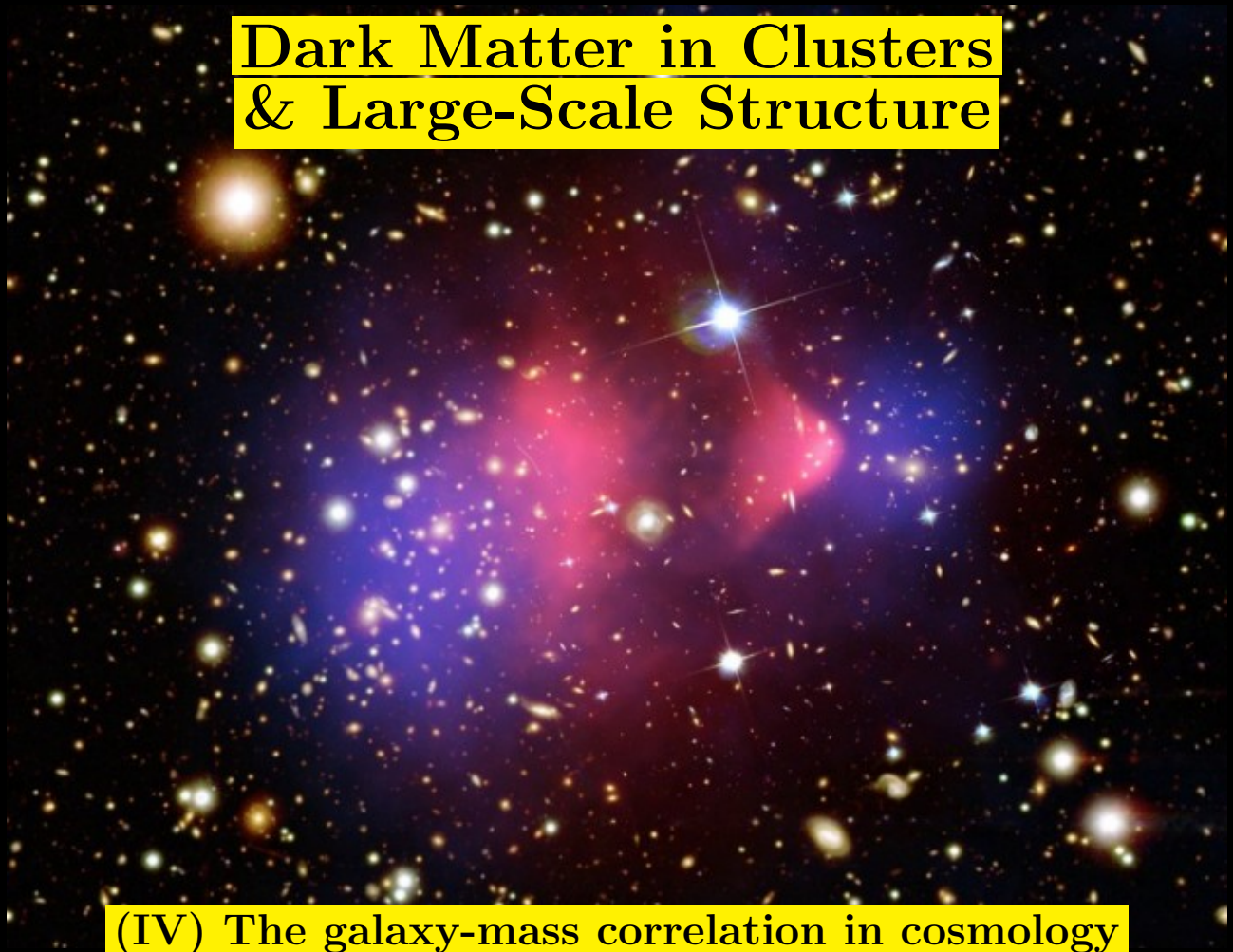

(IV) The galaxy-mass correlation in cosmology

The relation between light and matter

- Cosmologists predict the large-scale distribution of matter (e.g., through simulations);
- Astronomers observe the large-scale distribution of galaxies (e.g., 2dFGRS, SDSS).

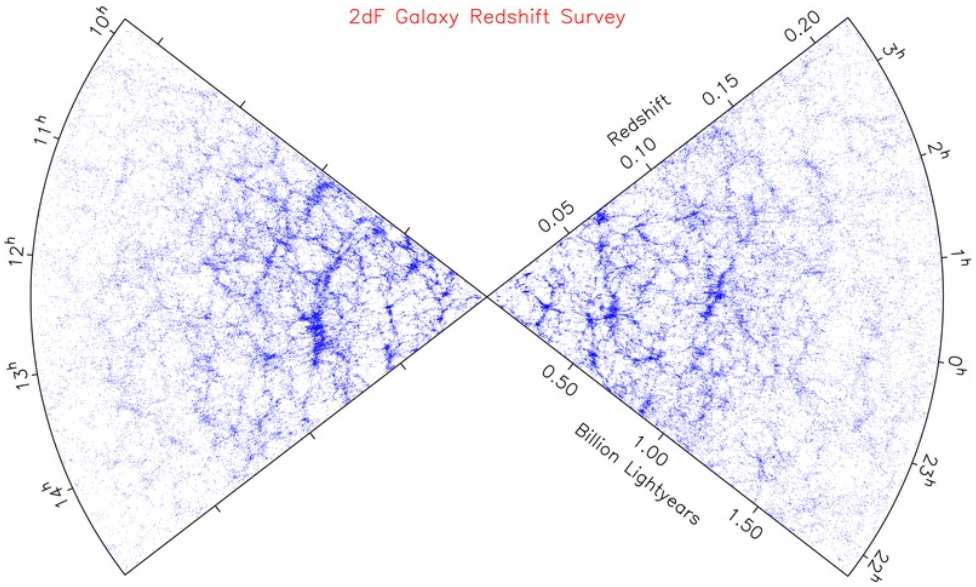

The relation between light and matter

- Cosmologists predict the large-scale distribution of matter (e.g., through simulations);
- Astronomers observe the large-scale distribution of galaxies (e.g., 2dFGRS, SDSS).
- how are these two related?

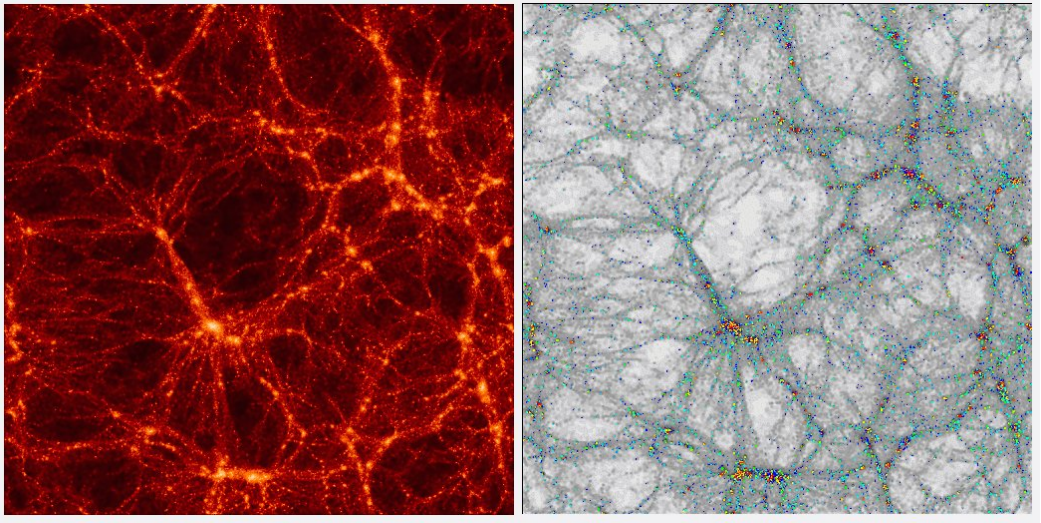

The mass of, and associated with galaxies

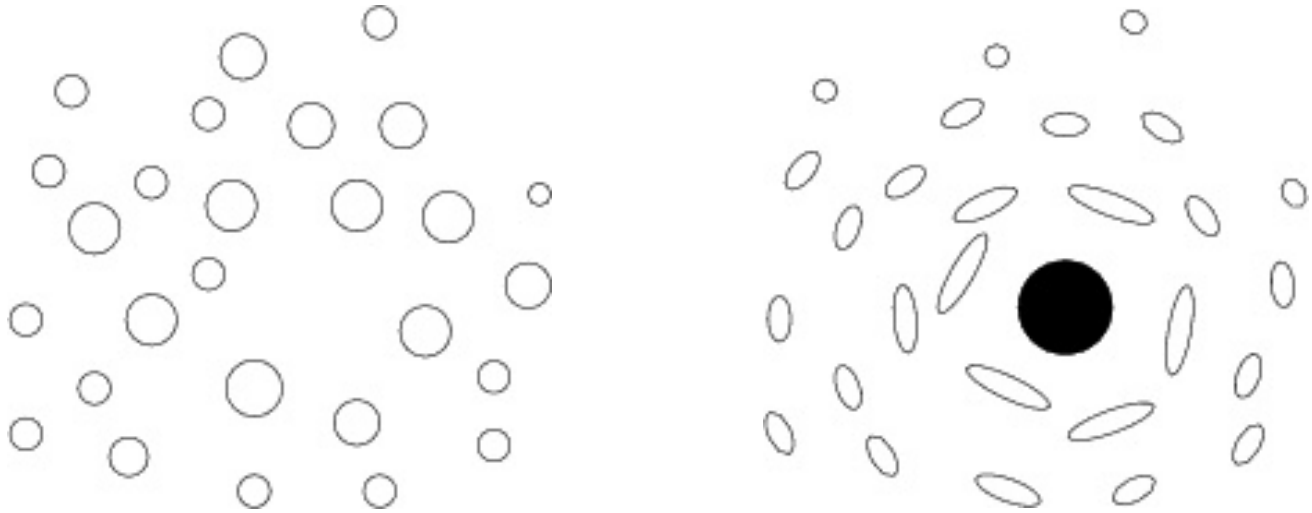

Whereas galaxies not massive enough to show a weak lensing signal individually, signal of many galaxies can be superposed;

consider sets of foreground (lens) and background galaxies;

in the mean, in a foreground-background galaxy pair, the ellipticity of the background galaxy will be preferentially oriented in the direction tangent to the connecting line.

Introduction

Investigating the mass profile of galaxies, and the correlation between galaxies and underlying mass distribution, are related problems:

- for small separations, shear near a galaxy is dominated by the mass of the galaxy itself;
- for larger separation, one starts to measure the mass with which the galaxy is associated (such as host group/cluster);
- on even larger scales, the correlation between mass and galaxy distribution is measured;
  which can also used to measure the bias factor (as function of scale).

These large-scale correlations can also be investigated by using the magnification effect.

Principle of galaxy-galaxy lensing

- The tangential shear $\gamma_{\rm t}(\theta)$ around an individual galaxy cannot be measured, due to shape noise.
- But one can statistically superpose the shear signal around many (similar) galaxies, to get the mean $\langle\gamma_{\rm t}\rangle\,(\theta)$.
- $\langle\gamma_{\rm t}\rangle\,(\theta) = \bar{\kappa}(\theta) - \langle\kappa\rangle\,(\theta)$, i.e., the difference between the average density *inside* the circle and the mean density *on* the circle.
- Measuring the GGL signal $\langle\gamma_{\rm t}\rangle\,(\theta)$ thus yields immediate information about the mean mass profile of the galaxy population.
- If the galaxies have known redshift, this can be translated into physical quantities, since $\kappa = \Sigma/\Sigma_{\rm cr}(z_{\rm d}, z_{\rm s})$, to yield $\Delta\Sigma(R = \theta D_{\rm d}) = \bar{\Sigma}(R) - \langle\Sigma\rangle\,(R)$ – hence, it measures an overdensity around galaxies.
- The signal can then be interpreted in terms of appropriate models, or one can obtain model-free results on biasing parameters (see below).

First detection

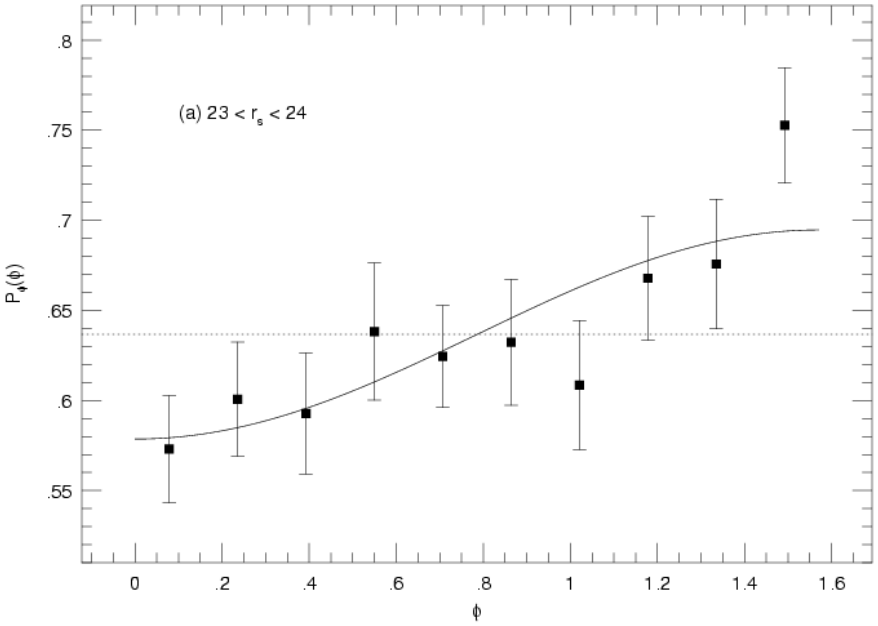

Effect first found by Brainerd et al. (1996), on a single $9'.6 \times 9'.6$ field;
'fg galaxies': $m \in [20, 23]$;
'bg galaxies': $m \in [23, 24]$;
$\Delta\theta \in [5'', 34'']$;
cos-curve measured.

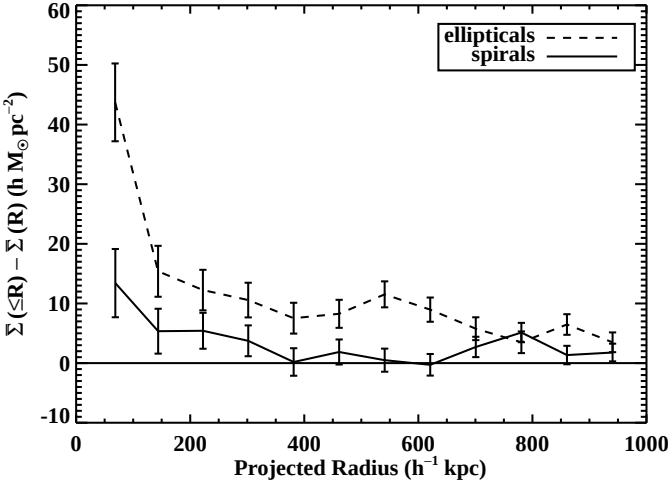

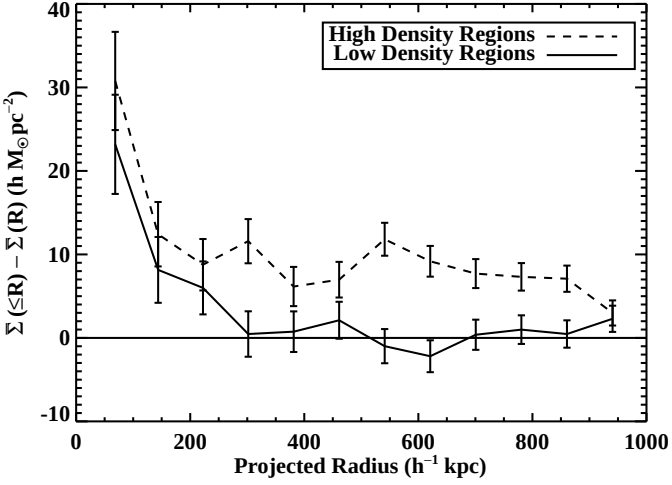

Early SDSS results

Figures (McKay et al 2001) show that the signal is dominated by early-type (ellipticals); not too surprising, as an L_*-E is more massive than an L_*-spiral (at least at small radii); furthermore, signal beyond $\sim 200h^{-1}$ kpc comes from galaxies in dense regions; may have two reasons:

- ellipticals tend to live in dense environments, and they yield the signal, or
- matter other than the galaxy contributes to lensing signal

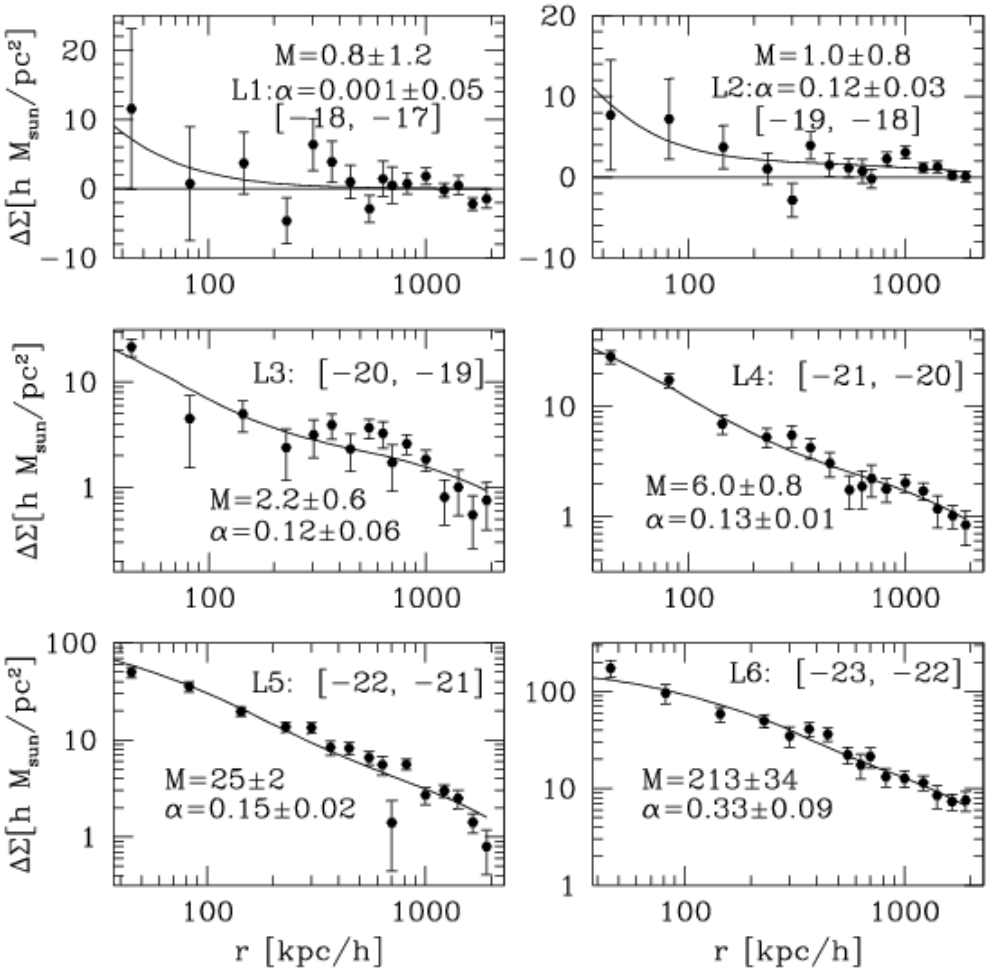

Later SDSS results

Figure from Seljak et al. (2004);

GGL signal for different luminosity bins of (foreground) galaxies; curves are fits from halo model.

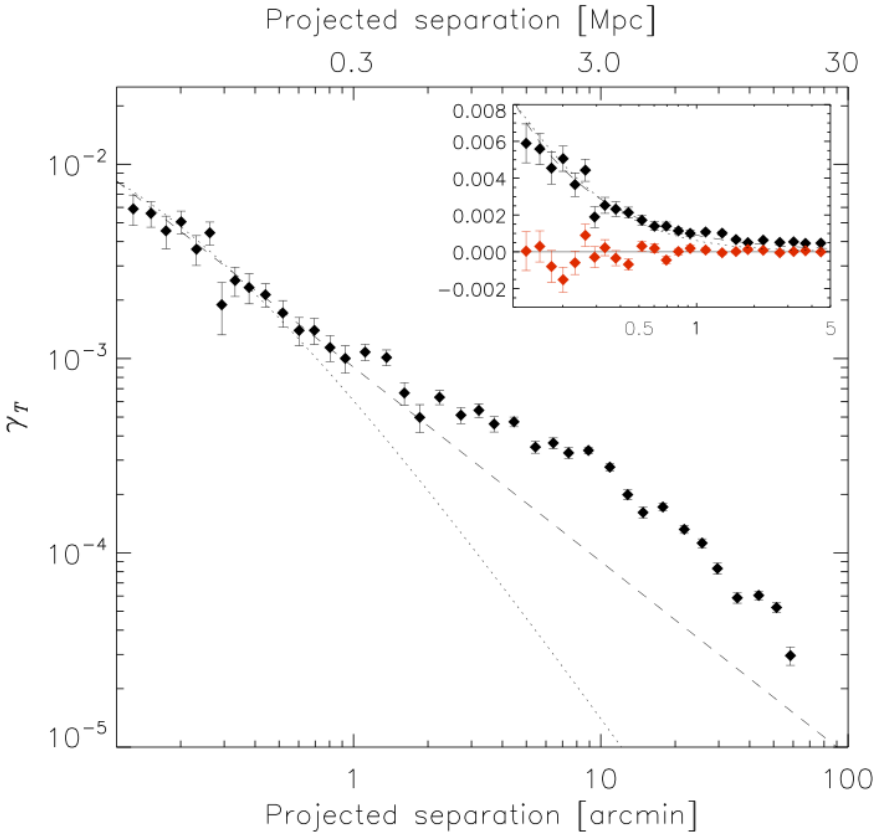

Tangential shear profile around 'bright' galaxies in the RCS2 survey (van Uitert et al. 2011);
for small separations, profile well fitted by either SIS or NFW profile;
for large separations, signal clearly exceeds these simple models:
the mass correlated with galaxies extends much further than the dark matter halo in which the galaxy is embedded – galaxies and mass are correlated at large separations.

The halo model

Interpretation of GGL signal often done in term of halo occupation distribution (HOD), also calle dhalo model.

Ingredients of the model, Part I:

- The mass distribution in the Universe can be considered as the sum of the density profiles of dark matter halos.
- Each halo is described by a position $\boldsymbol{x}_i$ and mass M_i.
- The density profile of a halo depends on its mass and redshift (NFW profile).
- The mass function of DM halos, $n(M, z)$, is known from simulations.
- The correlation function of halos with mass M_1, M_2, is given by

$$\xi(M_1, M_2; x) = b_{\rm h}(M_1)\, b_{\rm h}(M_2)\, \xi_{\rm lin} \ ,$$

  where the $b_{\rm h}(M)$ denote the bias of halos of mass M relative to the underlying matter distribution – halos cluster differently from the overall dark matter distribution. Can be obtained from N-body simulations.

- Combining these ingredients, the correlation function of matter can be derived,

$$\xi_{\rm m} = \xi_{\rm m}^{\rm 1h} + \xi_{\rm m}^{\rm 2h} \ ,$$

  where the first term descibes matter correlations within the same halo, whereas the second the correlation between two different halos.

This halo model yields astonishingly accurate description of the matter correlation function (or power spectrum) of the LSS.

Ingredients of the model, Part II – now with galaxies:

Consider galaxies with luminosities (or stellar masses) in a given interval.

- Let $\langle N|M\rangle$ be the mean number of galaxies (with the prescribed properties) that live in a halo of mass M. The functional form of $\langle N|M\rangle$ can be obtained from observations (galaxies in groups and clusters), further constraints come from number counts.
- Assume that N is Poisson distributed.
- If a halo has 1 galaxy, it lives the center of the halo. If it has more than one galaxy, one lives at the center, the other are satellite galaxies.
- Use a radial distribution function for the satellite galaxies, e.g., also an NFW profile.

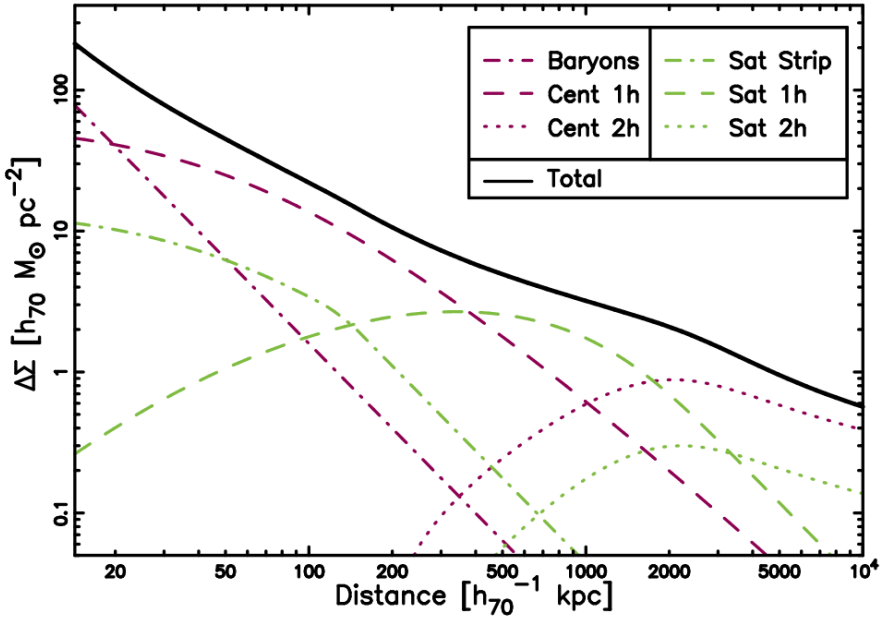

Illustration of halo model:
$M_{200} = 10^{12} M_\odot$;
$M_* = 5 \times 10^{10} M_\odot$;
satellite fraction $\alpha = 0.2$
from Velander et al. (2012)

$$\Delta\Sigma_{\rm cent} = \Delta\Sigma^{\rm 1h}_{\rm cent} + \Delta\Sigma^{\rm 2h}_{\rm cent}$$

$$\Delta\Sigma_{\rm sat} = \Delta\Sigma^{\rm strip}_{\rm sat} + \Delta\Sigma^{\rm 1h}_{\rm sat} + \Delta\Sigma^{\rm 2h}_{\rm sat}$$

$$\Delta\Sigma = \Delta\Sigma_{\rm bar} + (1-\alpha)\Delta\Sigma_{\rm cent} + \alpha\Delta\Sigma_{\rm sat}$$

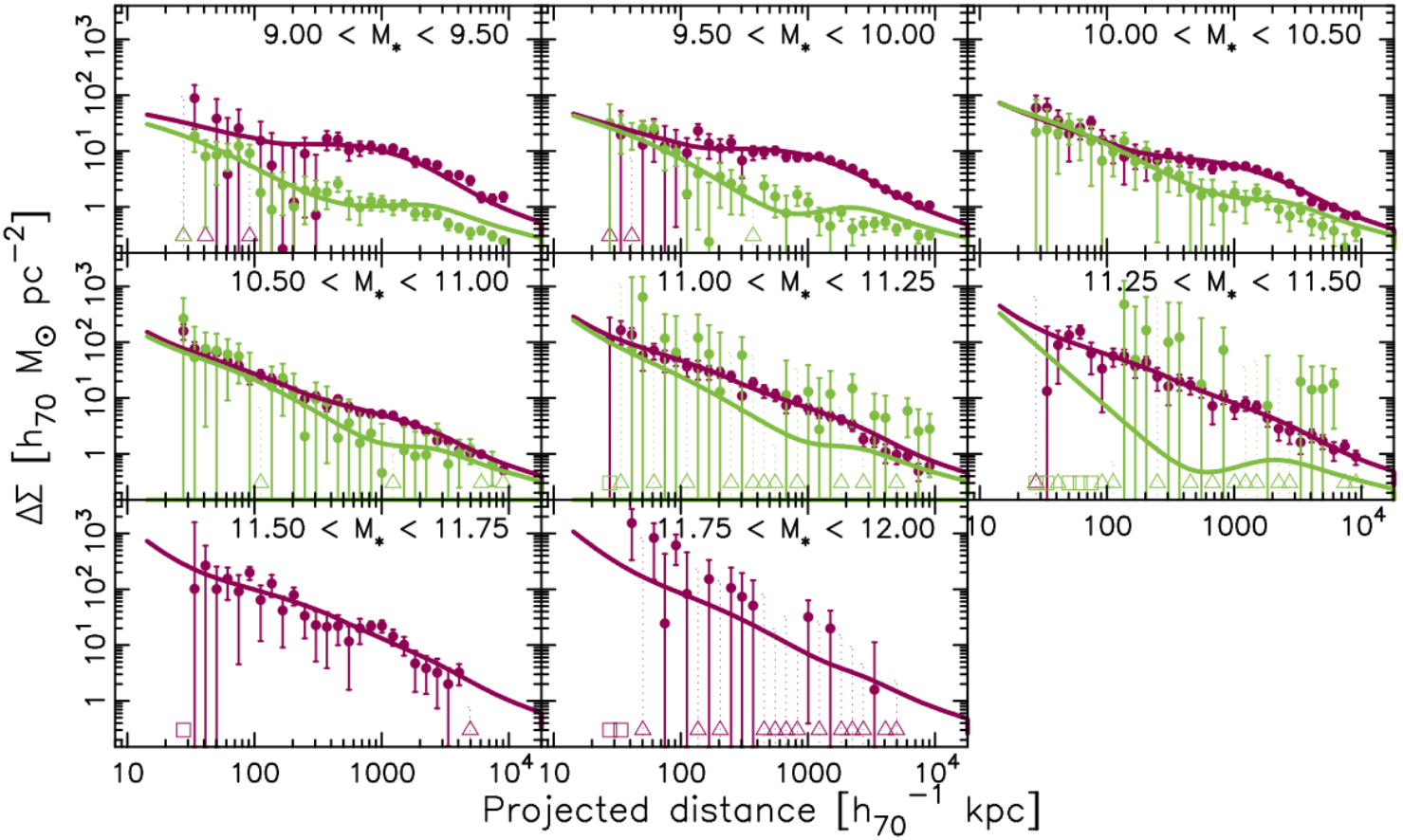

Velander et al. (2012)

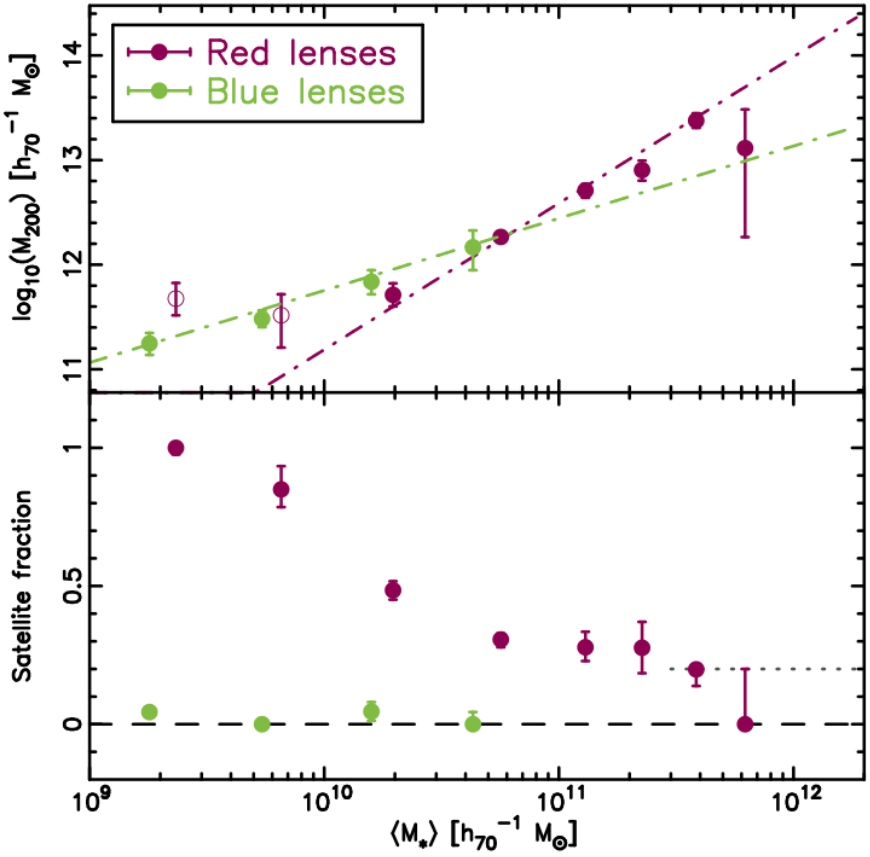

Relation between stellar mass and mean halo mass (top) and satellite fraction α as function of stellar mass (bottom),

for early- (purple) and late-type (green) galaxies

almost all late-type galaxies are centrals, the satellite ffraction of early-type galaxies strongly depends on galaxy mass (or luminosity)

Velander et al. (2012)

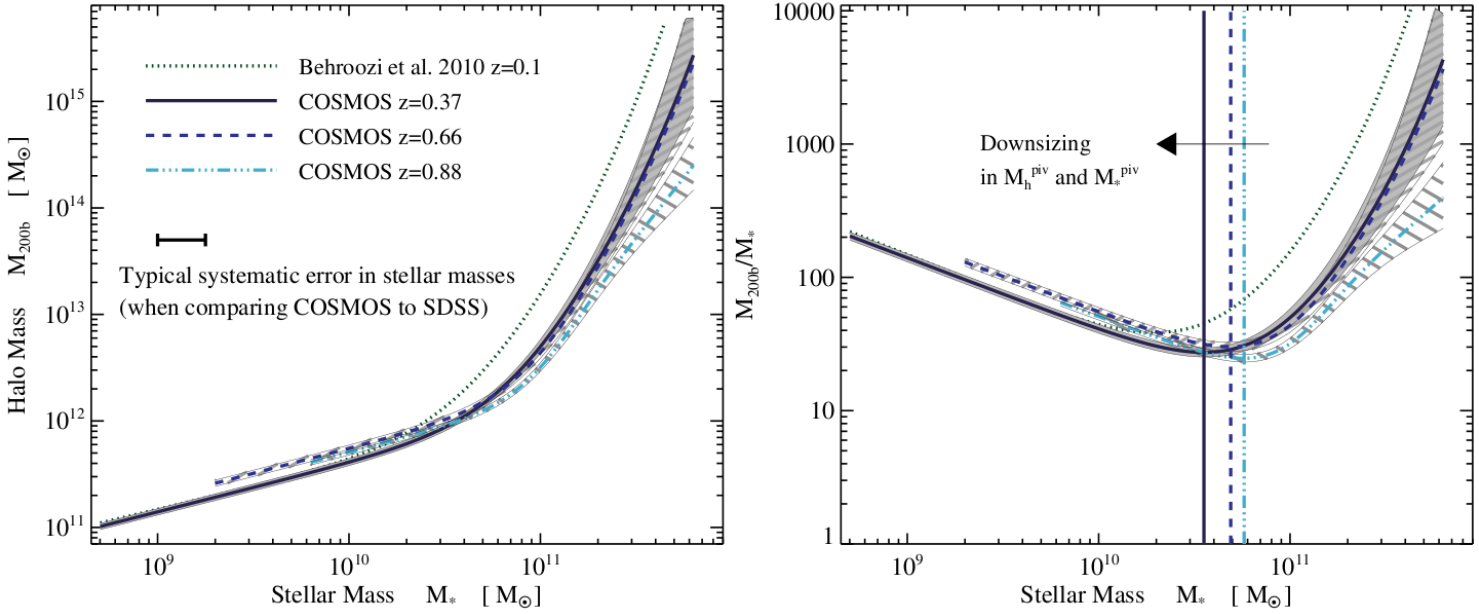

Combining galaxy correlations and galaxy-galaxy lensing in the framework of the halo model, the relation between stellar mass and dark matter halo mass can be derived from COSMOS survey (Leauthaud et al. 2012)

A clearly preferred scale for most efficient transformation of stars into gas.

Biasing of galaxies

- Galaxies are distributed differently than the overall mass distribution, they are **biased**.
- Seen from the luminosity- and galaxy type-dependence of the galaxy correlation function.
- Galaxies form in preferred locations, namely in overdense regions.
- Biasing of galaxies carries important information about galaxy formation and evolution.
- Quantifying biasing is also needed to use redshift surveys for cosmology.

Biasing is a function of scale and redshift:

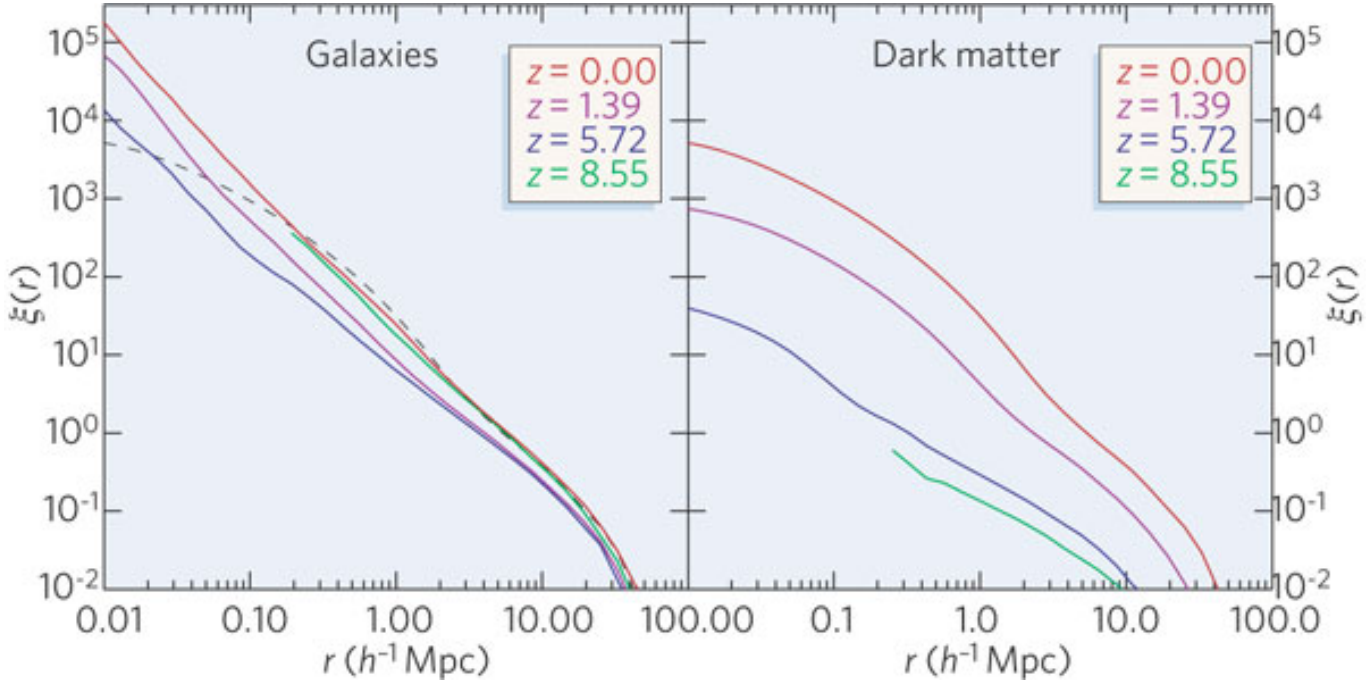

(from Springel et al. 2006)

Galaxy biasing from lensing

The correlation between galaxies and mass, as measured by galaxy-galaxy lensing, is also sensitive to galaxy biasing;

therefore, it provides a unique tool to study the bias factor as function of scale and redshift.

The principle

Consider two populations of galaxies, one a 'background' population with redshift distribution $p_{\rm b}(z)$, and a foreground population with $p_{\rm f}(z)$;

the former is used for shear measurements, the latter as signposts for density enhancement of matter.

Aperture mass of radius θ was defined as

$$M_{\rm ap}(\theta) = \int {\rm d}^2\vartheta\; U(|\boldsymbol{\vartheta}|)\,\kappa(\boldsymbol{\vartheta}) = \int {\rm d}^2\vartheta\; Q(|\boldsymbol{\vartheta}|)\,\gamma_{\rm t}(\boldsymbol{\vartheta})\;. \tag{78}$$

Fractional number density contrast of foreground galaxies is

$$\Delta n_{\rm g}(\boldsymbol{\vartheta}) = \frac{N(\boldsymbol{\vartheta}) - \bar{N}}{\bar{N}} = b \int {\rm d}w \; p_{\rm f}(w) \, \delta \left(f_K(w) \boldsymbol{\vartheta}; w \right) \; , \tag{79}$$

where 3-D fractional number density contrast of galaxies $\delta_{\rm g}$ was assumed to be related to density enhancement by
$\delta_{\rm g} = b \, \delta$, b **being the bias factor.**
This is the case for *linear deterministic biasing*; for *linear stochastic biasing* (more realistic), one defines the **bias factor** b and the **correlation coefficent** r by

$$\left\langle \delta_{\rm g}^2 \right\rangle = b^2 \left\langle \delta^2 \right\rangle \; ; \quad \left\langle \delta_{\rm g} \delta \right\rangle = b \, r \, \left\langle \delta^2 \right\rangle \; . \tag{80}$$

Define aperture counts

$$\mathcal{N}(\theta) = \int {\rm d}^2 \vartheta \; U(|\boldsymbol{\vartheta}|) \, \Delta n_{\rm g}(\boldsymbol{\vartheta}) \; ; \tag{81}$$

hence, $\mathcal{N}(\theta)$ provides a filtered measure of the number density of galaxies.

One now has:

- $\left\langle M_{\rm ap}^2 \right\rangle(\theta)$ is proportional to P_δ;
- $\left\langle \mathcal{N}^2 \right\rangle(\theta)$ is proportional to $P_{\rm g}$;
- $\langle M_{\rm ap}\,\mathcal{N} \rangle(\theta)$ is proportional to $P_{\delta{\rm g}}$

With the previous definitions, we have

$$P_{\rm g} = b^2 P_\delta \; ; \quad P_{\delta{\rm g}} = b\, r\, P_\delta \; ; \tag{82}$$

all quantities depend on scale (and redshift).

Combining these relations, one obtains

$$b^2 = f_1(\theta; \Omega_{\rm m}, \Omega_\Lambda)\; \Omega_{\rm m}^2\; \frac{\left\langle \mathcal{N}^2 \right\rangle(\theta)}{\left\langle M_{\rm ap}^2 \right\rangle(\theta)} \; , \tag{83}$$

and

$$r = f_2(\theta; \Omega_{\rm m}, \Omega_\Lambda)\; \frac{\langle M_{\rm ap}\,\mathcal{N} \rangle(\theta)}{\sqrt{\left\langle \mathcal{N}^2 \right\rangle(\theta)\; \left\langle M_{\rm ap}^2 \right\rangle(\theta)}} \; ; \tag{84}$$

f_1, f_2: depend on redshift distribution of fg and bg galaxies, on the cosmological parameters, but only very weakly on θ and shape of the power spectrum.

More precisely, one defines the bias function as

$$b(k) = \sqrt{\frac{P_{\rm g}(k)}{P_\delta(k)}}$$

correlation parameter r defined as

$$r(k) = \frac{P_{{\rm g}\delta}(k)}{\sqrt{P_\delta(k)\, P_{\rm g}(k)}}$$

Both, b and r are expected to depend on galaxy type, redshift, and length scale; all of this can be studies by galaxy-galaxy lensing – get the mass from lensing (shear) and the galaxies directly.

Aperture measures & correlation functions

To avoid problems with laying apertures on data fields (with holes and gaps), it is essential to realize that

- $\langle M_{\rm ap}^2 \rangle$ can be calculated from shear correlation function;
- $\langle \mathcal{N}^2 \rangle$ can be calculated from angular correlation function of (fg) galaxies;
- $\langle M_{\rm ap}\, \mathcal{N} \rangle$ can be calculated in terms of the mean tangential shear $\langle \gamma_{\rm t} \rangle\, (\theta)$ of the galaxy-galaxy lensing signal.

Hence, besides the mass profiles of galaxies, G-G lensing measures the product $b\, r$.

Results using this method have been published by Hoekstra et al. (2002) combining RCS and VIRMOS-DESCART data.

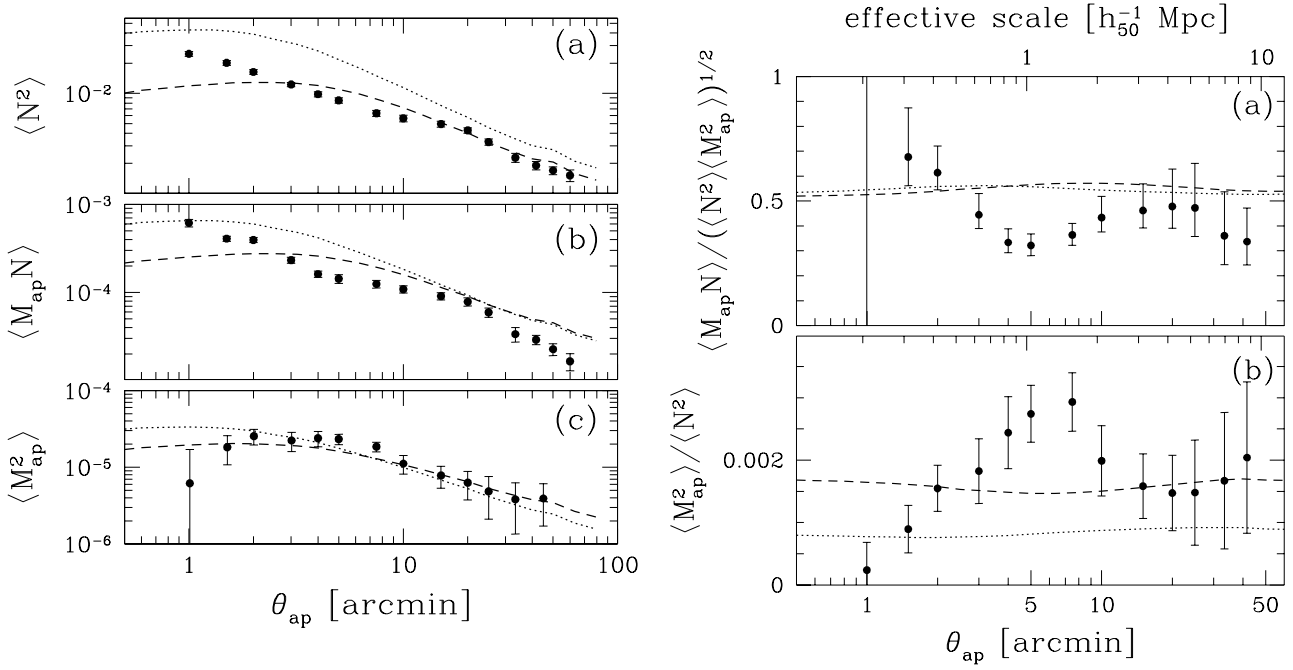

Dotted (dashed) curves correspond to OCDM (ΛCDM) model with $b = 1$, $r = 1$; right figures shows near independence of f_1, f_2 on aperture radius.

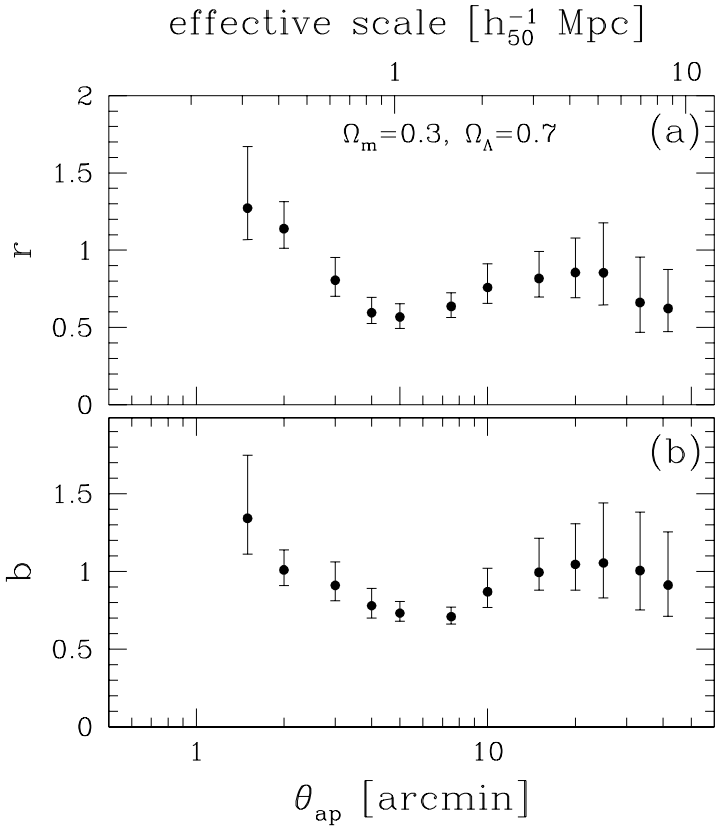

Measured value of r and b as function of angular scale and effective scale (top axis), for ΛCDM model;
ratio $b/r \approx 1.09 \pm 0.04$ on scales $1' \leq \theta \leq 60'$, with little dependence on θ;
but r and b seem to vary with scale, with $r \sim 1$ on small scales, but as low as 0.6 on $\sim 1\,h^{-1}\,$Mpc.

First application of this method yielded encouraging result;
can be made much more accurate, through larger surveys and phot-z information.

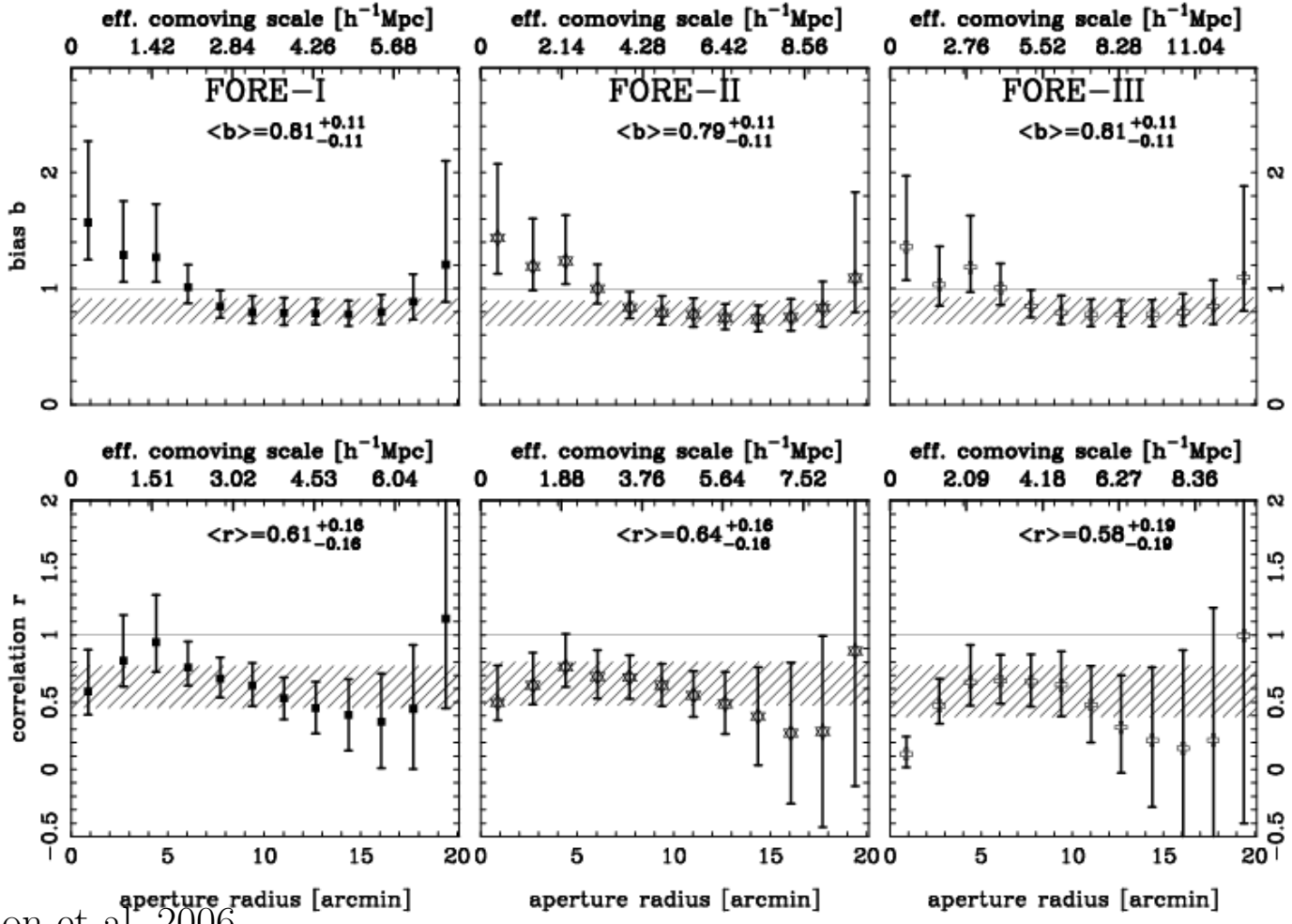

Simon et al. 2006

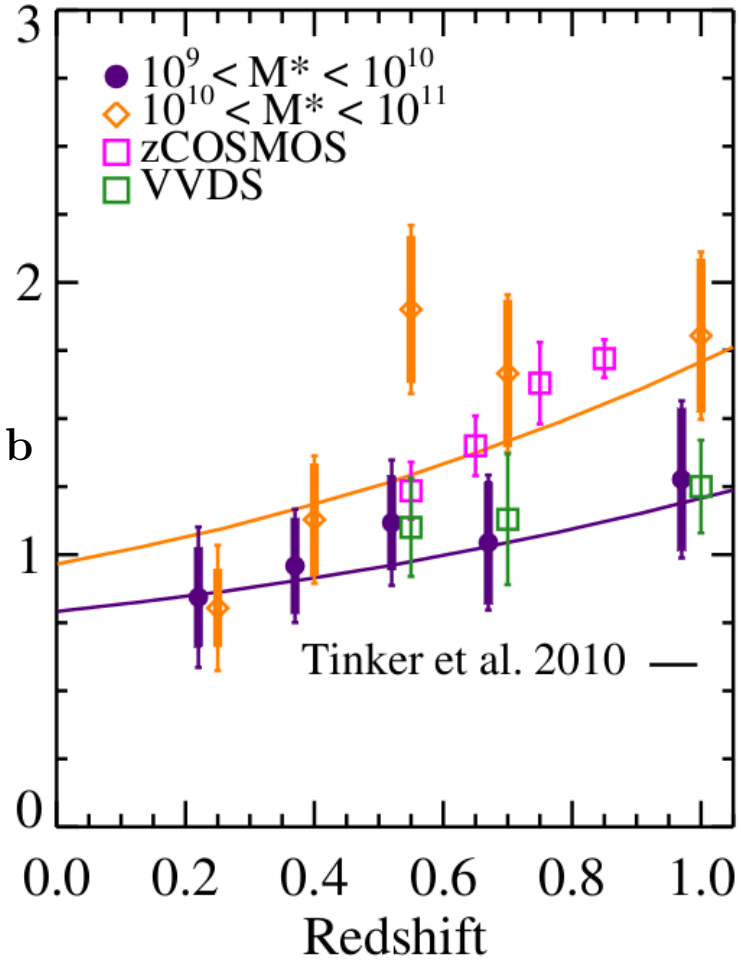

Results from COSMOS survey (Jullo et al. 2012)

- Bias of galaxies increases with redshift
- Bias increases with stellar mass of galaxies
- Correlation coefficient $r \approx 1$ (though with large error bars): no evidence for stochasticity of bias

Cluster-shear correlations

Idea: Weak lensing signal of many clusters are superposed to get average mass profile;

clusters can be binned according to richness, luminosity, ...

Recent results were presented in a series of papers from SDSS collaboration, with very high significance

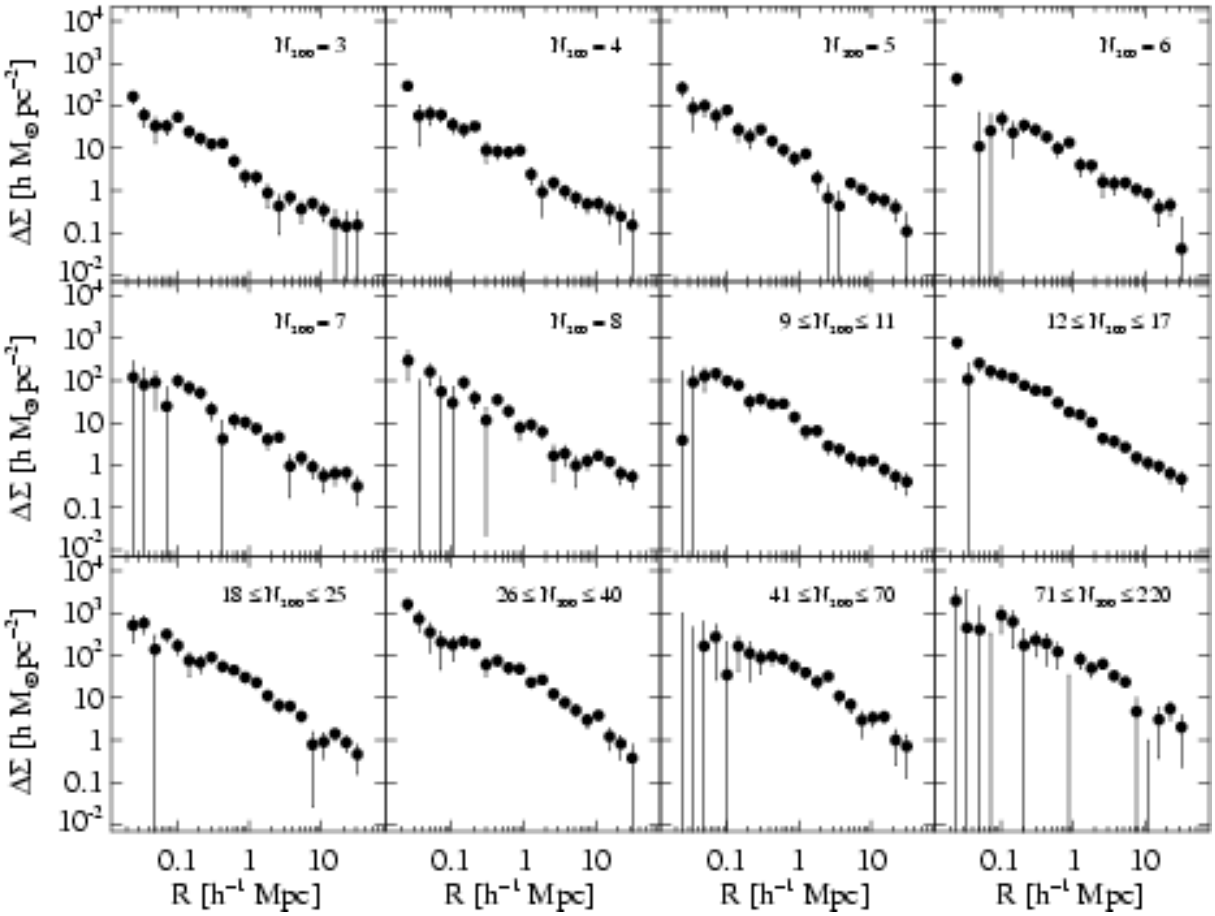

from Sheldon et al. (2007); note that shear signal is measured out to $> 20h^{-1}$ Mpc!

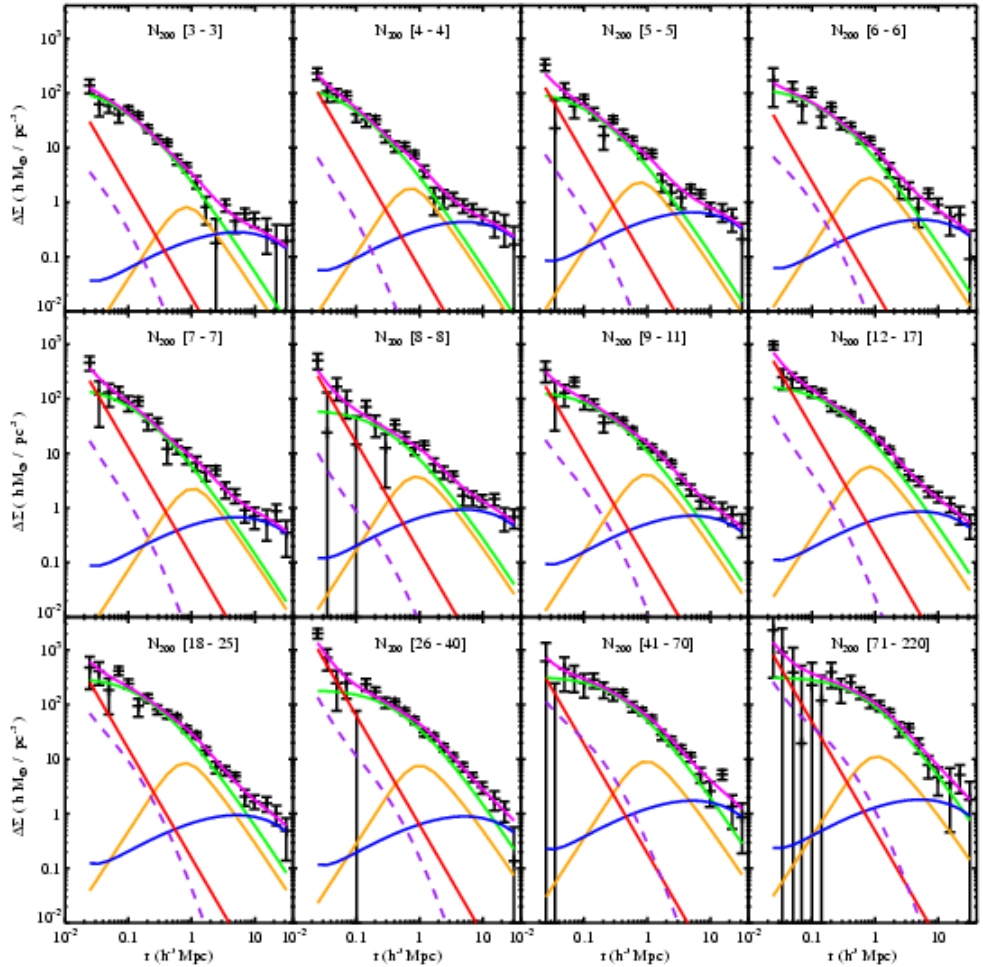

NFW fit

miscentered halos (orange)

BCG

neighboring halos

non-linear shear (purple)

Sum

the binning can also be performed in luminosity from Johnston et al. (2007)

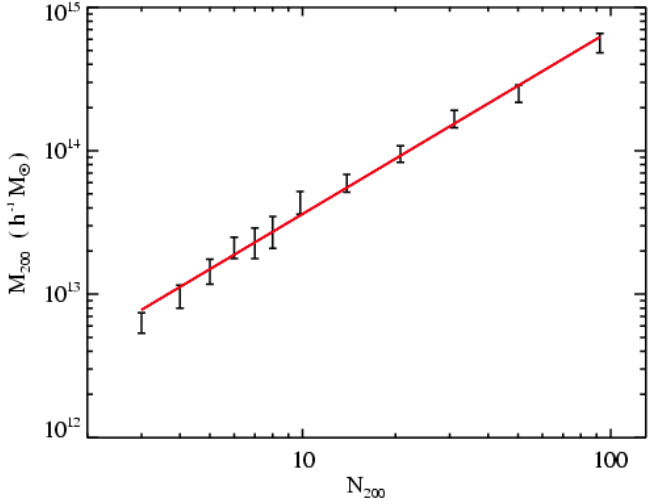

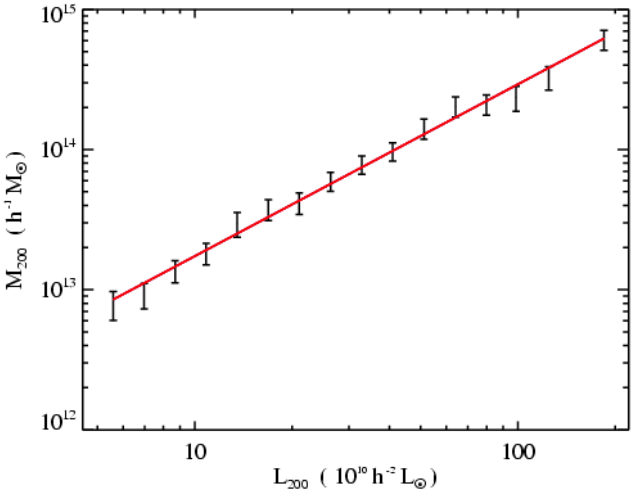

Results:

mass-richness (left) and mass-luminosity (right) relation, obtained by fitting NFW-profiles plus corrections to weak lensing signal in richness and luminosity bins

yields mass calibration for scaling relations of clusters

from Johnston et al. (2007)

Galaxy-galaxy-galaxy lensing

GGL measures correlation of galaxies with mass

One can correlate shear (i.e. mass) with **pairs** of galaxies and thus get the excess mass related to pairs – galaxy-galaxy-galaxy lensing

Probes higher-order biasing; constrains galaxy evolution models

Theory deveolped in Schneider & Watts (2005); first studied on data by Simon et al. (2007) using the RCS survey

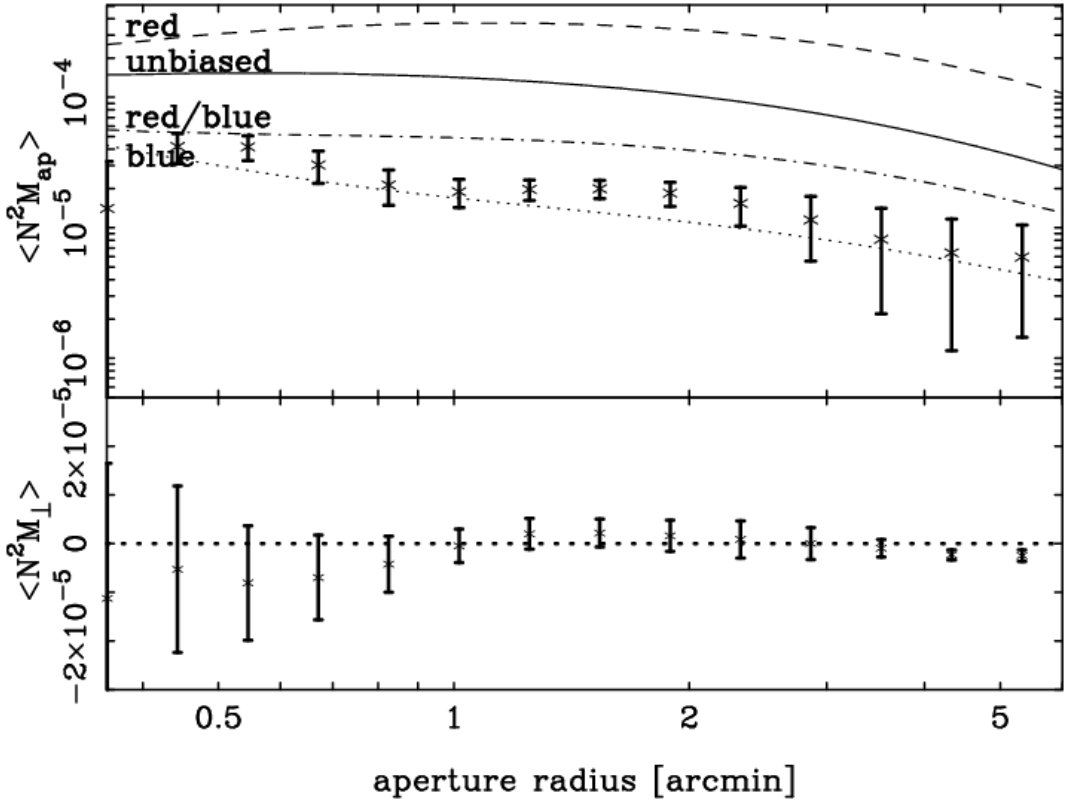

GGGL signal from the RCS, together with simplified HOD model predictions (Simon et al. 2007)

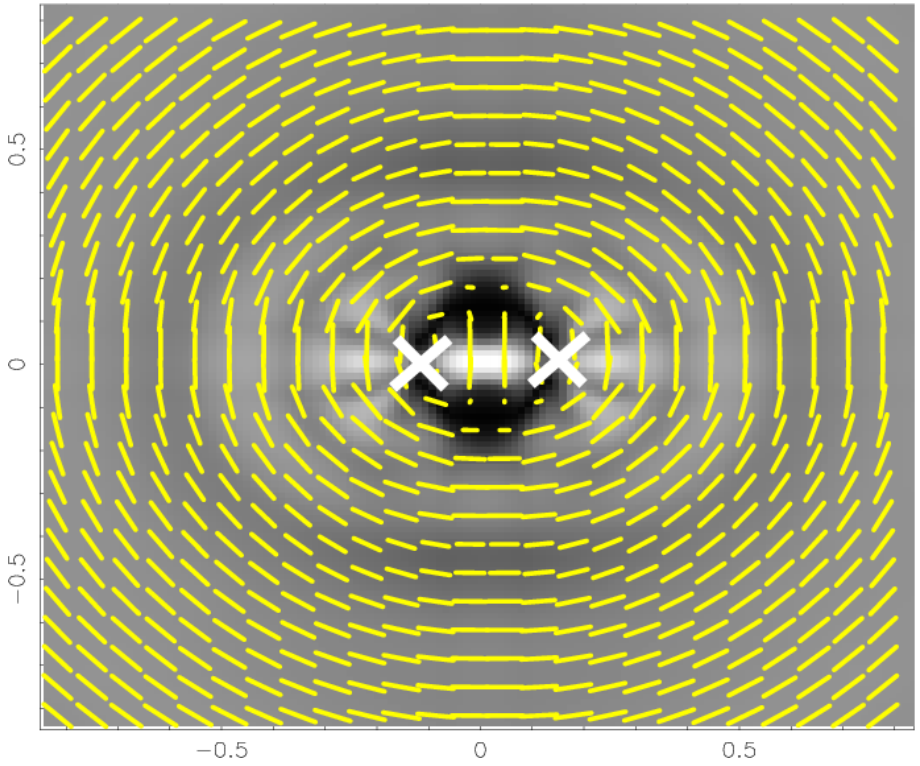

Shear around pairs of galaxies, by just taking the sum of shears associated with the two individual galaxies (Simon et al. 2007)

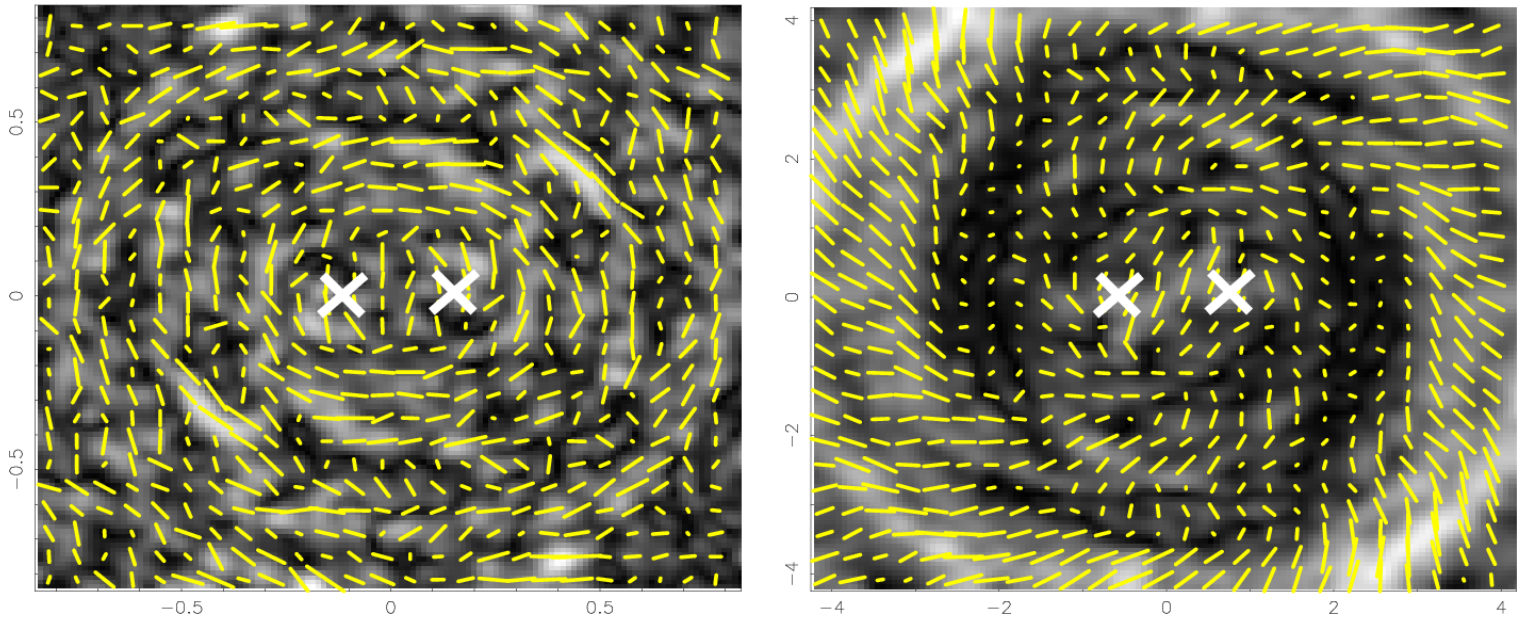

Shear around pairs of galaxies, with (shear from G1 + shear from G2) subtracted – i.e., excess shear over sum of the GGL signal (Simon et al. 2007)

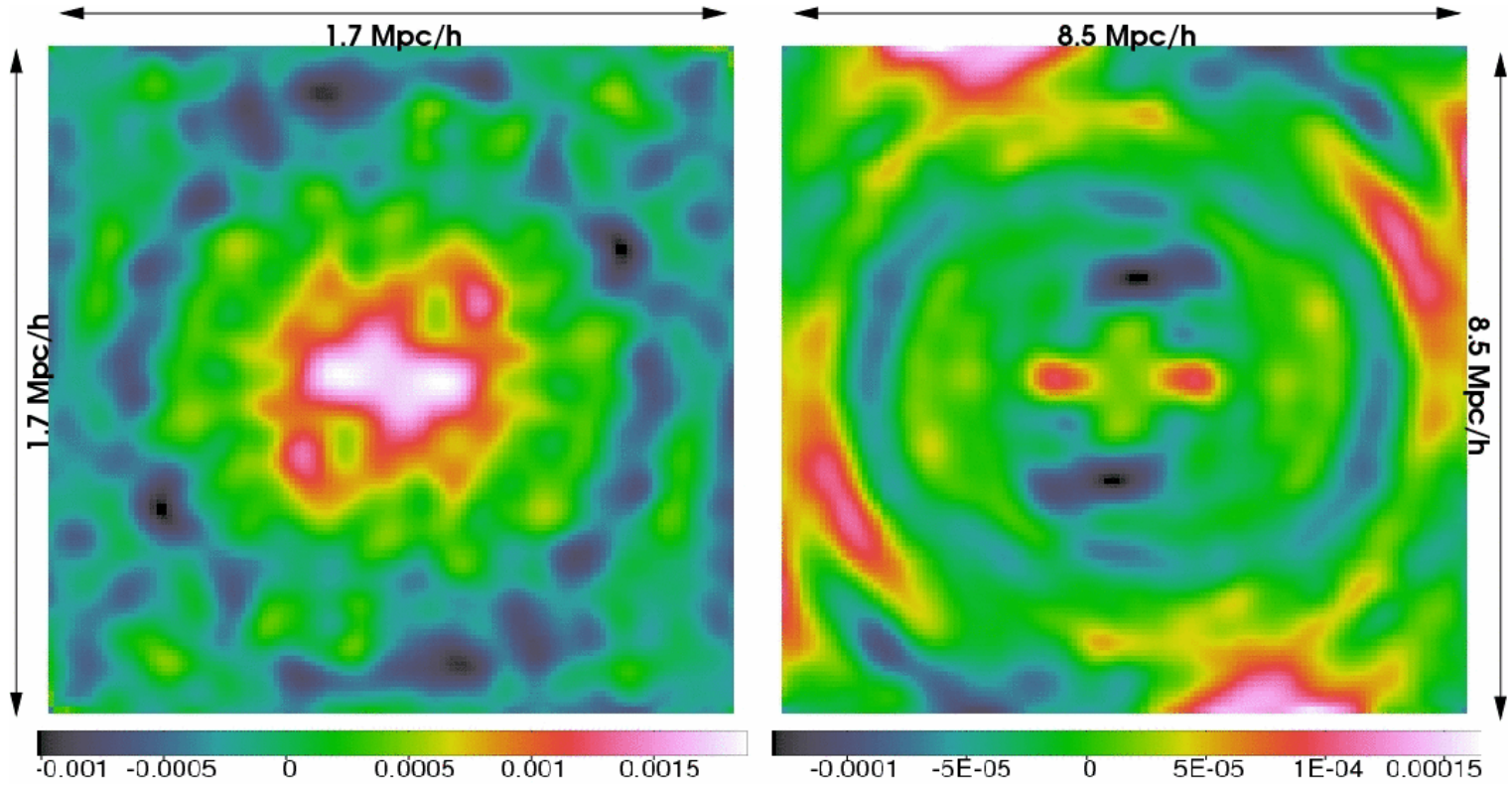

Mass reconstruction from the excess shear around galaxy pairs – i.e., excess mass around galaxy pairs over that of the sum of two galaxies (Simon et al. 2007)

Higher-order galaxy-shear correlations are highly sensitive probes of galaxy evolution models

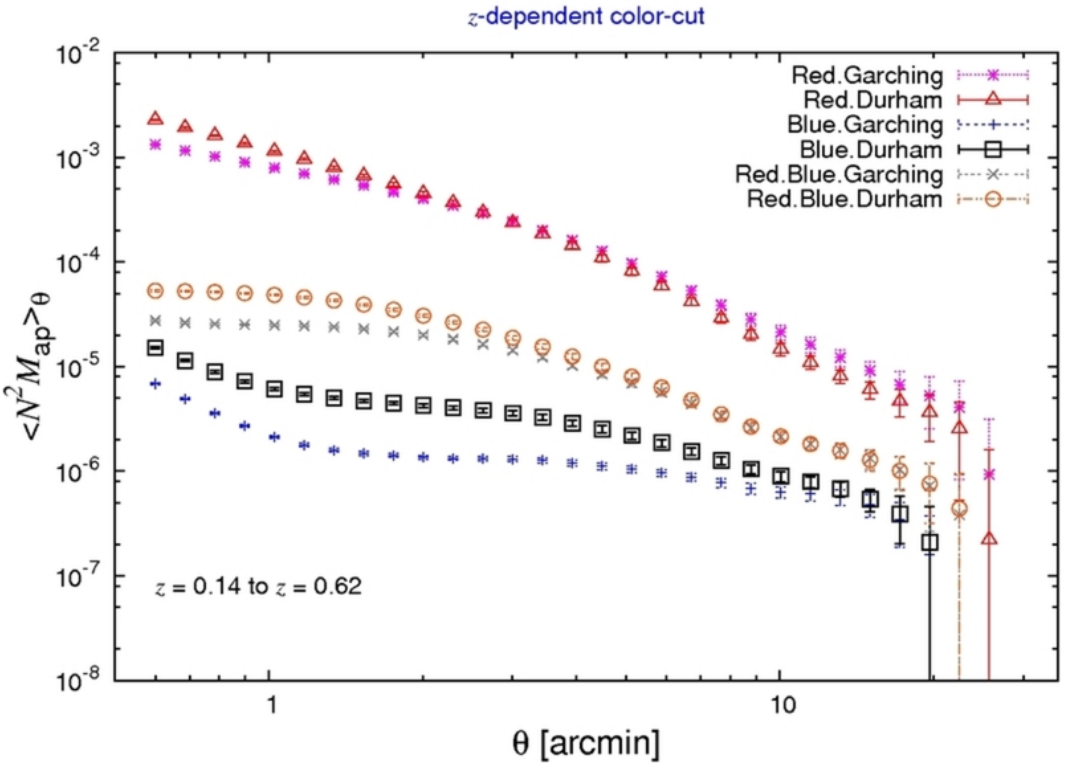

Saghiha et al. (2012)

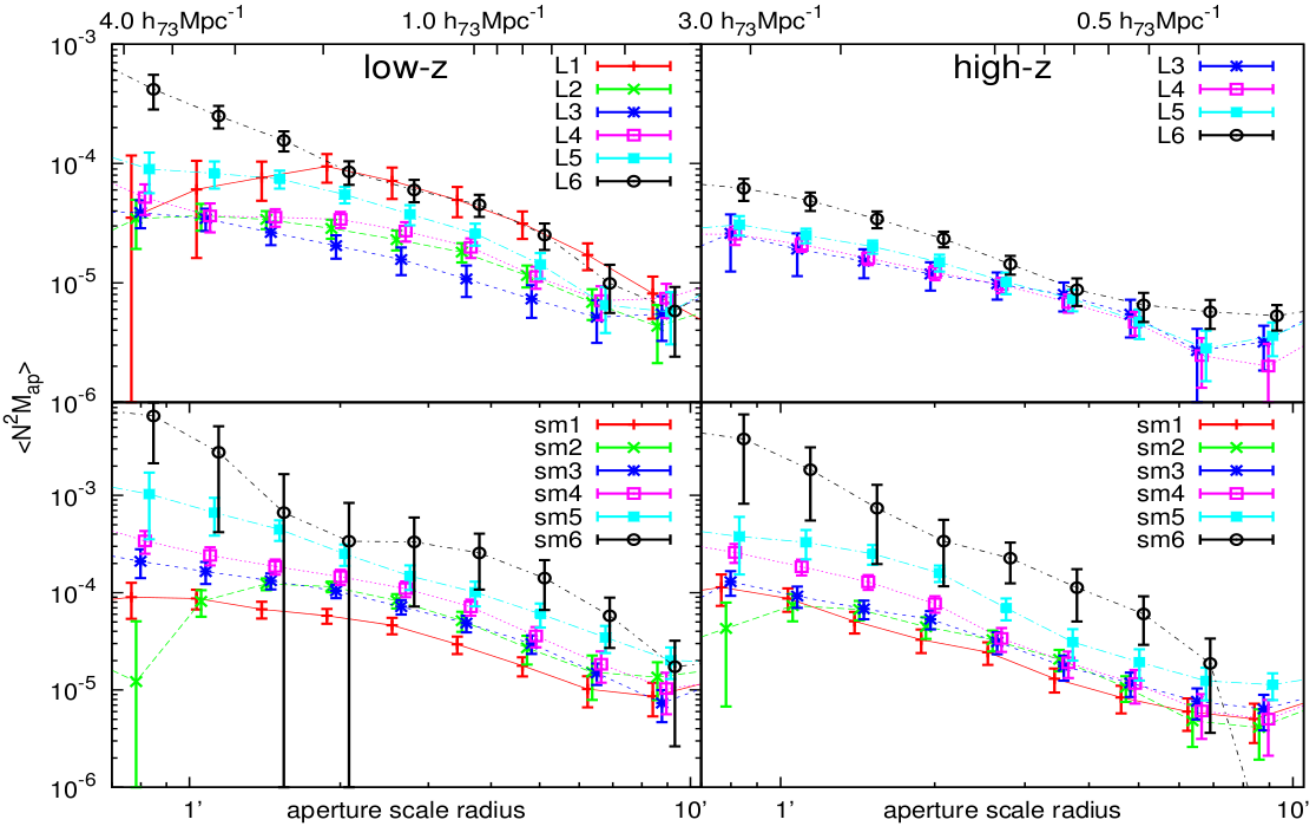

Results from CFHTLenS collaboration (Simon et al. 2012)

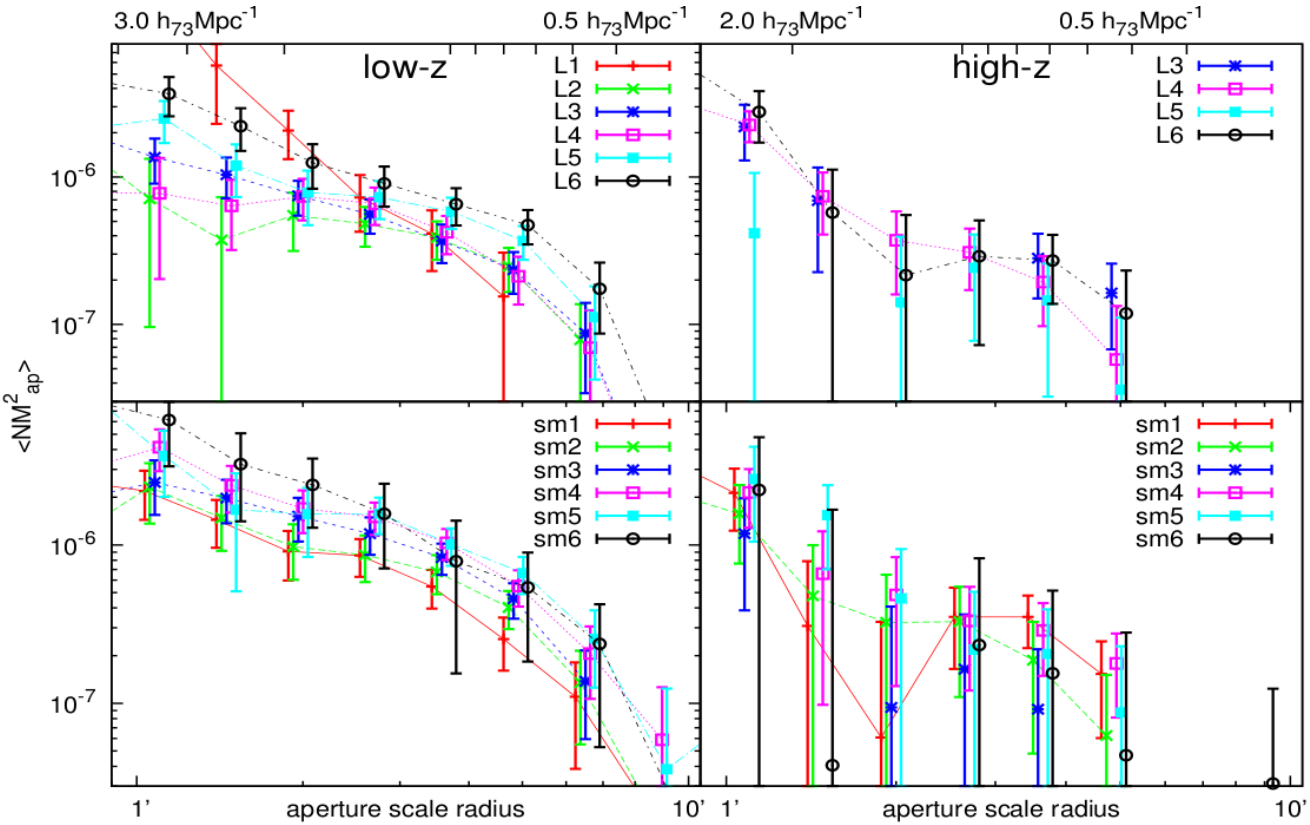

Results from CFHTLenS collaboration (Simon et al. 2012)

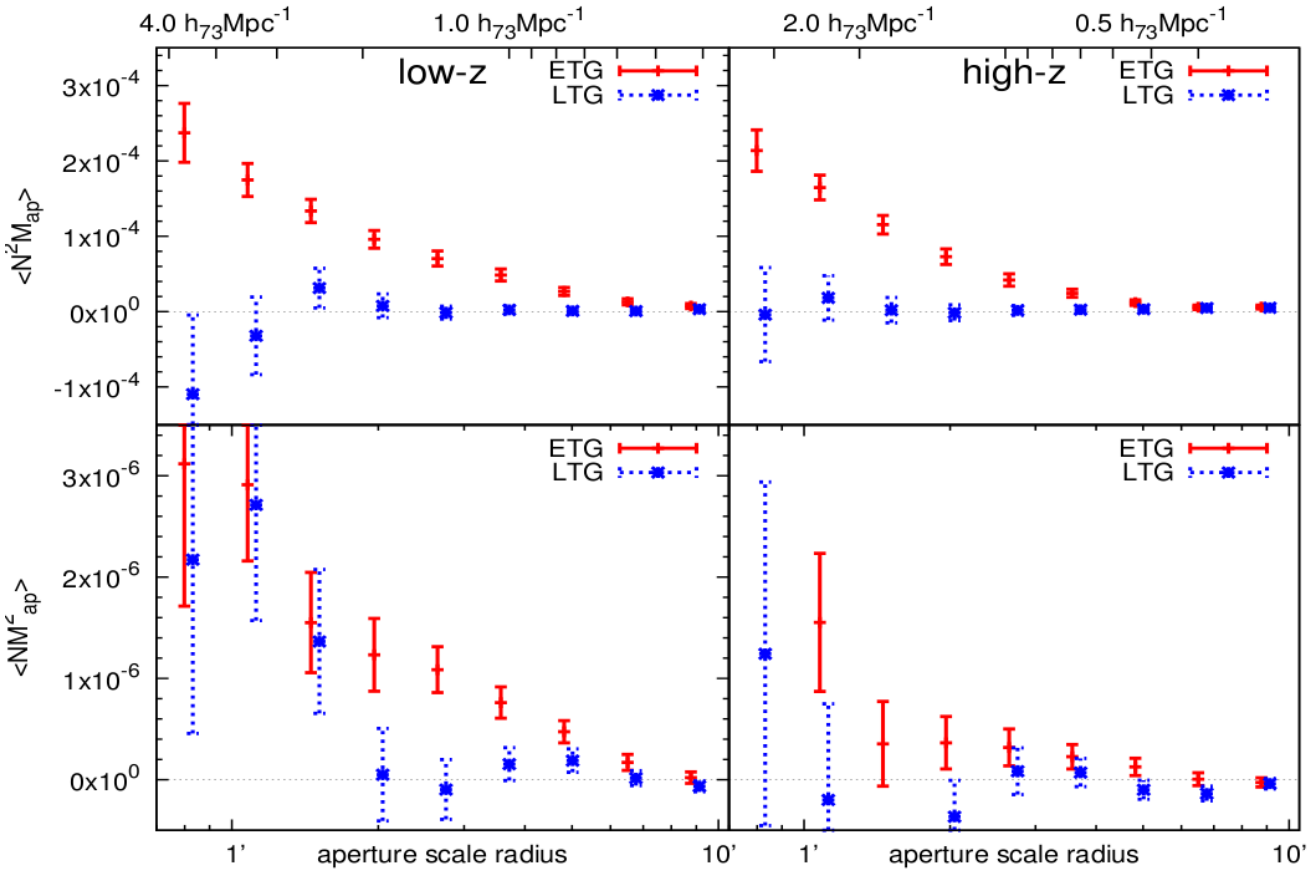

Results from CFHTLenS collaboration (Simon et al. 2012)

Conclusions

- Galaxy-galaxy lensing provides a unique tool for studying the relation between galaxies and mass.
- GGL signal easier to detect than cosmic shear, since it is linear in the shear.
- GGL yields the (mean) halo mass of galaxies, as function of galaxy mass, luminosity and type.
- Galaxy bias and galaxy-mass correlation coefficient can be determined directly, by combining GGL with cosmic shear and galaxy correlation function.
- GGL and its generalizations offers a unique mean to determine mass properties of group and cluster halos.
- Higher-order galaxy-mass correlations detcted with high significance; they are sensitive probe of galaxy evolution models.

Virial radius of dark matter halo

Simple model for halo formation (spherical collapse model) yields that 'virialized region' of a halo has a mean density of $\sim 200\,\rho_{\rm cr}$;

hence, 'virial radius' of a halo is related to 'virial mass' by

$$M = \frac{4\pi}{3} r_{200}^3\, 200\,\rho_{\rm cr}(z) = \frac{100 r_{200}^3\, H^2(z)}{G} \tag{85}$$

Note: The orbital time for a particle at radius r_{200} with circular velocity

$$v = \sqrt{\frac{GM_{200}}{r_{200}}}$$

is about the age of the Universe – makes sense!

Universal mass profile

CDM simulation yield the result that the mean density profile of dark matter halos follows a 'universal' law – the Navarro, Frenk & White profile

$$\rho(r) = \frac{\rho_{\rm s}}{(r/r_{\rm s})(1+r/r_{\rm s})^2} \; ; \tag{86}$$

r_s: scale radius; $\rho_{\rm s}$: normalization;

these two parameters can be expressed in terms of the mass M_{200} (which is equivalent to r_{200}) and the concentration

$$c = \frac{r_{200}}{r_{\rm s}} \; . \tag{87}$$

Simulations show that c is strongly correlated with mass (and redshift).